POLITECNICO DI TORINO

Corso di Laurea in Ingegneria Aerospaziale

Tesi di Laurea

Test Mass Release for LISA ESA mission

Control Design and MonteCarlo Analysis

Relatori
Dott.ssa Elisa Capello
Ing. Nicoletta Bloise
Dott.ssa Elisabetta Punta
Ing. Sabrina Dionisio

Candidato
Leonardo CAPICCHIANO
matricola: 265652

ANNO ACCADEMICO 2019-2020

Sommario

Questa tesi si concentra sullo studio di un controllo a struttura variabile non lineare, di tipo "sliding mode". La missione di riferimento è la missione ESA LISA con data di lancio fissata per il 2034 e una vita operativa di cinque anni, con l'obiettivo di essere utilizzata come osservatorio spaziale per la rilevazione di onde gravitazionali generate da diverse sorgenti, quali i sistemi di stelle binarie oppure collisioni di buchi neri supermassicci. Tale osservatorio è costituito da tre satelliti disposti in una costellazione triangolare equilatera, con il proprio centro in orbita attorno al Sole e alla distanza di un'unità astronomica. La distanza fra gli spacecraft dovrà essere mantenuta costante per tutta la durata della missione in modo tale che ogni minima variazione sia imputabile all'eventuale interazione con onde gravitazionali. In particolare, la strumentazione di rilevazione di ogni satellite sarà costituita da un interferometro laser e da due sistemi ottici che saranno composti a loro volta da un telescopio, da un piano ottico per l'interferometria laser e da un sistema di sospensione elettrostatica che controlla, all'interno di appositi contenitori, una massa cubica, chiamata "Test Mass", che sarà utilizzata come principale sensore di misurazione durante le operazioni scientifiche. L'obiettivo principale di questo lavoro riguarda lo sviluppo di un sistema di controllo rubusto e insensibile alle incertezze dei modelli matematici implementati, che sia capace di stabilizzare le test masses all'interno delle proprie gabbie, in un ambiente estremamente rumoroso e con forti disturbi esterni, durante la fase di test mass release. In particolare, per quest'ultima il design risulta essere particolarmente critico in quanto si ritrova a dover lavorare in una fase transitoria in cui le masse sono sganciate e libere di muoversi dopo la fase di acquisizione della costellazione da parte degli spacecraft. Di conseguenza, sono richieste elevate prestazioni in termini di accuratezza e stabilità per ottenere le condizioni iniziali ottimali per poter passare alla modelità scientifica, che costituisce la principale fase dell'intera missione. Il design di controllo proposto è accuratamente valuato in termini di prestazioni, in riferimento

a risultati che sono stati ottenuti attraverso una campagna MonteCarlo che comprende duecento simulazioni, con configurazioni differenti in termini di condizioni iniziali, rumori e disturbi esterni. Tutti i requisiti e vincoli considerati in questo lavoro fanno riferimento ai documenti forniti da ESA e riguardanti la precedente missione LISA Pathfinder, che aveva l'obiettivo di testare e validare i sistemi di controllo e gli equipaggiamenti da utilizzare nella missione LISA. Le simulazioni prendono in considerazione le prestazioni di due modalità in cui è stata divisa la fase di test mass release, ovvero le modalità "*Wide Range*" and "*High Resolution*". Queste saranno differenti fra loro per diverse autorità di controllo, condizioni iniziali e configurazioni ambientali, in termini di rumori e disturbi. La soluzione proposta, quindi, sarà concentrata nel design del Super Twisting Sliding Mode Control per il controllo sia della posizione che dell'assetto delle due masse cubiche al fine di contrastare elevati disturbi, rumori e incertezza intrinseche del modello implementato. Infine, un'analisi approfondita verrà anche effettuata su un controllo SMC del primo ordine, implementato prima su LISA Patfinder ma fallimentare, mediante la stessa campagna MonteCarlo, al fine di confrontare i due tipi di controllo e mostrare i vantaggi riguardo l'implementazione della strategia di controllo proposta. Infine, una breve analisi sarà effettuata in modo tale da valutare quantitativamente l'influenza dei forti disturbi e rumori esterni che vanno ad interagire strettamente con le test masses.

Abstract

This thesis is focused on a second order controller named Super Twisting Sliding Mode Control (STW SMC) designed for the Laser Interferometer Space Antenna (LISA) mission. This ESA space mission, which will be launched on 2034, will be used as in-space observatory for a lifetime of five years to detect gravitational waves generated from sources like binary stars systems and merging of supermassive black holes. The space observatory consists in three satellites in a triangular constellation at 1 AU from the Sun on a heliocentric orbit. The distance between spacecrafts will have to be fixed and each small variation will be assigned to possibly gravitational waves. In detail, the sensor instrument is composed by a laser interferometer and two Optical Assembly (OA) clusters on each spacecraft(S/C), which are composed by a telescope, an optical bench for the laser interferometer and an electrostatic suspension system which houses suspended cubic Test Mass (TM). The electrostatic suspension system is the actuation system involved in the control design. The main purpose of this work is to develop a robust controller to stabilize the TMs to their own cages center in a noisy space environment with high disturbances during the TMs release, a very critical transient phase in which the TMs are unlocked and released in their proper cages after the constellation acquisition. High levels of stability and precision are required to obtain optimal initial conditions to switch to the scientific in-orbit operations. The proposed control system is tested in terms of performance such as stability, maximum overshoot, settling time, violation time, steady-state error, and accuracy (3) through a MonteCarlo simulation campaign. The results are analysed for two hundred runs at different configurations, randomly defined in a wide range of values fixed by ESA documents for noises, disturbances and initial conditions. As reference data to compare the obtained outcomes in respect of the required performance and constraints, reports are given from the previous LISA Pathfinder mission, which had the purpose to verify and test different technologies which will be implemented on LISA itself such as measurement instrumentation. The analysis involves two operative modes: (1) "Wide Range" (WR) and (2) "High resolution" (HR). In the first mode, the TMs are caught and stabilized after their release from plungers with a coarse precision to obtain good initial

conditions to switch to the HR mode. The second mode allows a better control and performance within ESA requirements to reach good initial conditions for the Science Mode (SCI), with a converging time within 5000s. In the WR mode, the reduced control authority and the higher magnitude of noises and disturbances are a challenging configuration for the control design. The solution proposed consists in a STW SMC, which is a nonlinear technique applied to obtain a precise and robust control for both position and attitude to effectively counteract the strong disturbances in the challenging space environment and high uncertainties given by onboard sensors and actuators. The mathematical model defines a coupled nonlinear dynamics between the spacecraft and TMs, but there is no coupling between the two TMs. Finally, a second reduced MonteCarlo campaign is proposed to compare the implemented STW SMC and a first order SMC controller to highlight the different properties of the two algorithms in terms of advantages and drawbacks.

Acknowledgements

"This work was supported by the European Space Agency under contract No. 4000124985/18/NL/CRS. The view expressed herein can in no way be taken to reflect the official opinion of the European Space Agency."
Vorrei ringraziare il meraviglioso team di cui ho fatto parte, fra cui la dottoressa Elisa Capello, la dottoressa Elisabetta Punta e l'ingegner Nicoletta Bloise, che in questo ultimo semestre mi hanno accompagnato in questa esperienza e con cui ho lavorato giorno e notte al fine di ottenere un ottimo lavoro. Vi ringrazio per l'atmosfera di sana collaborazione creatasi fin dall'inizio e per gli aiuti e gli utili consigli che mi avete dato. In particolare, vorrei ringraziare la professoressa Capello per avermi fatto appassionare al suo campo, per l'opportunità ricevuta e per il costante supporto sia morale che professionale, per la passione, la disponibilità e la pazienza dimostrata nei miei confronti in un periodo molto difficile e stressante. Vorrei ancora ringraziare l'ingegner Sabrina Dionisio per avermi dato l'opportunità di lavorare e di stare a contatto con lei e i suoi collaboratori, che tanto hanno contributo affinché questi risultati venissero raggiunti. Grazie a tutti per l'esperienza che avete condiviso con me e di cui farò tesoro per ciò che verrà. Inoltre, vorrei ringraziare i miei familiari, fra cui Salvatore, mio padre, Anna, mia madre e mio fratello, Maurizio. Grazie per aver creduto in me sin dal quando ero bambino e di essermi stati accanto nei momenti difficili, che mi hanno permesso di diventare la persona che sono e di cui spero possiate essere orgogliosi. Senza di voi e senza i vostri sacrifici niente di tutto ciò sarebbe stato possibile, a testimonianza del fatto che la forza in ciò che si fa viene dalle persone che si amano. Tutto questo è anche un vostro risultato.

Contents

List of Tables

List of Figures

Chapter 1

Introduction

The main focus of this thesis is the analysis and study of a control system for the Laser Interferometer Space Antenna (LISA), which is an in-space mission under development by the European Space Agency (ESA) with a launch date in 2034 and an estimated lifetime of five years.

It will be a space observatory complementary to the existing Virgo and LIGO, the two others terrestrial observatories with the goal to test Einstein's theory of gravity, through the detection of the gravitational waves, which are distorsion of space-time travelling with a waves shape at the speed of light, from different sources such as compact binary systems of neutron stars or mergers of supermassive black holes, which involve huge masses and related gravitational strong interactions and effects (Amaro-Seoane et al., 2017, Moore, Gerosa, and Klein, 2019). The mission will be constituted by three satellites in a equilateral triangle formation which have to be kept with a side length of $2.5x10^6 km$ in their own orbital plane with an inclination about 60 *degrees* relative to the ecliptic plane. The constellation will be on a heliocentric orbit at $1AU$ from the CoM of the Sun, following the Earth orbit with a phase angle of 20 *degrees*. Each one of the three spacecrafts will have, as on-board sensing instrumentation, two Optical Assembly (OA) composed by a telescope, an optical bench for the laser interferometer and a cage which houses a cubic Test Mass (TM) controlled through electrostatic suspension. These latter together constitute the Gravitational Reference Sensor (GRS). On each spacecrafts there will be two TMs, with the properties of $46mm$, roughly $2kg$ and gold-coating of gold/platinum, will be equipped as sensors and they must be kept fixed to their own cages center in free fall conditions for scientific operation purposes. The Drag Free and Attitude Control System (DFACS)

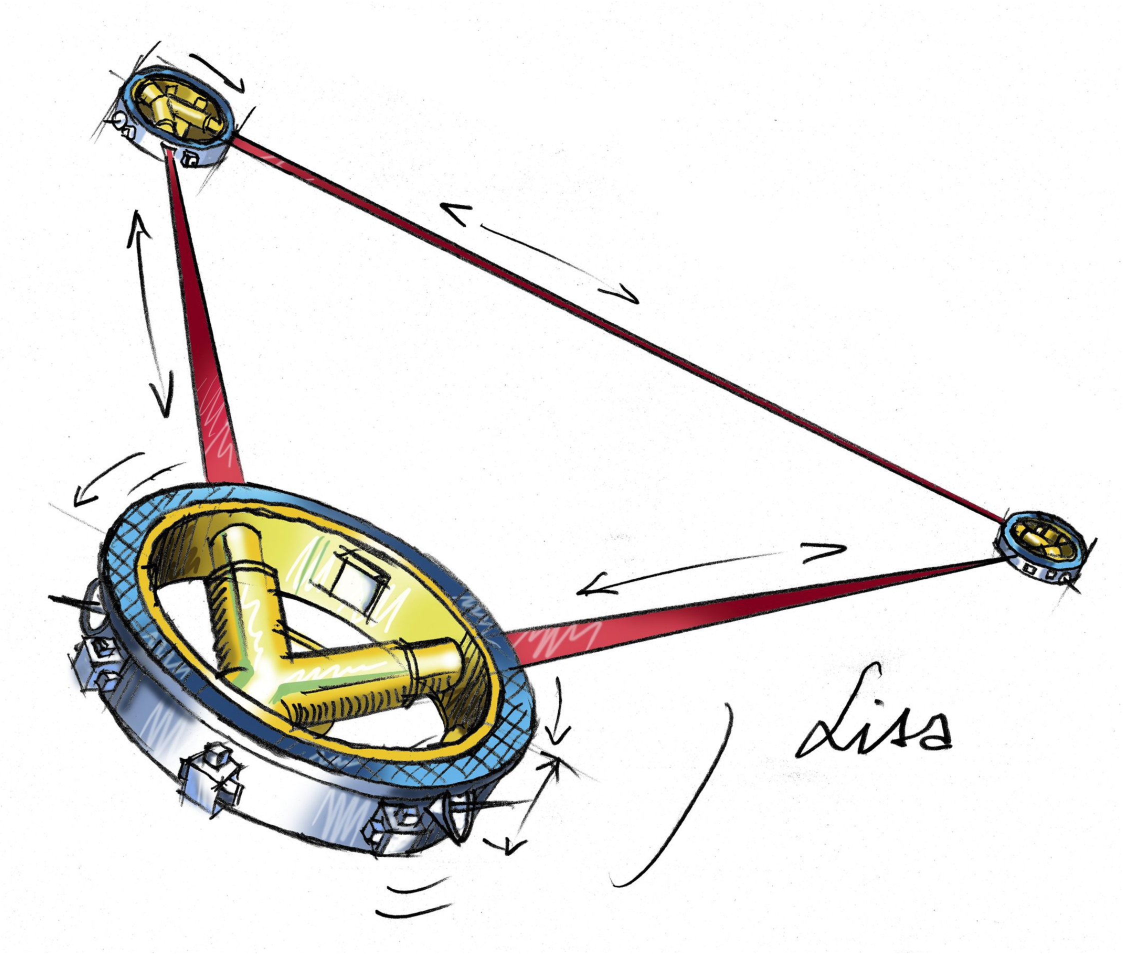

Figure 1.1. LISA Mission Concept

will control all the 15 Degrees of Freedom (DoF) in the way to counteract any external disturbance, which could interact with the TMs and the inertial sensors, with a residual acceleration less than $3x10^{-14} m/s^2/\sqrt{Hz}$ over the frequency bandwidth of 1 to $30mHz$. The measurements will be done in respect of the differential variations in the length of the OAs arms, pointed from one to the other two satellites, on which the TMs are kept fixed and are sensed by the laser interferometers, which are sensitive to low frequency gravitational signals in a range between $0.2mHz$ and $1Hz$.

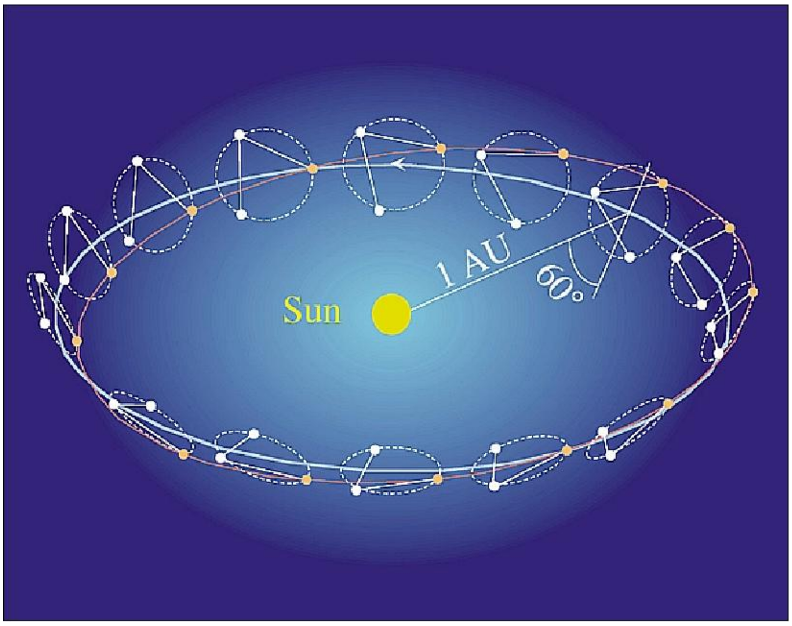

Figure 1.2. LISA Mission Configuration

The technologies which will be on LISA constellation such as inertial sensors, optical metrology system, micro-propulsion cold gas thruster, the electrostatic suspension and the performance of DFACS and TMs control, in this case, about the TMs release were tested in the previous LISA Pathfinder mission (Montemurro et al., 2006, Antonucci et al., 2012). The reference values, constraints and performance requirements used for this work are taken from the available reports of LISA Pathfinder and given by ESA, (Schleicher et al., 2018).

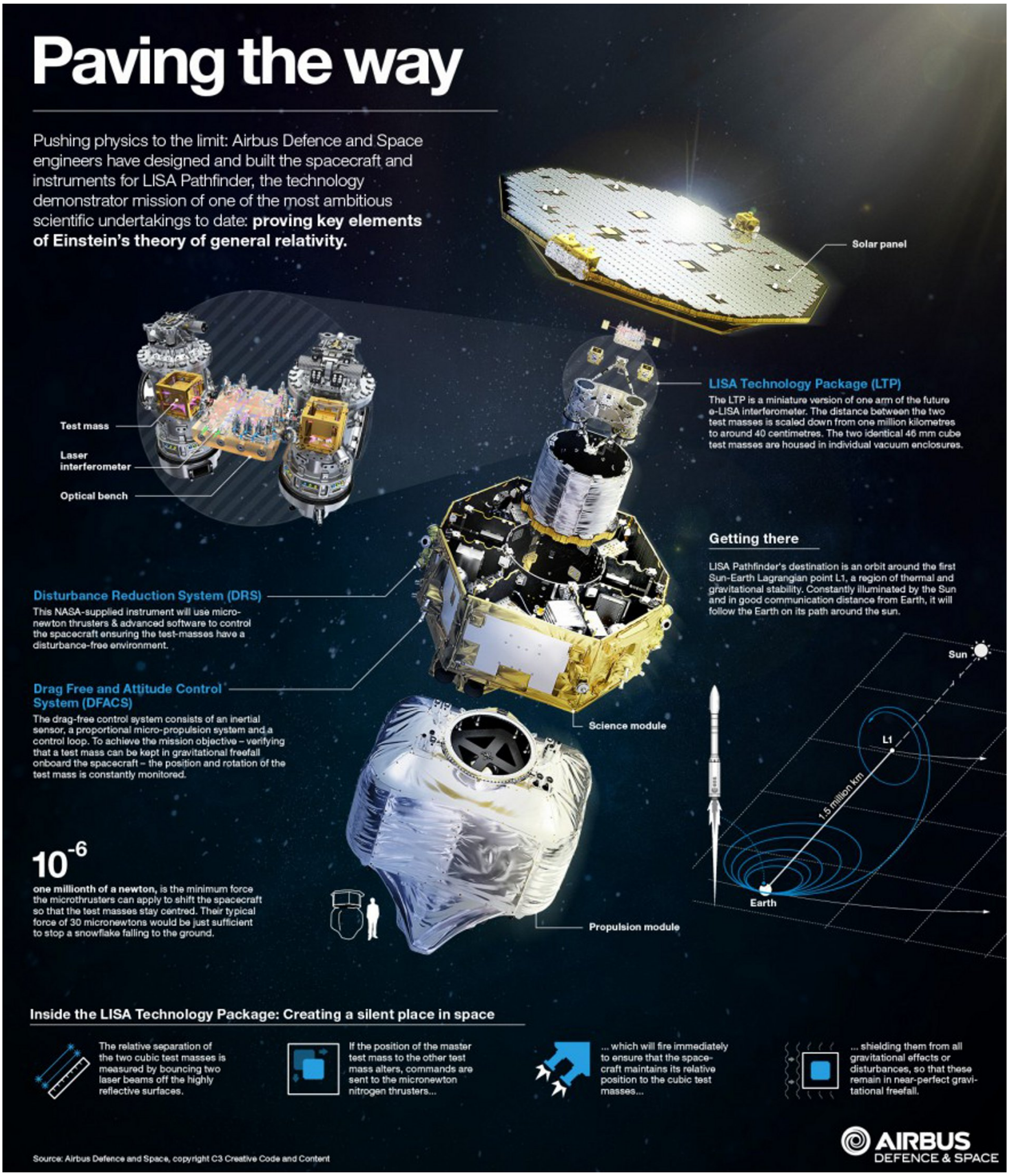

Figure 1.3. LISA Pathfinder equipment

1.1 Work objectives

The focus of this work is the TM release phase. This one is an in-orbit operation in which the TMs are locked by plungers at the beginning, until they are ready to be released and controlled by a closed loop control through electrostatic actuators both for position and attitude. Then, the TMs are released by the plungers which define the initial conditions considered for this phase. After the plungers retraction, the TMs have to be robustly and precisely controlled to be kept fixed to the center of their own cages to achieve optimal initial condition for the next phase to switch to the scientific operations.

In reference of the results of the previous related mission, called LISA Pathfinder and mentioned above, had the objective to demonstrate and validate the technologies which will be applied for LISA Mission, a first order SMC controller was implemented for the TMs release phase, (Montemurro et al., 2006, Antonucci et al., 2012). The application of this kind of control could not stabilize the TMs but, as opposite, it allowed the masses to hit the inner walls of their own housing cages with a consequent diverging behaviour, which is incompatible to the scientific operations. This is the reason which led this work about the proposed application of the STW SMC and its comparison with a first order SMC control. So, the STW SMC is proposed as solution to achieve the purpose of which above and to satisfy the constraints and performance requirements given by ESA, taking into account that SMC control is widely used for the attitude and position maneuvers of spacecraft, as in (Yeh, 2010, Pukdeboon, 2011, Tiwari, Janardhanan, and Nabi, 2014, Capello, Punta, and Bartolini, 2017, Capello et al., 2017). Since the design of robust flight software plays an important role in space research, SMC techniques are well suited as they are able to guarantee stringent requirements even with parameters other than nominal ones. In this case, the critical aspect of the presented design is the strong influence caused by the environmental disturbance and noises in respect of a reduced control authority, which make a challenging design to achieve the requested performance. In the way to obtain optimal results and to make compatible the control design to the other mission phases, two operative modes named *WideRange* (WR) and *HighResolution* (HR) are implemented. These latter have a different configuration about disturbance, sensors noises, initial conditions and actuation authority. Moreover, the presented work is structured in two parts. In the first one, the STW SMC is presented and designed for the TM release phase through MATLAB/Simulink environment. A MonteCarlo campaign is performed taking into account two hundred simulations in a wide range of randomly defined critical initial conditions, noises and disturbance in reference of the bounds imposed by ESA. The performance are analyzed both for states, sliding surface and their first derivative in terms of stability, maximum overshoot, accuracy (3σ) (ESSB HB-E-003 Working Group, 2011), steady-state error and settling time. These results are consequently presented through graphics and tables to show the goodness of the proposed control keeping the control performance within ESA requirements and to show the suitability with this kind of space applications. In the second part, a comparison in terms of performance of a first order controller in respect of the STW SMC mentioned above, in the way to highlight their own different properties, to validate and to justify the design of the second order controller designed and presented in this work. So, the MonteCarlo simulations take into account the comparisons between the two control strategies and their different performance in terms of critical initial conditions and critical disturbance variation.

1.2 Overview of the thesis

This thesis is structured in five chapters. In the Chapter 1 is given an overview of LISA mission about its main objectives, about its configurations in terms of the technologies implemented and the operative phases, such as the TMs release phase which is the main subject of study in this work. It is also given a description about the reasons and the main objectives of this document in reference of the previous reports about LISA Pathfinder mission. The second Chapter 2 deeply describes the operative configuration of the simulation environment about the operative modes defined and simulation architecture in terms of the adopted models of the environmental disturbance and noises, sensors and actuators. The mathematical model, which is included in the simulation architecture in the plant block, is defined in a detailed way in the Chapter 3. This latter shows the nonlinear dynamics for the S/Cs and TMs and the description of the adopted reference frames. The Chapter 4 is focused on the SMC control theory in general and its main properties. As the same, the two control strategies are described about the first order SMC and STW SMC and their own implementation on the LISA mission. In the Chapter 5 are described the MonteCarlo campaign and the evaluation criteria used for the performance analysis. These latter take into account the first order SMC and the STW SMC results which include the validation campaign for LISA mission, about the comparison between the two control strategies and performance analysis for a disturbance evaluation. In the end, the Chapter 6 includes the conclusions about the obtained results of this work and possible future developments in reference of the tips which could be carried out from this thesis.

Chapter 2

Simulation environment

This chapter has the purpose to describe in a detailed way the two operative modes, mentioned in the Chapter 1 as WR and HR modes, modeled for the control design. Moreover, is presented the architecture of the simulation environment about its fundamental components and considered variables. In the end, the environment disturbance and sensors noises, of which the S/Cs and TMs are affected, are modeled and described to be similar to the real environment configuration expected for LISA mission. In the following, a brief list of noises and disturbance involved is given as introduction.

- Direct internal disturbance
- GRS sensor noises
- GRS actuation noises
- Self gravity (SG) and stiffness disturbance
- Solar pressure

2.1 Operative configuration

As previously mentioned, the TMs release phase is modeled to be split in two operative modes which have different disturbance and noises configuration in reference of their requirements.

The WR mode has the purpose, after the release of the TMs from the plungers, which defines the initial conditions, to capture, to stabilize and to keep precisely fixed the TMs to the center of their own cages in the way to reach a smaller steady-state error and obtain optimal initial conditions to switch to the HR mode. In addition, the maximum overshoot for position DoF is fundamental to not allow the masses to hit the cages inner walls to prevent diverging behaviours, possible structural damages or scratches which could distort the lasers measurements. In this case, the actuation authority given by the electrostatic suspension, which is the Gravitational Reference Sensor (GRS) actuation, is strong enough to counteract the challenging environment:

- GRS actuation force authority: $\simeq 10^{-6}N$
- GRS actuation torque authority: $\simeq 10^{-8}Nm$

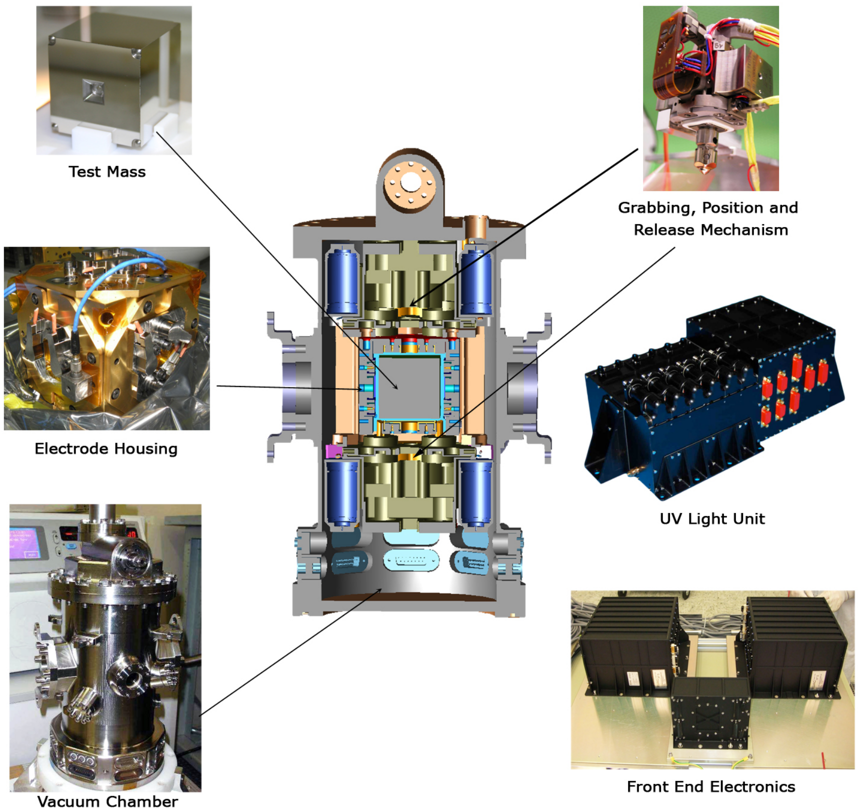

Figure 2.1. Inertial Sensor Subsystem

The HR mode has the purpose to improve the performance, mostly in terms of accuracy (3σ) and converging time, within ESA requirements, to achieve optimal initial conditions requested to switch to the science mode operations, which is the main LISA phase where the detection of the gravitational waves take place. So, the TMs release phase is the most challenging in terms of control design because of the reduced control authority wrt disturbance and noises values, which are comparable to the maximum actuation authority. As following are given the order of magnitude of the GRS actuation:

- GRS actuation force authority: $\simeq 10^{-9} N$
- GRS actuation torque authority: $\simeq 10^{-11} Nm$

2.2 Simulation architecture

In this section is given a simplified block diagram of the simulation environment of which in the Fig.2.1.

This is the DFACS simulation environment which consists in a MATLAB/Simlink model composed by five fundamental blocks. The plant block contains the S/C and TMs dynamics described in the following Chapter 3 but also their coupling with the optical assembly. The S/C and TMs forces and torques are taken as input and elaborated through the implemented dynamics, giving the following parameters as outputs:

- *TMs DoF* are given by the nonlinear dynamics are constituted by the linear, angular positions and velocities.
- *S/C attitude* defines the angular rotations in terms of quaternions.

The actuators block takes as input the digital control commands both for S/C and TMs which are elaborated through the actuators dynamics to obtain the effective actuation in reference of the maximum available effort, applied through saturation blocks. The output parameters are now described:

- F_{GRS} is a vector identifying the GRS actuation force.
- T_{GRS} is a vector identifying the GRS actuation torque.
- F_{MPS} is a vector identifying the actuation force of the Micro Propulsion System (MPS) which is the actuator system allowed to control the S/C attitude in the TM release phase.

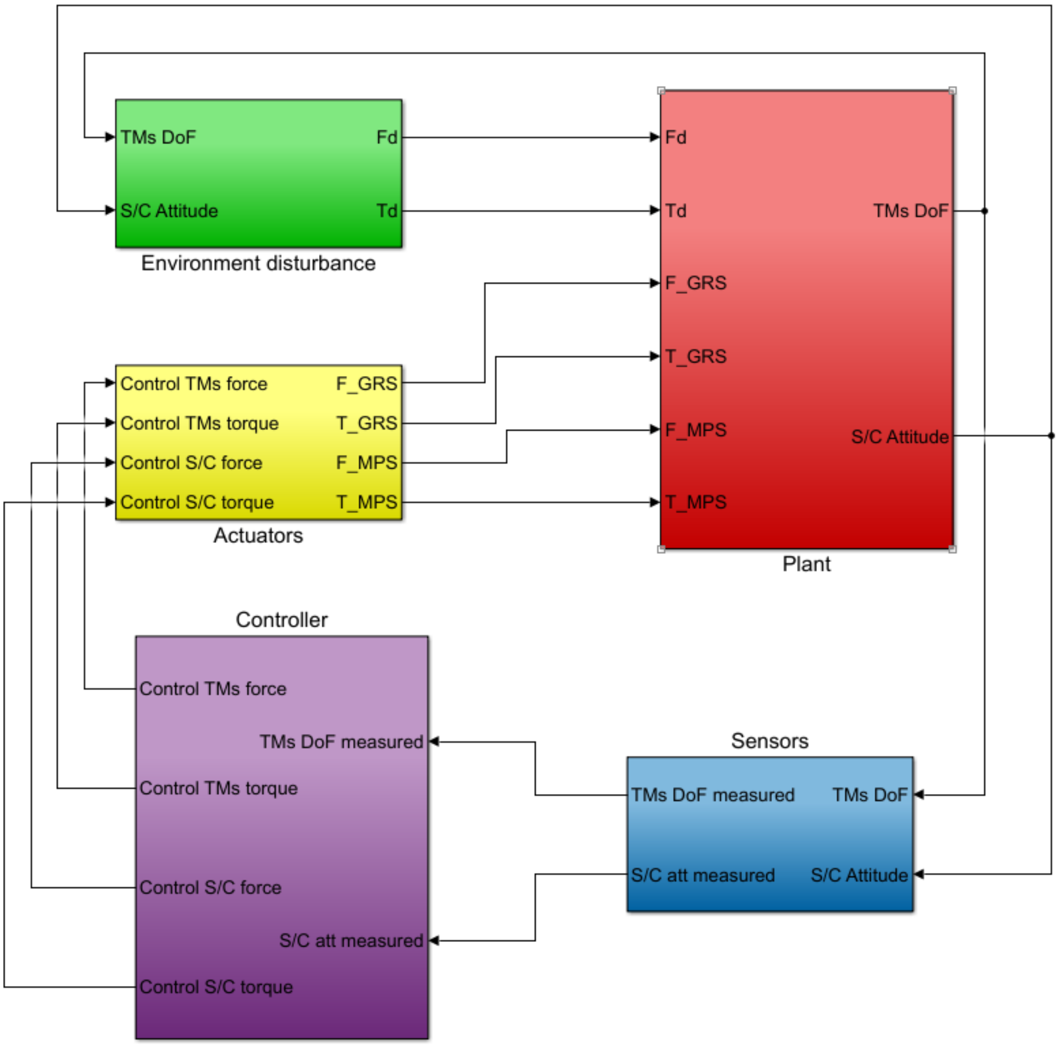

Figure 2.2. STW SMC simulation architecture

- T_{MPS} is a vector identifying the MPS actuation torque.

The disturbance block takes into account the environmental noises and disturbance, both for position and attitude, better described in this chapter. The output parameters are:

- F_d is a vector identifying the disturbance and noises forces in respect of their own model.
- T_d is a vector identifying the disturbance and noises torques in respect of their own model.

The controller block contains the control architecture in which the control algorithm is implemented in reference of the desired values. The desired and actual positions and attitude angles are needed for the definition of the sliding manifold. The Proportional, Integrative and Derivative (PID) controller is also considered for the S/C attitude control but it is not explained in this work. The control output commands are evaluated taking as input parameters the measured TMs DoF and S/C attitude.

- $Control\ TMs\ force$ is evaluated through the STW algorithm, in reference of the measured TMs DoF, and it is obtained to be evaluated after through the implemented actuation dynamics.
- $Control\ TMs\ torque$ is evaluated through the STW algorithm as the same for the control TMs force.
- $Control\ S/C\ force$ is evaluated through the PID algorithm in reference of the S/C dynamics and it is needed to counteract the solar pressure.
- $Control\ S/C\ torque$ is evaluated through the PID controller in reference of the S/C dynamics and it is needed to counteract the solar pressure.

The sensors block contains the noise shape blocks, saturation and filters about the GRS sensors for the TMs position and attitude, and the Star Tracker (STR) for the sensing of the S/C attitude. It takes as input the TMs DoF and S/C attitude as reference and which have to be compared with the sensed motion to give in output the following parameters:

- $TMs\ DoF\ measured$ given by the GRS sensors for both position and attitude.
- $S/C\ attitude$ given by the STR.

2.3 Disturbance and noises

In the simulation environment, external disturbance and sensor noises are affecting the S/Cs and masses in the TMs release phase, and they are modeled as follows. In the micro-gravity environment the self gravity is considered as disturbance exerted by the external components of the S/C on the TMs. This disturbance is composed by the sum of three components:

- Static self gravity, taking into account the mean distance between the S/C and TMs CoM.
- Self gravity fluctuations generated by thermoelastic deformation.
- Self gravity gradient due to the TMs, OAs and S/C relative motion.

The self gravity disturbance is assumed to be about 50% of the maximum actuation authority both for position and attitude, which are different in the WR and HR mode, as in (Merkowitz et al., 2005).

To model the self gravity gradient cross-coupling effects to the DoF of the TMs, a stiffness matrix is modeled according to the Hook's law.

$$\mathbf{F}_{TT} = STT\mathbf{r}_M \quad \mathbf{F}_{RT} = SRT\mathbf{q}_M \quad \mathbf{M}_{TR} = STR\mathbf{r}_M \quad \mathbf{M}_{RR} = SRR\mathbf{q}_M$$

$$STT, SRT, STR, SRR \in R^{3x3}$$

With the four mentioned matrices described below.

- STT: Cross-coupling between translation components
- SRT: Cross-coupling between TM rotation and translation
- STR: Cross-coupling between TM translation and rotation
- SRR: Cross-coupling between rotation components

which defines the complete stiffness matrix:

$$K = \begin{bmatrix} STT & SRT \\ STR & SRR \end{bmatrix}$$

In order to have a diverging behaviour of the TM the forces, or torques, they have to be positive in respect of the TM motion. In this case, the matrices must be positive to have an unstable motion.
Moreover, the matrices are not constant but they can vary in a defined range of values through a random evaluation of the MonteCarlo algorithm for environment initialization.

The solar radiation pressure is an external disturbance exerted from the Sun and due to the photons emitted which interacts with the S/Cs surface through momentum exchange, generating a consequent external pressure with a magnitude dependent on the distance from the Sun and its own activity. This pressure is among the biggest disturbances which acts on the S/C and it is controlled through an outer control loop given by a PID controller, to shield the TMs and keep them in the free fall conditions. A simple model of this force could be:

$$\mathbf{F}_S = p_S(1 + K)S\mathbf{n} \tag{2.1}$$

with the following terms:

- K is the reflectivity parameter which can be included from 0 to 1;
- p_S is solar pressure which is a function of the distance from the Sun;
- $S\mathbf{n}$ is the normal surface of the S/C projected to the Sun vector;

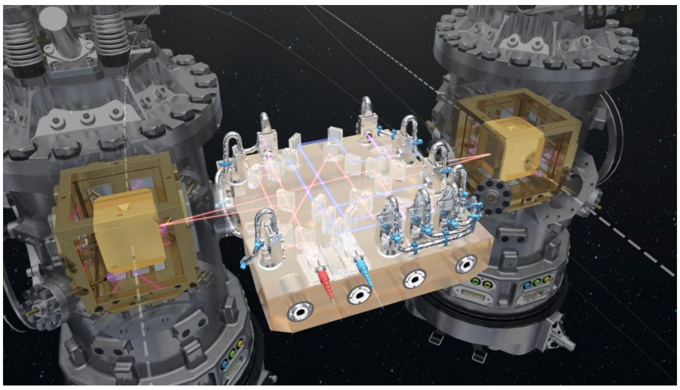

Figure 2.3. Gravitational Reference Systems

The GRS is equipped with capacitive sensors featured with six pairs of electrodes related to capacitive bridge circuits which sense variations in capacitances and are triggered by the relative motion between the TM and the electrodes themselves. An example of GRS system is given in the Fig.2.3. The combined information given by the mentioned circuits allowed to measure the three translational and three rotational DoF of the TMs. Moreover, the gaps between the electrodes and the TM are about $4mm$ that are much bigger than other similar applications, such as space accelerometers, which are typically around 100 microns. In reference of the WR and HR modes, different range of values are considered to model this noise:

- Max linear position noises (WR): $10^{-3}[m]$
- Max angular position noises (WR): $10^{-3}[rad]$
- Max linear position noises (HR): $10^{-4}[m]$
- Max angular position noises (HR): $10^{-4}[rad]$

The GRS has to provide also to the TM control through electrostatic forces and torques given by the same electrodes which are used as actuation control in the TM release phase, as mentioned above. Moreover, the actuators are affected by their own noises which are different for the WR and HR mode:

- Max linear acceleration (WR): $10^{-7}[m/s^2]$
- Max angular acceleration (WR): $10^{-5}[rad/s^2]$
- Max linear acceleration (HR): $10^{-9}[m/s^2]$
- Max angular acceleration (HR): $10^{-8}[rad/s^2]$

Chapter 3

Mathematical Model

This chapter describes the nonlinear dynamics adopted for the TMs and S/Cs in terms of position and attitude, which results from direct application of the Newton-Euler approach. Moreover, a decoupled dynamics between the two TMs is assumed.

3.1 Reference Frames

In the following the reference frame are presented for the definition of the S/Cs and TMs dynamics.

- The *Inertial frame(IF)* is centered into the Sun Center of Mass (CoM) $(\mathbf{O}_i)$. Where the axes are $\{\mathbf{I}_1, \mathbf{I}_2, \mathbf{I}_3\}$ and $\{\mathbf{I_1}, \mathbf{I_2}\}$ define the ecliptic plane of the satellites and $\mathbf{I}_3$ is normal to it, as in Figure 3.1.

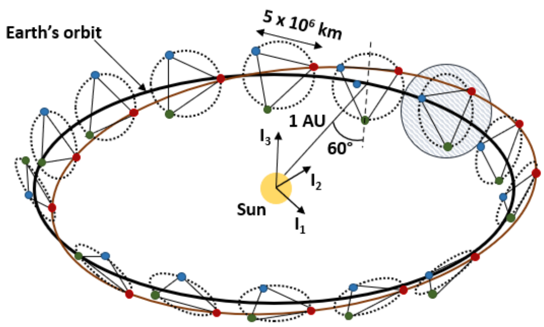

Figure 3.1. Inertial Reference Frame

- The *Local Constellation Frame (CFi)* is the target frame for the S/C attitude during the measurement of the SCI phase. It is centered to the i-th S/C CoM($_{Si}$), where (i=1,2,3). Where the axes are $\{\mathbf{c}_{1i}, \mathbf{c}_{2i}, \mathbf{c}_{3i}\}$ and $\mathbf{c}_{1i}$ is the bisector of the two constellation arms joining the S/C CoM with the CoMs of the other two S/C. $\mathbf{c}_{2i} = \mathbf{c}_{3i} \wedge \mathbf{c}_{1i}$ lies in the constellation plane.

- The *Spacecraft Frame (SFi)* is centered into the i-th spacecraft, where (i=1,2,3), S/C CoM $(\mathbf{O}_{Si})$ where the axes are $\{\mathbf{s}_{1i}, \mathbf{s}_{2i}, \mathbf{s}_{3i}\}$ and $\{\mathbf{s}_{1i}, \mathbf{s}_{2i}\}$ that define the optical plane of the telescopes and $\mathbf{s}_{3i}$ is the bisector of the two telescope optical axes, as in Figure 3.2.

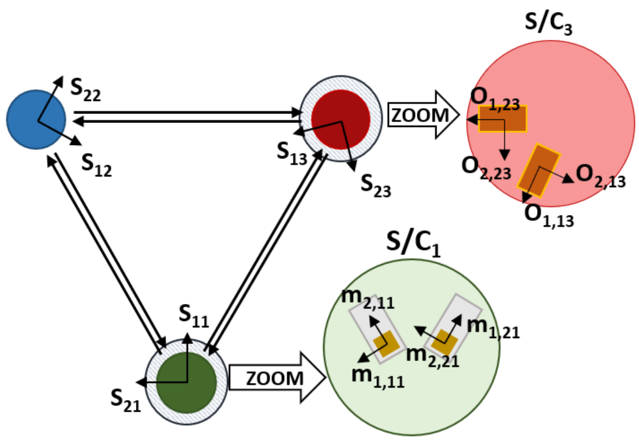

Figure 3.2. S/C, OA and TM frame

- The *Optical Assembly Frame (OFij)* centered to the OAji CoM $\mathbf{O}_{Oji}$ The axes $\{\mathbf{o}_{1ji}, \mathbf{o}_{2ji}\}$ are in the optical plane previously defined and $\mathbf{o}_{1ji}$ is the telescope optical axis. $\mathbf{o}_{3ji}$ is assumed to be perpendicular to the optical plane and thus parallel to $\mathbf{s}_{3i}$. In the real system, a displacement occurs between the two axes, and it is an uncertainty of the implemented nonlinear model. The index $i = 1,2,3$ is the S/C number and $j = 1,2$ is the OA number. The Fig.3.2 is given as reference.

- The *Test Mass Frame (MFji)* is centered to the i-th TM CoM $(\mathbf{O}_{Mji})$ on the j-th spacecraft, where the axis are $\{\mathbf{m}_{1ji}, \mathbf{m}_{1ji}, \mathbf{m}_{3ij}\}$ with $\mathbf{m}_{1ji}$ is orthogonal to the $+x$ face of the TM and $\mathbf{m}_{3ji}$ is orthogonal to the $+z$ face, as in Figure 3.2. The index $i = 1,2,3$ is the S/C number and $j = 1,2$ is the TM number in reference of the j-th OA.

3.2 Main Mathematical Models

The relevant dynamics about the S/C identifies three linear positions, for drag-free purpose only, and three angular positions, considered for attitude control against the solar pressure. Both of two are actuated through the MPS. In addition, one angle is considered between the two OA axes on each S/C.
In the following, the equations of both S/C and TM nonlinear dynamics are given. For the presented equations, the subscript "I" indicate the IF. The subscript "S" is referred to the SF. The subscript "C" is referred to the CF and the subscript "M" is related to the MF. The notation and variables of which below are completely described in a detailed way in the Appendix A and Appendix B.

- S/C translation dynamics

$$\ddot{\mathbf{r}}_I = -\mu_{\odot}\frac{\mathbf{r}_I}{|\mathbf{r}_I|^3} + m_s^{-1}T_S^I(\mathbf{F}_T + \mathbf{d}_S) - m_S^{-1}\sum_{i=1,2} T_{Oi}^I \mathbf{F}_{Ei} \tag{3.1}$$

The $\mathbf{r}_I$ is S/C position vector, $\mu_{\odot}$ is the gravitational parameter of the Sun, m_s is the S/C mass, $\mathbf{F}_T$ is vector of the actuation force of the S/C controller, $\mathbf{d}_s$ is the vector of the force disturbance acting on the S/C, $\mathbf{F}_E$ is the vector of the actuation force of the TM, the T_S^I is the rotation matrix $IF \rightarrow SF$ and T_{Oi}^I is the rotation matrix $IF \rightarrow OFi$.

- S/C rotation dynamics

$$\dot{\boldsymbol{\omega}}_{SI} = \boldsymbol{\Lambda}(\boldsymbol{\omega}_{SI}) + J_S^{-1}(\mathbf{M}_T + \mathbf{D}_S - \sum_{l=1,2}((\mathbf{b}_{Sl} + T_{Ol}^S\mathbf{b}_M) \wedge T_{Ol}^S\mathbf{F}_{El} + T_{Ol}^S\mathbf{M}_{El})) \tag{3.2}$$

$$\dot{\mathbf{q}}_{SI} = \frac{1}{2}\mathbf{q}_{SI} \otimes \boldsymbol{\omega}_{SI} \tag{3.3}$$

The $\boldsymbol{\Lambda}(...)$ defines the gyroscopic acceleration, $\dot{\omega}_{SI}$ is the angular velocity of the S/C, J_S is the inertia matrix of the S/C, $\mathbf{M}_T$ is the actuation torque of the S/C controller, $\mathbf{D}_S$ is the momentum disturbance vector acting on the S/C, $\mathbf{b}_S$ is the vector from the S/C CoM to the OA pivot,

$\mathbf{b}_M$ is the vector from the OA pivot to the cage center, $\mathbf{M}_E$ is the actuation torque given by the TM controller, T_{OI}^{S} is the rotation matrix $SF \to OFl$. In addition, is also given the S/C attitude angles in terms of quaternions, with $\mathbf{q}_{SI}$ are the S/C quaternions.

- TM translation equation

$$\ddot{\mathbf{r}}_{Mj} = T_I^{Oj}\ddot{\mathbf{r}}_{Mj}^I - \Omega_{Oj}\mathbf{r}_{Mj} - 2\boldsymbol{\omega}_{Oj} \wedge \dot{\mathbf{r}}_{Mj}, \tag{3.4}$$

In which the $\mathbf{r}_{Mj}$ is the position vector of the j-th TM, $\boldsymbol{\omega}_{Oj}$ is the angular velocity of the j-th OA, Ω_{Oj} is the skew-symmetric matrix of the j-th OA and T_I^{Oj} is the rotation matrix $OFj \;\to\; IF$.

Moreover, the TM translational dynamics $\ddot{\mathbf{r}}_{Mj}^I$ w.r.t IF, can be defined as:

$$\begin{aligned} \ddot{\mathbf{r}}_{Mj}^I &= K_\Delta \Delta \mathbf{r}_{Ij} + m_M^{-1} T_{Oj}^I (\mathbf{F}_{Ej} + \mathbf{d}_{Mj}) + \\ -m_S^{-1} T_S^I (\mathbf{F}_T + \mathbf{d}_S) &+ m_S^{-1} T_{Oj}^I \mathbf{F}_{Ej} - T_S^I \Omega_{SI} \mathbf{b}_S - T_{Oj}^I \Omega_{Oj} \mathbf{b}_M \end{aligned} \tag{3.5}$$

In which the $K_\Delta\Delta(\mathbf{r}_{Ij})$ is the gravity gradient acceleration, Ω_{SI} is the skew-symmetric matrix S/C w.r.t. IF, $\boldsymbol{d}_{Mj}$ is the force of the disturbance acting on the j-th TM and m_M is the TM mass.

- TM rotation model

$$\dot{\boldsymbol{\omega}}_{MIj} = \boldsymbol{\Lambda}(\boldsymbol{\omega}_{MIj}) + J_M^{-1}(K_{Rj}\boldsymbol{\Theta}_{Mj} + T_{Oj}^{Mj}\mathbf{M}_{Ej} + \mathbf{D}_{Mj}) \tag{3.6}$$

In which $\boldsymbol{\omega}_{MIj}$ is the j-th TM angular velocity, J_M is the inertia matrix of the TM, K_{Rj} is the j-th TM angular stiffness term, Θ_{Mj} is the j-th TM vector of the Euler angles, $\mathbf{D}_{Mj}$ is the momentum disturbance acting on the j-th TM and T_{Oj}^{Mj} is the rotation matrix $OFj \to MFj$.

$$\dot{\mathbf{q}}_{\mathbf{MIj}} = \frac{1}{2}\mathbf{q}_{MIj} \otimes \boldsymbol{\omega}_{MIj} \tag{3.7}$$

In addition, is also given the TM angular displacements in terms of quaternions, with $\mathbf{q}_{MI}$ are the TM quaternions.

Chapter 4

Design of Control Systems

4.1 Sliding Mode Control

Sliding Mode Control is a non linear control method which is characterized by a high precision and robustness against external disturbances, system noises and uncertainties given by the implemented plant model. The main key feature is the sliding manifold (σ) to reach the desired dynamics in a finite time and keep the desired trajectory.

The system dynamics both for position and rotation for each TM is fully decoupled in six Single Input Single Output (SISO) systems related to the respective DoF to be controlled. For each of these latter, the control consists at least in a single independent command input. This simplification allowed to ease the control design both for the first and second order approach.

Consider the following uncertain nonlinear control system:

$$\dot{x} = f(x,t) + u, \tag{4.1}$$

where $x \in \mathbb{R}$ is the state, $u \in \mathbb{R}$ is the control input, and $f(x,t) \in \mathbb{R}$ is a possibly uncertain, yet bounded term. The sliding variable $\sigma(x,t) \in \mathbb{R}$ is chosen for the considered system and it has relative degree one with respect to u. The sliding manifold is defined

$$\sigma(x,t) = 0, \tag{4.2}$$

which defines the desired trajectory to reach and to keep as main goal. In detail, for the position control, the components of the following vector $\overline{\sigma} =$

$[\overline{\sigma}_1, \overline{\sigma}_2, \overline{\sigma}_3] = [\sigma_x, \sigma_y, \sigma_z]^T$ are defined for the presented uncertain system which is

$$\overline{\sigma}_i = (\dot{\overline{x}}_i - \dot{\overline{x}}_{di}) + c_i(\overline{x}_i - \overline{x}_{di}), \tag{4.3}$$

where c_i is a positive constant, and for i = 1,2,3 it is referred the corresponding components of the following vectors: $\overline{\mathbf{x}} = [x_1, x_2, x_3]^T = [x, y, z]^T$ and $\dot{\overline{\mathbf{x}}} = [\dot{\overline{x}}_1, \dot{\overline{x}}_2, \dot{\overline{x}}_3]^T = [\dot{\overline{x}}, \dot{\overline{y}}, \dot{\overline{z}}]^T$ are the vectors of the TM positions and velocities, instead $\overline{\mathbf{x}}_{\mathbf{d}} = [\overline{x}_{d1}, \overline{x}_{d2}, \overline{x}_{d3}]^T = [\overline{x}_d, \overline{y}_d, \overline{z}_d]^T$ and $\dot{\overline{\mathbf{x}}}_d = [\dot{\overline{x}}_{d1}, \dot{\overline{x}}_{d2}, \dot{\overline{x}}_{d3}]^T = [\dot{\overline{x}}_d, \dot{\overline{y}}_d, \dot{\overline{z}}_d]^T$.

As the same for the attitude, the components of the vector $\tilde{\sigma} = [\tilde{\sigma}_1, \tilde{\sigma}_2, \tilde{\sigma}_3] = [\sigma_\phi, \sigma_\theta, \sigma_\psi]^T$ are defined below:

$$\tilde{\sigma}_i = (\dot{\tilde{x}}_i - \dot{\tilde{x}}_{di}) + \tilde{c}_i(\tilde{x}_i - \tilde{x}_{di}), \tag{4.4}$$

defined for the attitude, where $\tilde{c}_i$ is a positive constant, and for i = 1,2,3 it is referred the corresponding component of the following vectors: $\tilde{\mathbf{x}} = [\tilde{x}_1, \tilde{x}_2, \tilde{x}_3]^T = [\phi, \theta, \psi]^T$ and $\dot{\tilde{x}} = [\dot{\tilde{x}}_1, \dot{\tilde{x}}_2, \dot{\tilde{x}}_3]^T = [\dot{\phi}, \dot{\theta}, \dot{\psi}]^T$ are the vectors of the TM attitude and angular velocities, instead $\tilde{\mathbf{x}}_d = [\tilde{x}_{d1}, \tilde{x}_{d2}, \tilde{x}_{d3}]^T = [\phi_d, \theta_d, \psi_d]^T$ and $\dot{\mathbf{x}}_d = [\dot{\tilde{x}}_{d1}, \dot{\tilde{x}}_{d2}, \dot{\tilde{x}}_{d3}]^T = [\dot{\phi}_d, \dot{\theta}_d, \dot{\psi}_d]^T$ are the reference vectors of the desired attitude angles and angular velocities.

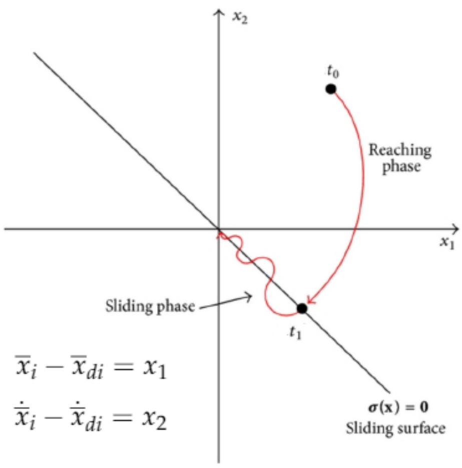

Figure 4.1. Control law - Example for position

4.2 First Order SMC

A first order SMC design is proposed as comparison with a second order STW SMC in terms of performance. The main properties of a sliding mode controller are maintained, as previously described in this chapter. Moreover, it is characterized by a discontinuous control due to its control law which assures a finite-time convergence of the sliding variables, as in (Utkin, 1992, *Sliding mode control and observation*).This design implies an actuation effort, in absolute value, always fixed to the saturation point. As consequence, the state trends are featured with a chattering phenomenon because the desired configuration is never reached in a real case due to disturbance, noises and plant imperfections and uncertainties.

In reference of the previous defined sliding surface, the design consists in the tuning of the parameter given by the following discontinuous control $u = -K\text{sgn}(\sigma)$ guarantees a convergence trend to the sliding surface σ
. As following the designed position control is presented:

$$u_i = -K_i\text{sgn}(\sigma_i),\ with\ i = 1{,}2{,}3, \tag{4.5}$$

where u_i is the control input, K_i is the control parameter and it has to be a positive constant value. For the position control, it is related to the actuation force F_{Ej}, described in the mathematical model in Chapter 3 for the j-th TM, and it is defined as the maximum actuation force

$$\overline{K}_i = F_{Ej,i_{max}}\ with\ j = 1{,}2, \tag{4.6}$$

where $F_{Ej} = [F_{Ej,1}, F_{Ej,2}, F_{Ej,3}]^T = [F_{Ej,x}, F_{Ej,y}, F_{Ej,z}]^T$ is equal to $\overline{u} = [\overline{u}_1, \overline{u}_2, \overline{u}_3]^T = [\overline{u}_x, \overline{u}_y, \overline{u}_z]^T$.

For the attitude control, instead the tuning parameter is related to the actuation torque M_{Ej}, always given in Chapter 3 for the j-th TM, and it is defined as the maximum actuation torque

$$\tilde{K}_i = M_{Ej,i_{max}} with\ j = 1{,}2, \tag{4.7}$$

where $M_{Ej} = [M_{Ej,1}, M_{Ej,2}, M_{Ej,3}]^T = [M_{Ej,\phi}, M_{Ej,\theta}, M_{Ej,\psi}]^T$ is equal to $\tilde{u} = [\tilde{u}_1, \tilde{u}_2, \tilde{u}_3]^T = [\tilde{u}_\phi, \tilde{u}_\theta, \tilde{u}_\psi]^T$.

4.3 STW SMC

The STW SMC is proposed as solution to be applied in the TM release phase because of its unique properties which allows to control robustly and precisely the TMs despite the high noises and disturbance of which above in Chapter 2. As described in (Levant, 1993, Levant, 2003; *Sliding mode control and observation*), the property of this control to be insensitive to the noises and uncertainties, given by the implemented plant, and to effectively counteract strong disturbances despite their influence higher than the actuation authority available, mostly for the HR mode, made a challenging design but one of the most suitable controller for this applications in extreme environments in reference of the strict requirements given by ESA and fundamental for the success of the scientific in-orbit operations.

The STW algorithm is a second order SMC with all the properties previously explained for the Sliding Mode Control. Moreover, this strategy allows a continuous control law and a reduction of chattering wrt a first order SMC, guaranteeing the convergence of both σ and its first derivative, as in (Levant, 1993, *Sliding mode control and observation*). The control input is defined as following

$$u = -\lambda|\sigma|^{\frac{1}{2}}\mathrm{sgn}(\sigma) + v, \tag{4.8}$$

$$\dot{v} = \begin{cases} -u, & \text{if } |u| > U_M \\ -\alpha\mathrm{sgn}(\sigma), & \text{if } |u| < U_M. \end{cases} \tag{4.9}$$

through which a finite time convergence of σ and $\dot{\sigma}$ is guaranteed. The STW control parameters λ, α and U_M are chosen to the following. Considering the dynamics:

$$\dot{\sigma} = a(x,t) + b(x,t)u \tag{4.10}$$

where $a(x,t)$ and $b(x,t)$ are unknown and are bounded by known constant as below:

$$\begin{cases} |\dot{a}| + b_M|\dot{b}| \leq C \\ 0 \leq |a| \leq a_M \\ 0 < b_m \leq b \leq b_M \\ |\frac{a_M}{b_m}| < qU_M \\ 0 < q < 1 \\ \alpha > \frac{C}{b_M} \\ \lambda > \sqrt{\frac{2}{(b_m\alpha - C)}\frac{(b_m\alpha + C)b_M(1-q)}{b_m^2(1-q)}} \end{cases} \tag{4.11}$$

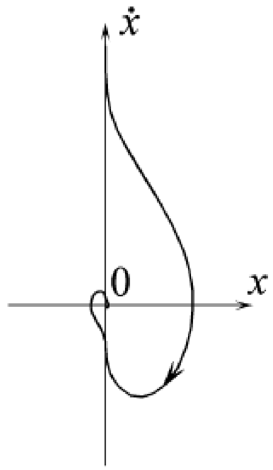

Figure 4.2. Example of the phase portrait of STW SMC

This algorithm is applied both for translation and rotation TMs dynamics. Now, considering the previously defined sliding surface, the designed position control is described:

$$\overline{u}_i = -\overline{\lambda}_i|\overline{\sigma}_i|^{\frac{1}{2}}sgn(\overline{\sigma}_i) + v \tag{4.12}$$

$$\dot{\overline{v}}_i = \begin{cases} -\overline{u}_i, & \text{if } |\overline{u}_i| > U_{Mi} \\ -\overline{\alpha}_i sgn(\overline{\sigma}_i), & \text{if } |\overline{u}_i| < U_{Mi} \end{cases} \quad for\ i = 1{,}2{,}3 \tag{4.13}$$

where $\overline{\lambda} = [\overline{\lambda}_1, \overline{\lambda}_2, \overline{\lambda}_3] = [\lambda_x, \lambda_y, \lambda_z]^T$, $\overline{\alpha} = [\overline{\alpha}_1, \overline{\alpha}_2, \overline{\alpha}_3] = [\alpha_x, \alpha_y, \alpha_z]^T$ and $\overline{U}_M = [\overline{U}_{M1}, \overline{U}_{M2}, \overline{U}_{M3}] = [U_{Mx}, U_{My}, U_{Mz}]^T$ which depend on the bounds on the system uncertain dynamics according to the conditions reported above. The input control $\overline{u} = [\overline{u}_1, \overline{u}_2, \overline{u}_3] = [u_x, u_y, u_z]^T$ has as main function to bring the control surface $\overline{\sigma}$ and its first derivative $\dot{\overline{\sigma}}$ to zero.

In a similar way, for the designed attitude control,

$$\tilde{u}_i = -\tilde{\lambda}_i |\tilde{\sigma}_i|^{\frac{1}{2}} \mathrm{sgn}(\tilde{\sigma}_i) + v \tag{4.14}$$

$$\dot{\tilde{v}}_i = \begin{cases} -\tilde{u}_i, & \text{if } |\tilde{u}_i| > U_{Mi} \\ -\tilde{\alpha}_i \mathrm{sgn}(\tilde{\sigma}_i), & \text{if } |\tilde{u}_i| < U_{Mi} \end{cases} \quad for\ i = 1,2,3 \tag{4.15}$$

where $\tilde{\lambda} = [\tilde{\lambda}_1, \tilde{\lambda}_2, \tilde{\lambda}_3] = [\lambda_\phi, \lambda_\theta, \lambda_\psi]^T$, $\tilde{\alpha} = [\tilde{\alpha}_1, \tilde{\alpha}_2, \tilde{\alpha}_3] = [\alpha_\phi, \alpha_\theta, \alpha_\psi]^T$ and $\tilde{U}_M = [\tilde{U}_{M1}, \tilde{U}_{M2}, \tilde{U}_{M3}] = [U_{M\phi}, U_{M\theta}, U_{M\psi}]^T$ which depend on the bounds on the system uncertain dynamics according to the conditions reported above. The input control $\tilde{u} = [\tilde{u}_1, \tilde{u}_2, \tilde{u}_3] = [u_\phi, u_\theta, u_\psi]^T$ has as main function to bring the control surface $\tilde{\sigma}$ and its first derivative $\dot{\tilde{\sigma}}$ to zero.

Finally, in the way to provide for ($\sigma = 0$; $\dot{\sigma} = 0$) the positions and rotations and their first derivative measurements are requested. In the implemented model, the position and rotation are measured through the GRS sensors but there is no sensing for their first derivative. This problem is overcame through the application of the discrete derivative.

Chapter 5

Simulation results

In this section are presented the results obtained through MonteCarlo campaign. In a first part the plots of two hundred runs overlapped are considered, both for the TM1 and the TM2, in the way to validate the SMC STW controller for its possible application on LISA mission for the TMs release phase. A second part describes the results obtained about one of the best run to show the effectiveness and suitability of the STW SMC control for the LISA environment and which are similar almost for the totality of the runs of the MonteCarlo campaign. In the third part are considered ten runs for a comparison between the first order SMC controller to be compared after with the STW SMC control, with the same conditions. Finally, the last part shows the results about one of the worse simulations as the SG disturbance vary, which turn out to be relevant as they are comparable to the maximum actuation authority, in order to value its effect to the TMs DoF. In the end, the results about STW SMC campaign are just given in terms of orders of magnitude in the performance analysis.

5.1 Montecarlo campaign

The MonteCarlo simulation are performed through a MATLAB/Simulink model previously described in Fig.2.2. The adopted solver is a fixed-step Runge Kutta 4 (ode4) and the simulation time is about 5000s and it is divided in 1000s for the WR mode and 4000s for HR mode. Thus, the switching time is obtained through a trade off between the possible available time for the TM release phase and the time needed by the TM control to reach the desired performance. The number of runs performed in this campaign are about two hundred for two TMs that are named Test Mass 1

(TM1) and Test Mass 2 (TM2), to evaluate the STW SMC performance. Ten simulations are performed for the comparison between the first order SMC and STW SMC control and, in the end, two simulations are considered for SG evaluations. Except for these latter, the other MonteCarlo simulations are evaluated with a SG fixed to the 50% of the maximum actuation authority. Moreover, for each run some variations are considered:

- Initial conditions, referred to the WR mode.
- Self gravity disturbance, for both forces and torques, and in terms shape and values in a defined range.
- TM stiffness, in reference of the model defined in the proper section of Chapter 2.

5.2 Performance evaluation criteria

The controller performance are evaluated taking into account the Monte-Carlo campaign outputs both for states and sliding surface. The evaluation criteria are described below. The sliding surface has no requirements given by ESA about its performance but it is a fundamental parameter to analyze in the way to define the goodness of the implemented control.

- Stability

  The stability evaluation defines the number of runs in which the states reach the convergence within a dead band interval, that is different for WR and HR mode, and in the steady-state accuracy range requirements given by ESA.

  So. it's defined a different dead band for each phase in which the run must reach the accuracy requirements to be considered as "*successful*" or "*failed*" on the other hand.

  - WR dead band = 700s of duration;
  - HR dead band = 2000s of duration, starting from 1000s which is the switching time from WR to HR.

The "$failed$" cases do not define simulations with divergent trends but it defines runs with a longer convergence time to reach the desired performance which is settled around 12000s. If a longer simulation time is considered, a 100% of success rate will be considered as stability results. For this analysis, the previously bounds, except for the accuracy, are defined independently because there are no detailed indications given by ESA.

- Steady-state accuracy

  The accuracy (3σ) performance is a statistical way to evaluate the steady-state error, that is the difference between the desired value and real value for the states when convergence trends are reached. So this analysis has to take into account the stability results because just the convergent runs could be considered. In the WR mode, the accuracy is evaluated in the last 200s and in the HR mode in the last 500s.

$$\sigma_X = \sqrt{\frac{\sum_{i=1}^{N}(x_i - \mu)^2}{N}}; \tag{5.1}$$

  In which are defined the following parameters:

  – σ_X: This is the standard deviation which is a measure of the dispersion of a set of values that are distributed on a bell shaped, or Gaussian, curve.

  – x_i: This term defines the evaluated variable, which could be about states or sliding surface parameters.

  – μ: Average value of the considered variable and calculated as the arithmetic average.

  – N: Number of converging simulation considered for this analysis in reference of the fixed simulation time and dead bands.

  In reference of the calculated σ_X, the 3σ bounds are defined as showed in the Fig.5.1 and fixed as performance evaluation criteria. In function of the σ multiplicative coefficient, three range could be set:

  – σ: It identifies the range in which there are the 68.27% of the set of values.

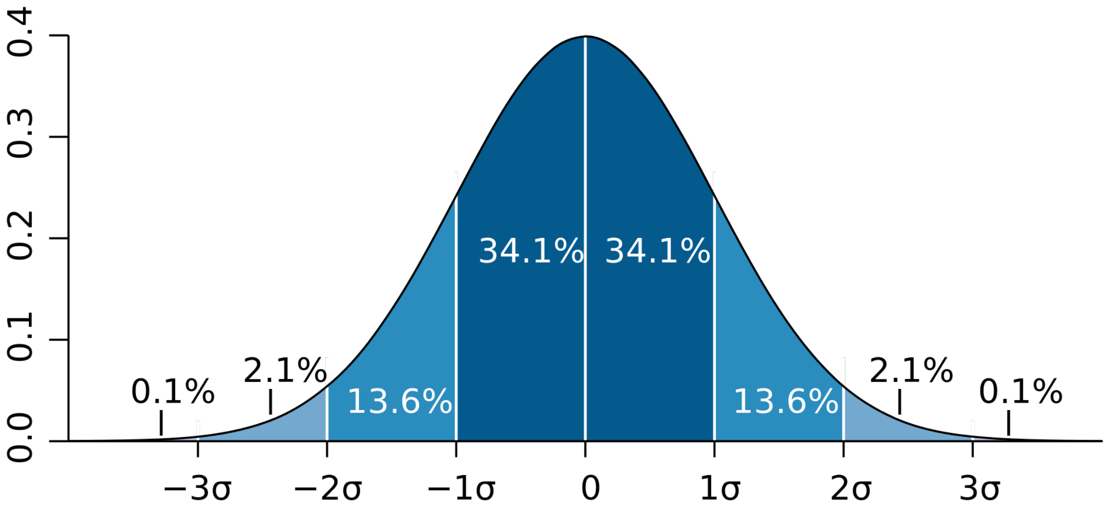

Figure 5.1. Standard distribution on a Gaussian curve

- 2σ: It identifies the range in which there are the 95.45% of the set of values.
- 3σ: It identifies the range in which there are the 99.73% of the set of values.

- Settling time

  The settling time is the time needed by each run to achieve the desired accuracy performance and to keep it for the remaining time. It is evaluated just for the successful runs. The failed runs have not a diverging behaviour but they have a longer converging time, as mentioned above. The performance analysis defines, for each mode, three time slots in which are evaluated the percentages of convergence of the considered runs.

- Maximum overshoot

  The maximum overshoot is the absolute peak reached by the states at the beginning of the WR mode and it is not just directly related to critical initial conditions but it is also a function of the environmental disturbance and noises. This analysis defines the absolute value reached by each simulation variables among the evaluated runs. This performance is fundamental for the positions displacements to know about possible collisions between the housing cages walls and the TMs.

- Input actuation

  The input actuation describes the digital commands given by the controller to the TMs actuators, both for position and attitude control. The input is saturated to the 98% of the maximum available actuation efforts to not overload the TMs actuation system. Moreover, both for forces and torques, the actuation authority is reduced of two order of magnitude switching from WR mode to HR mode.

- Chattering amplitude of the sliding surface

  The chattering is evaluated when a converging behaviour is reached by sliding variable both for translation and rotation. It is considered in the last $200s$ in WR mode and in the last $500s$ in HR mode. In terms of performance, chattering range are defined in a similar way of 3σ to establish a threshold in which the sliding variable trends can be considered convergent.

- Convergence time of the sliding surface

  The convergence time defines the time needed to the the control to reach a converging trend within the 3σ bounds calculated for WR and HR mode and which have to be kept for the remaining time. It's an optimal index to establish the goodness of the implemented control to achieve the desired values, which are to bring both σ and $\dot{\sigma}$ to zero, against the environmental disturbance and noises.

5.3 STW SMC results

In this section the MonteCarlo campaign results are showed about the STW SMC controller through the evaluation of two hundred overlapped plots. The red lines in the zoom boxes represents the ESA accuracy requirements.

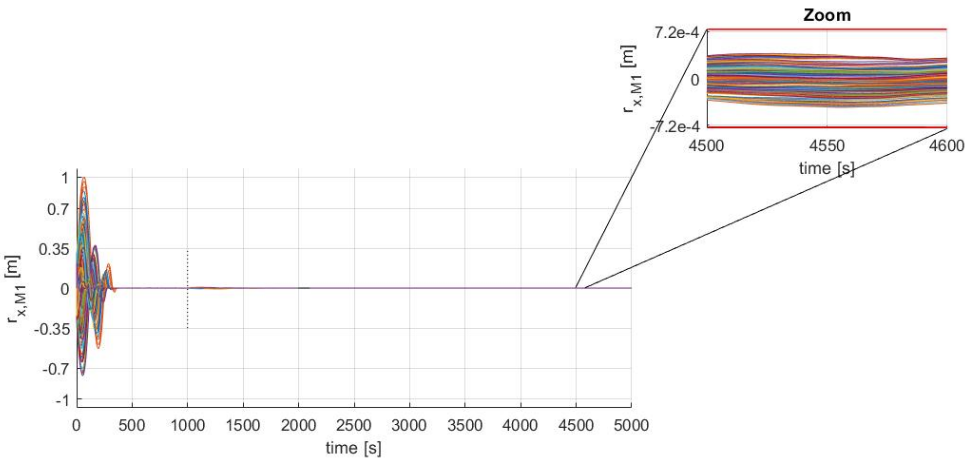

Figure 5.2. STW SMC - TM1 Linear position along X axis

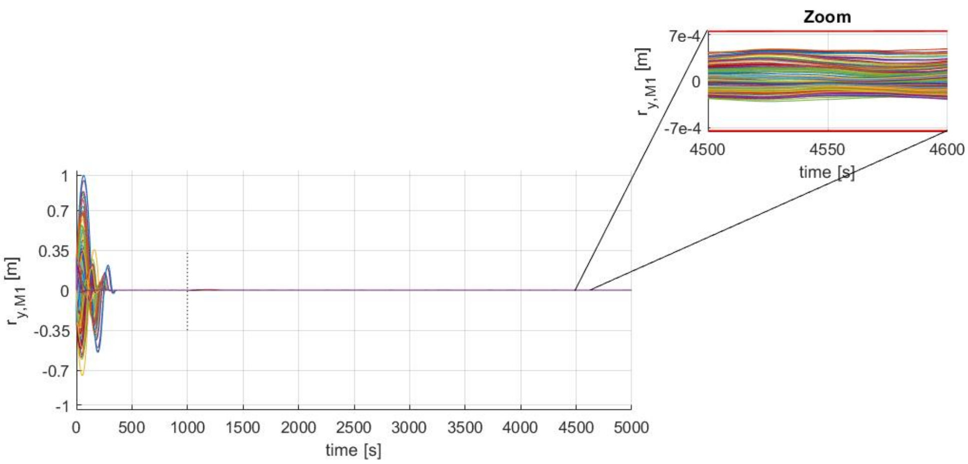

Figure 5.3. STW SMC - TM1 Linear position along Y axis

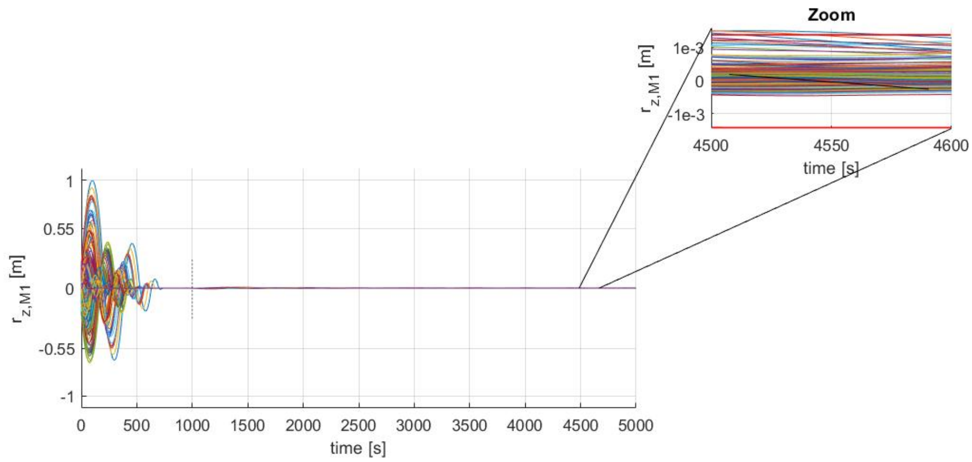

Figure 5.4. STW SMC - TM1 Linear position along Z axis

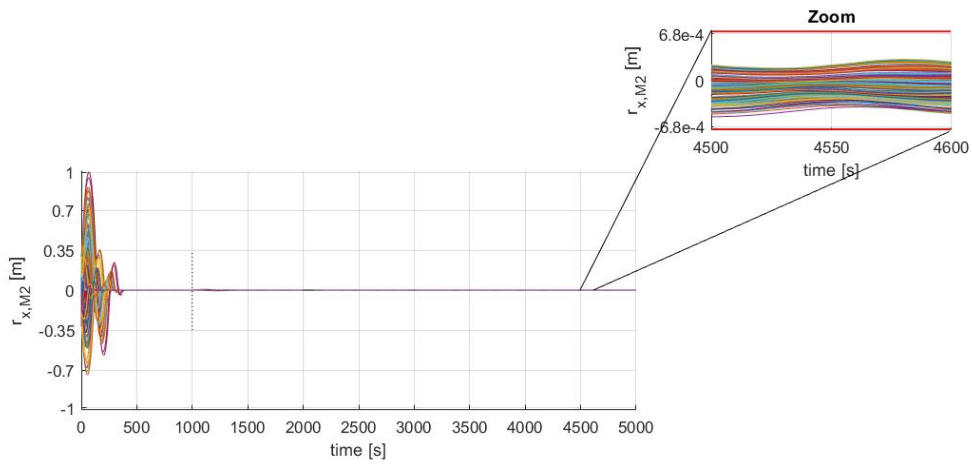

Figure 5.5. STW SMC -TM2 Linear position along X axis

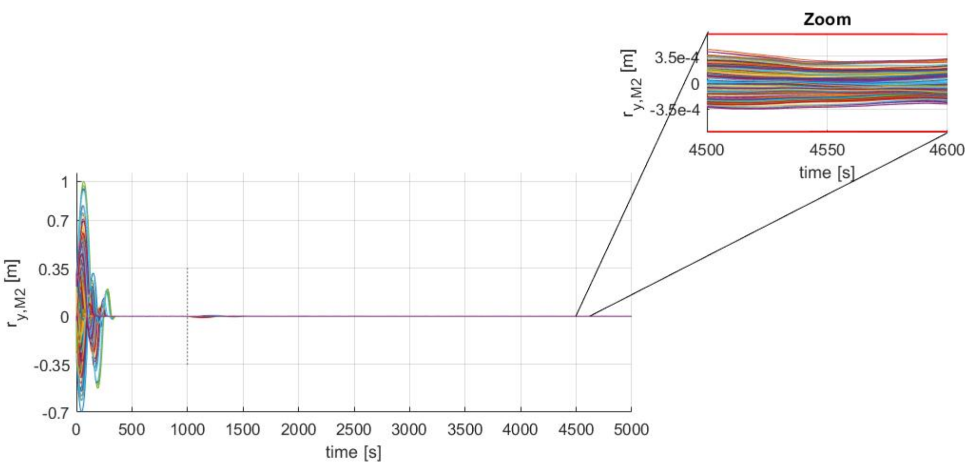

Figure 5.6. STW SMC - TM2 Linear position along Y axis

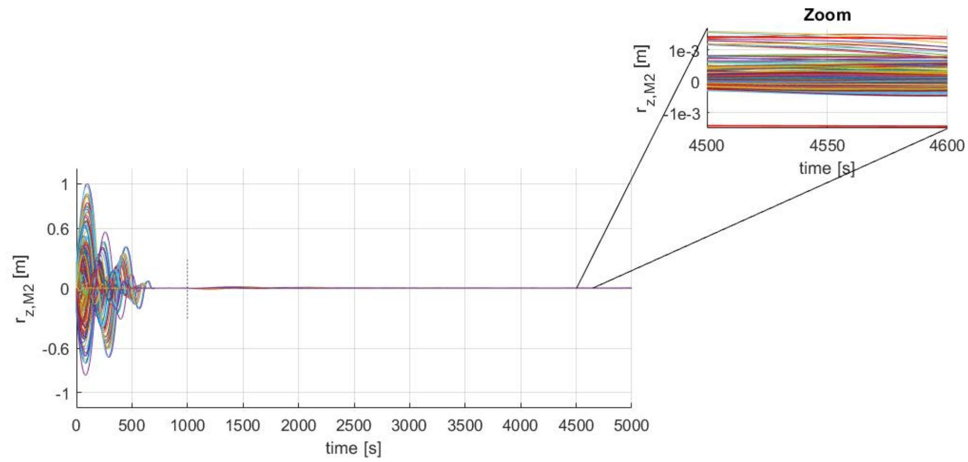

Figure 5.7. STW SMC - TM2 Linear position along Z axis

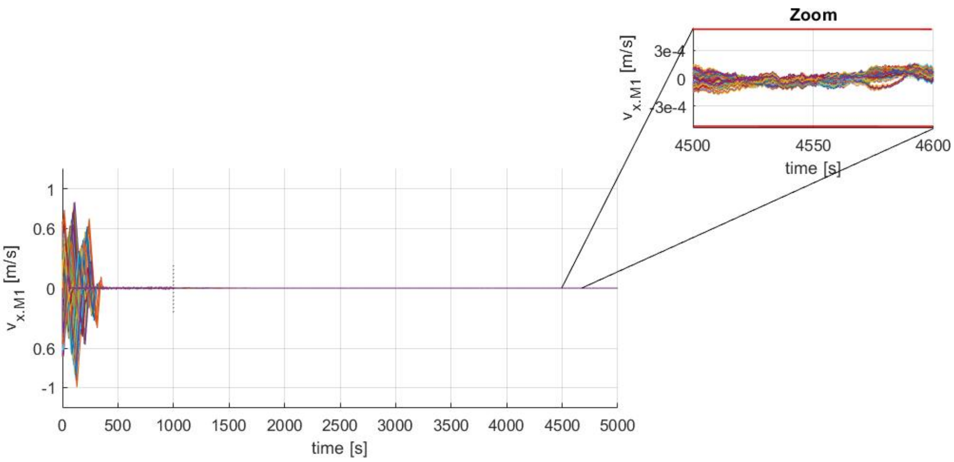

Figure 5.8. STW SMC - TM1 Linear velocity along X axis

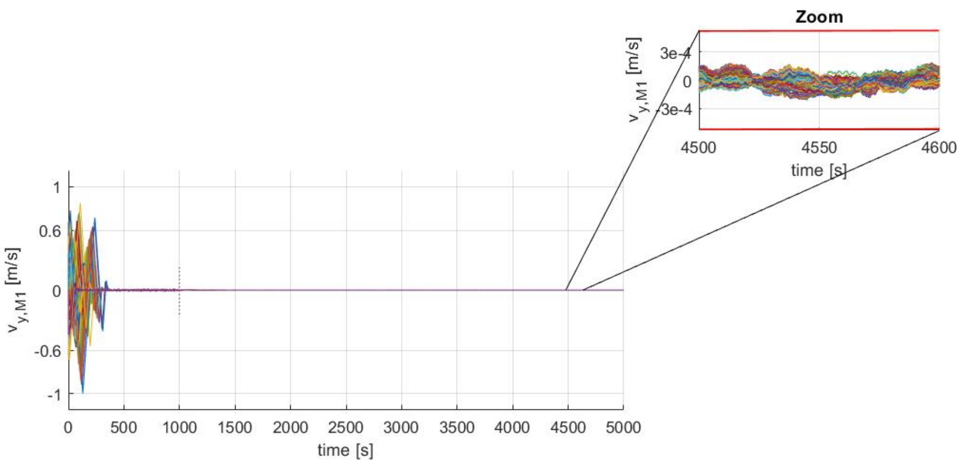

Figure 5.9. STW SMC - TM1 Linear velocity along Y axis

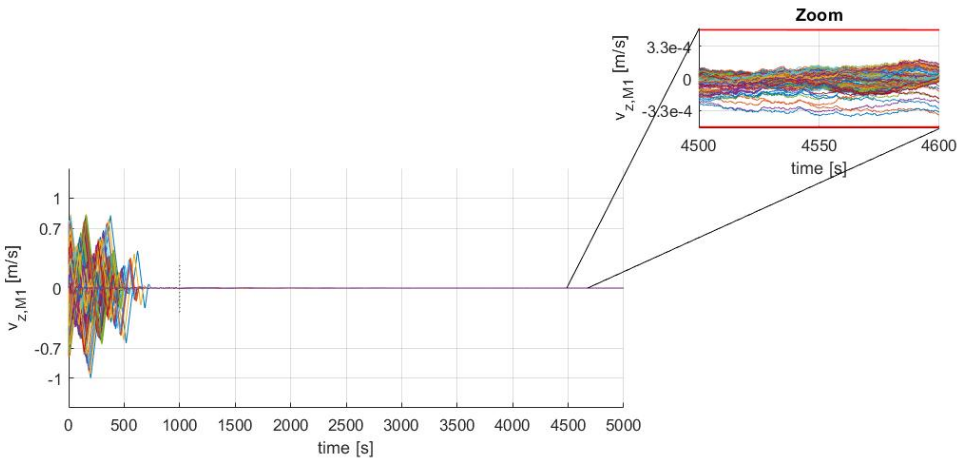

Figure 5.10. STW SMC - TM1 Linear velocity along Z axis

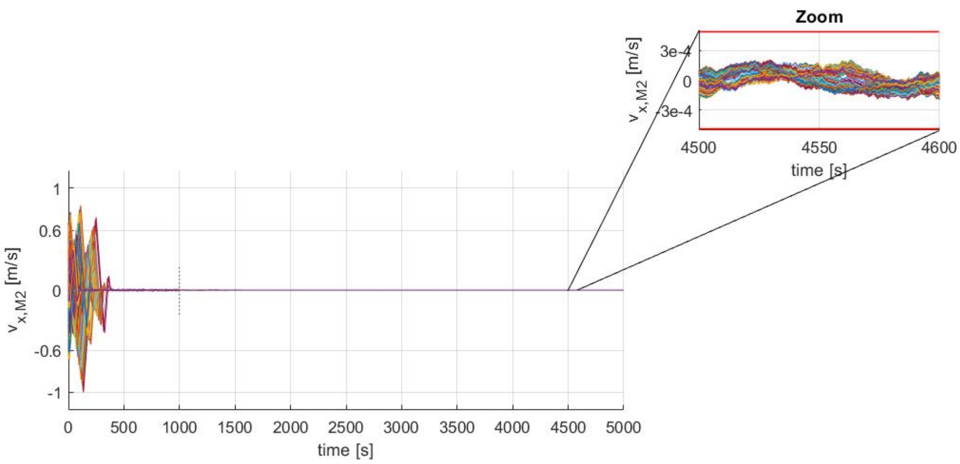

Figure 5.11. STW SMC - TM2 Linear velocity along X axis

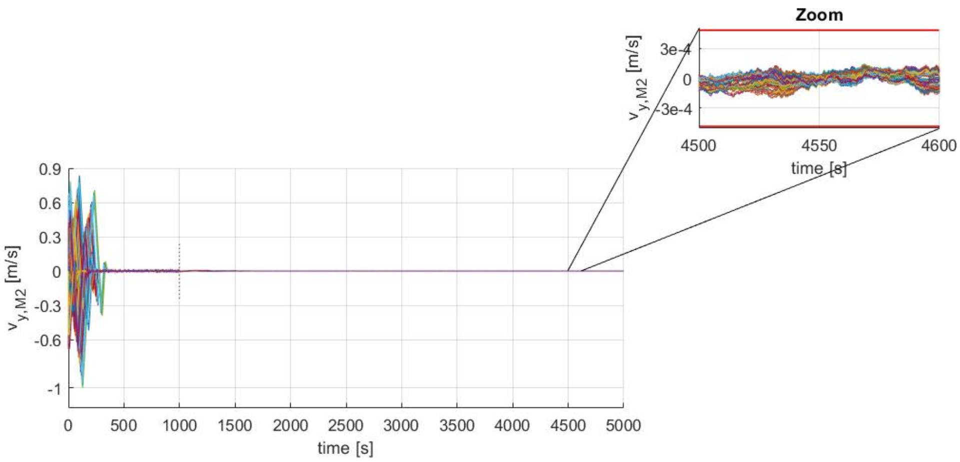

Figure 5.12. STW SMC - TM2 Linear velocity along Y axis

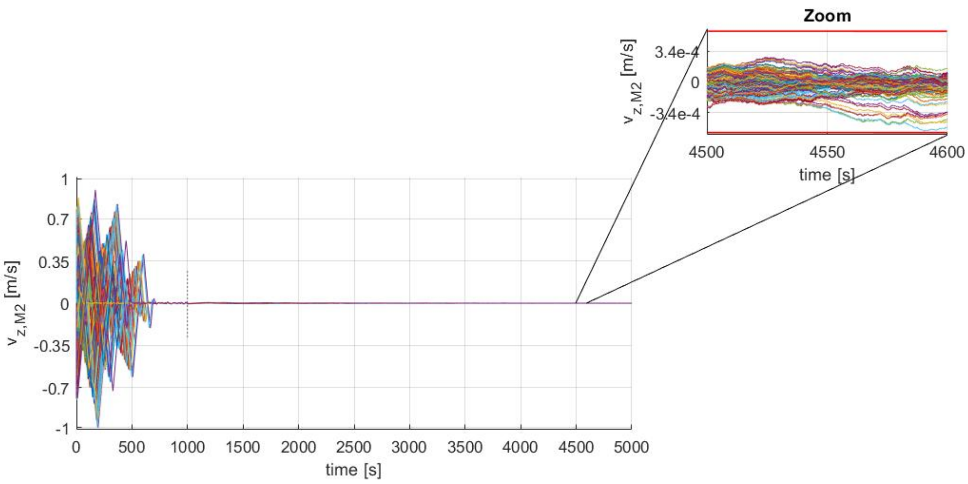

Figure 5.13. STW SMC - TM2 Linear velocity along Z axis

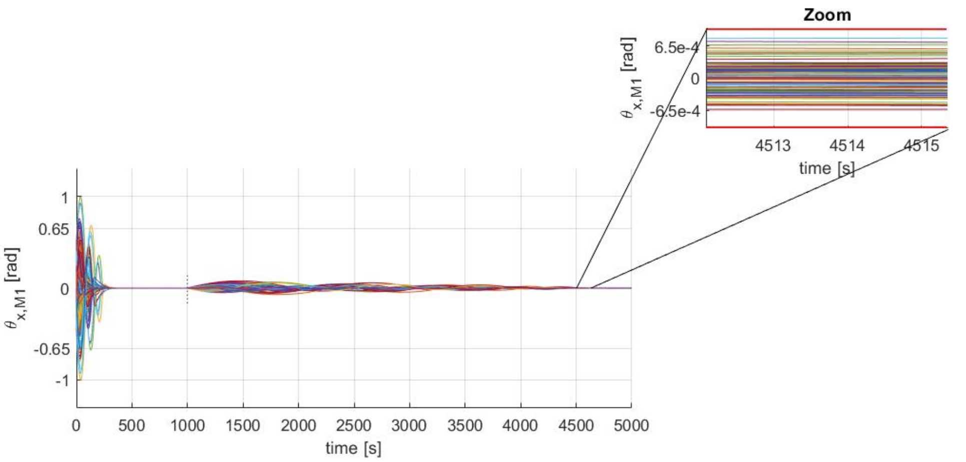

Figure 5.14. STW SMC - TM1 Angular position around X axis

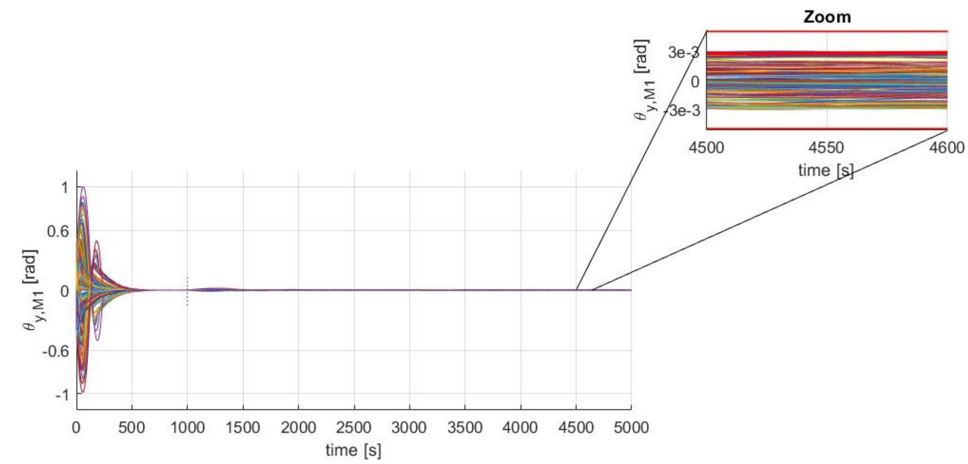

Figure 5.15. STW SMC - TM1 Angular position around Y axis

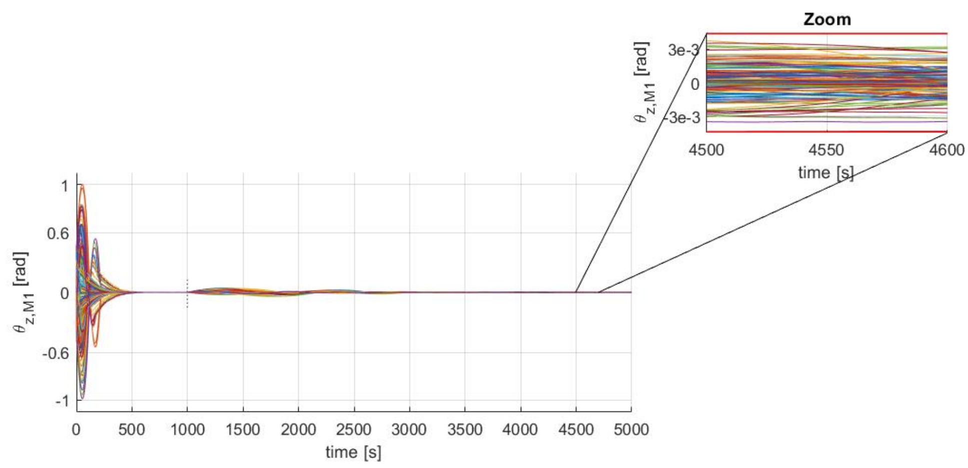

Figure 5.16. STW SMC - TM1 Angular position around Z axis

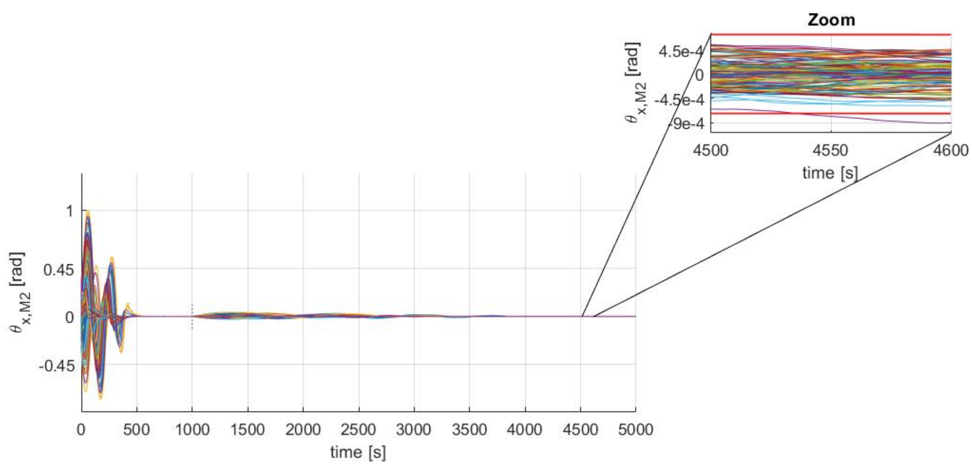

Figure 5.17. STW SMC - TM2 Angular position around X axis

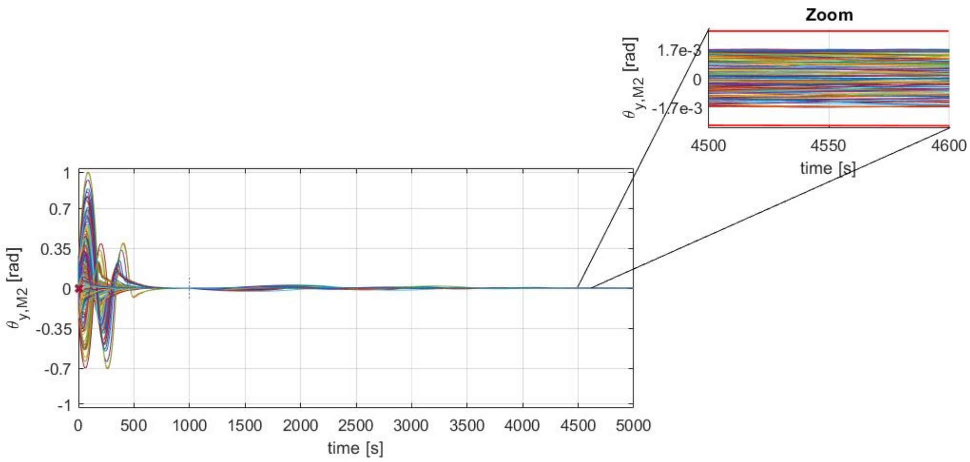

Figure 5.18. STW SMC - TM2 Angular position around Y axis

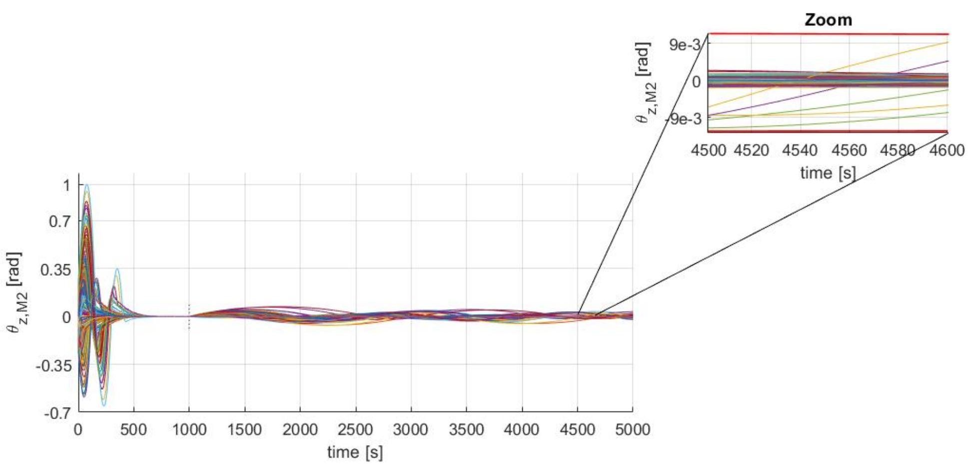

Figure 5.19. STW SMC - TM2 Angular position around Z axis

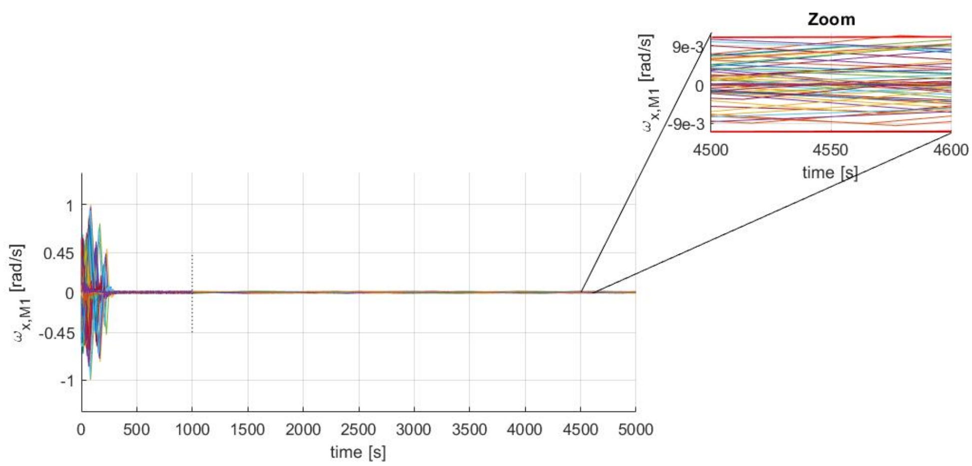

Figure 5.20. STW SMC - TM1 Angular velocity around X axis

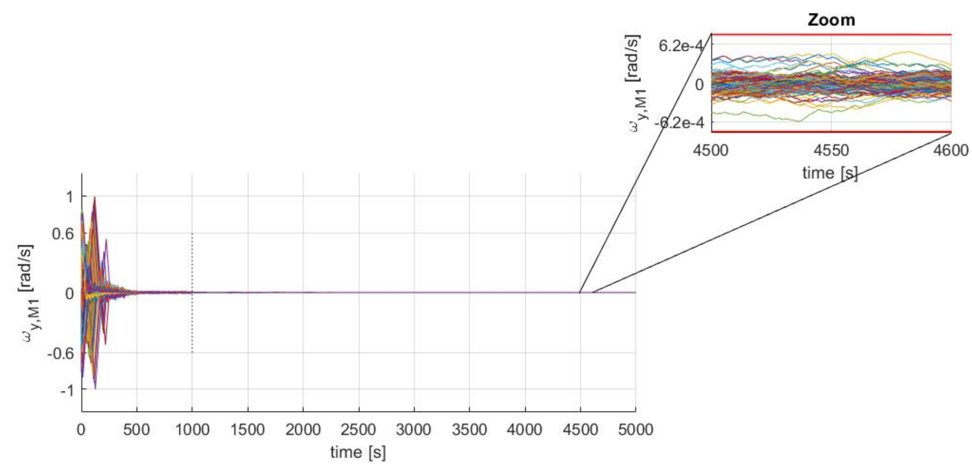

Figure 5.21. STW SMC - TM1 Angular velocity around Y axis

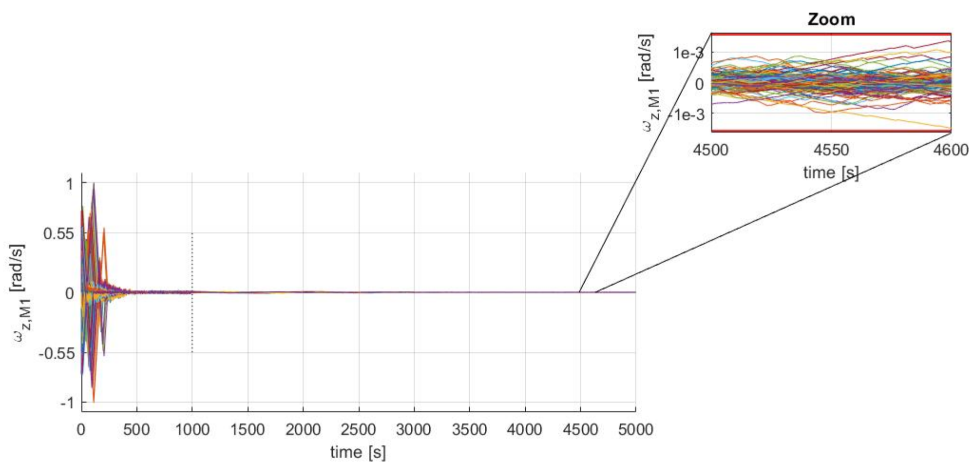

Figure 5.22. STW SMC - TM1 Angular velocity around Z axis

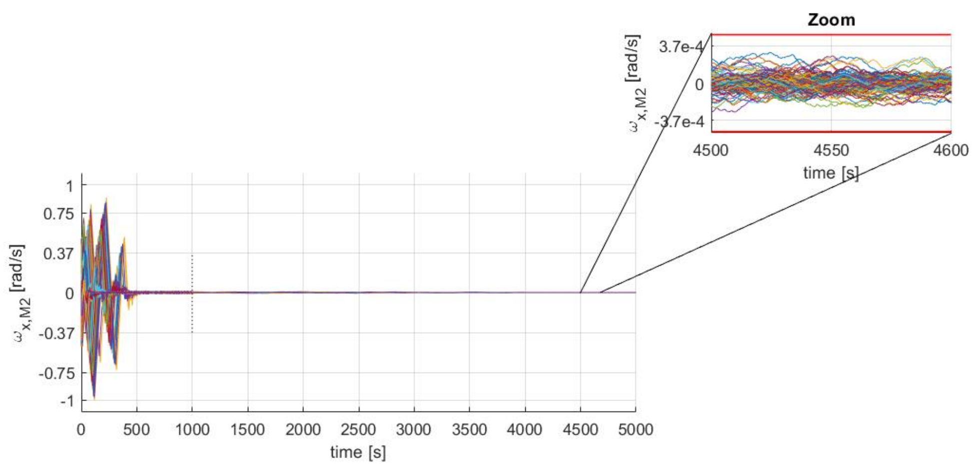

Figure 5.23. STW SMC - TM2 Angular velocity around X axis

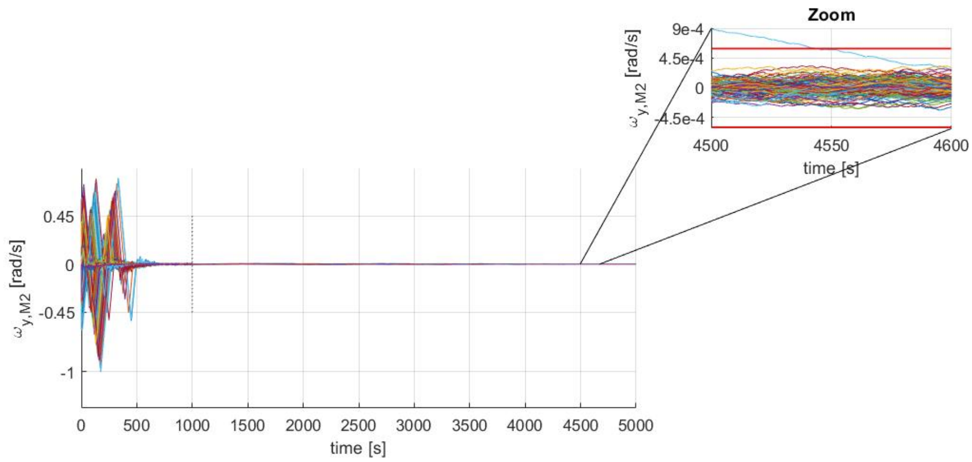

Figure 5.24. STW SMC - TM2 Angular velocity around Y axis

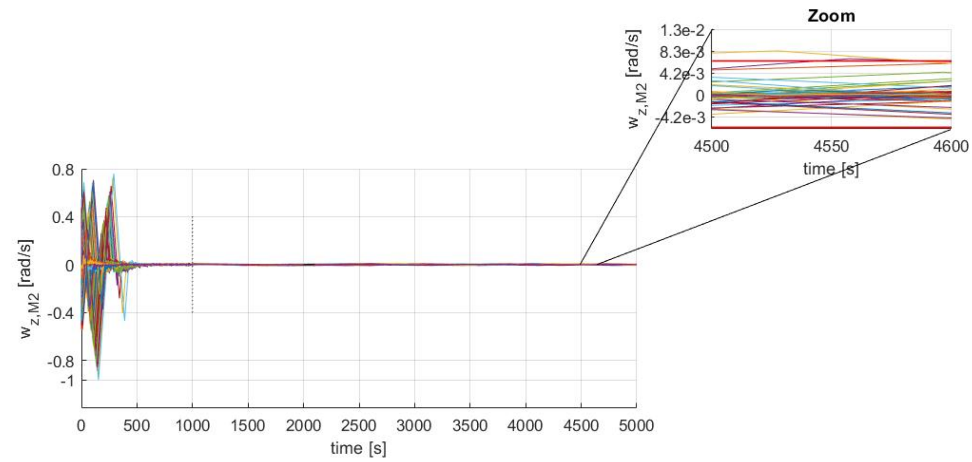

Figure 5.25. STW SMC - TM2 Angular velocity around Z axis

5.4 STW SMC - Performance analysis

This performance analysis is done to test the STW SMC control strategy designed in this work and to validate it for a possible implementation in the TMs release phase for LISA mission. All reference data are taken from the MonteCarlo campaign results for both TMs. In detail, the linear positions are showed from the Fig.5.2 to Fig.5.43; the angular displacements are from the Fig.5.14 to Fig.5.19; the linear velocities from Fig.5.11 to Fig.5.13 and, finally, the angular velocities are defined from Fig.5.20 to Fig.5.25. In terms of accuracy, as verified through the performance analysis of the MonteCarlo results, the STW SMC designed was able to counteract and to stabilize the masses against the high environmental disturbance and system noises of which in the TMs release phase. Among the two hundred runs the 100% are considered successful in the WR mode for the two TMs. The HR mode has 100% of successful runs in terms of position control and just the $6-7\%$, respectively for the TM2 and TM1, of slow converging runs about the attitude control, with a settling time needed beyond the $5000s$ fixed as simulation time to reach the accuracy requested by ESA. The similar failure rate put in evidence the symmetry in TMs behaviour both for position and control attitude. Through the settling time analysis, it can be shown that all the variables for both TMs reach the desired accuracy mostly before $200s$ in WR mode except for the attitude angles which have a settling time mostly in the second time slot. In the HR mode, the $93-98\%$ of the 200 simulations have a settling time below the $4800s$. The failed $6-7\%$ runs are not considered in the HR settling time evaluation because the time needed is around $12000s$ to achieve the desired accuracy performance. The following tables 5.1 and 5.2 precisely describes the setting time results.

Table 5.1. STW SMC performance - TM1 Settling time in WR and HR mode

	[0; 199]s	[200; 800]s	[801; 1000]s
WR	[x;y;z]	[x;y;z]	[x;y;z]
r_{M1}	[73%; 83%; 50%]	[27%; 17%; 50%]	[0%; 0%; 0%]
v_{M1}	[77.5%; 85%; 50.5%]	[22.5%; 15%; 49.5%]	[0%; 0%; 0%]
θ_{M1}	[53%; 2%; 6%]	[47%; 98%; 94%]	[0%; 0%; 0%]
ω_{M1}	[92.5%; 66.5%; 84%]	[7.5%; 33.5%; 16%]	[0%; 0%; 0%]
	[1001; 1200]s	[1201; 4800]s	[4801; 5000]s
HR	[x;y;z]	[x;y;z]	[x;y;z]
r_{M1}	[86%; 90%; 32.5%]	[14%; 10%; 65.5%]	[0%; 0%; 2%]
v_{M1}	[70.5%; 74.5%; 0%]	[29.5%; 25.5%; 100%]	[0%; 0%; 0%]
θ_{M1}	[61.5%; 92.5%; 48%]	[30.5%; 7.5%; 52%]	[8%; 0%; 0%]
ω_{M1}	[89%; 56.5%; 43%]	[11%; 43.5%; 57%]	[0%; 0%; 0%]

Table 5.2. STW SMC performance - TM2 Settling time in WR and HR mode

	[0; 199]s	[200; 800]s	[801; 1000]s
WR	[x;y;z]	[x;y;z]	[x;y;z]
r_{M1}	[74%; 82%; 46%]	[26%; 18%; 54%]	[0%; 0%; 0%]
v_{M1}	[76.5%; 84%; 46%]	[23.5%; 16%; 54%]	[0%; 0%; 0%]
θ_{M1}	[43%; 3.5%; 4%]	[57%; 94%; 96%]	[0%; 2.5%; 0%]
ω_{M1}	[77%; 46%; 67%]	[23%; 54%; 33%]	[0%; 0%; 0%]
	[1001; 1200]s	[1201; 4800]s	[4801; 5000]s
HR	[x;y;z]	[x;y;z]	[x;y;z]
r_{M1}	[71%; 50%; 6.5%]	[29%; 50%; 91.5%]	[0%; 0%; 2%]
v_{M1}	[70%; 22.5%; 0%]	[30%; 77.5%; 100%]	[0%; 0%; 0%]
θ_{M1}	[47%; 44.5%; 70.5%]	[53%; 55.5%; 22%]	[0%; 0%; 7.5%]
ω_{M1}	[36.5%; 14.5%; 83.5%]	[63.5%; 85.5%; 13%]	[0%; 0%; 3.5%]

The maximum overshoot evaluation is done just for the WR mode which is the only phase where the overshoot took place. So, both the TMs in this case have similar performance for all the simulation variables due to their symmetric behaviour. The performance analysis shows that the positions maximum absolute value reached by states among the whole amount of runs is about $1e-3\ m$ and they are not allowed to hit the inner walls of the

TMs housing cages, which is one of the strict requirements needed to assure a converging behaviour and preventing any kind of damage in a real configuration. The Table 5.3 describes the order of magnitude of the maximum overshoot in absolute value which are reached by each simulation variables:

Table 5.3. STW SMC - TMs Maximum overshoot

$TM1$	x	y	z
$r_{M1}[m]$	1e-3	1e-3	1e-3
$v_{M1}[m/s]$	1e-5	1e-5	1e-5
$\theta_{M1}[rad]$	1e-2	1e-2	1e-2
$\omega_{M1}[rad/s]$	1e-4	1e-4	1e-4
$TM2$	x	y	z
$r_{M2}[m]$	1e-3	1e-3	1e-3
$v_{M2}[m/s]$	1e-5	1e-5	1e-5
$\theta_{M2}[rad]$	1e-2	1e-2	1e-2
$\omega_{M2}[rad/s]$	1e-4	1e-4	1e-4

The accuracy evaluation, as in Table 5.4 and Table 5.5, takes into account both the WR and HR mode even if the first one has no requirements imposed by ESA. As previously mentioned in the stability analysis, for both WR and HR modes, the 100% of the whole runs, except for the angular displacements in HR mode, reach the required accuracy performance to achieve the optimal initial conditions requested to switch to the SCI operations. So for the attitude control, in the WR mode the 100% of runs reach the requested performance and in the HR mode just the $6 - 7\%$ of failing runs need a converging time around 12000s to reach the same successful results. As mentioned in the Chapter 2, these failed runs are influenced by the strongest SG disturbance and GRS noises with a magnitude similar or even greater to the maximum actuation authority and coupled with varying critical initial conditions.

Table 5.4. STW SMC - TM1 Accuracy in WR and HR mode (3σ)

WR	x	y	z
$r_{M1}[m]$	$\pm 1e-6$	$\pm 1e-6$	$\pm 1e-6$
$v_{M1}[m/s]$	$\pm 1e-6$	$\pm 1e-6$	$\pm 1e-7$
$\theta_{M1}[rad]$	$\pm 1e-5$	$\pm 1e-5$	$\pm 1e-5$
$\omega_{M1}[rad/s]$	$\pm 1e-5$	$\pm 1e-5$	$\pm 1e-5$
HR	x	y	z
$r_{M1}[m]$	$\pm 1e-6$	$\pm 1e-6$	$\pm 1e-6$
$v_{M1}[m/s]$	$\pm 1e-8$	$\pm 1e-8$	$\pm 1e-8$
$\theta_{M1}[rad]$	$\pm 1e-5$	$\pm 1e-4$	$\pm 1e-4$
$\omega_{M1}[rad/s]$	$\pm 1e-5$	$\pm 1e-7$	$\pm 1e-6$

Table 5.5. STW SMC - TM2 Accuracy in WR and HR mode (3σ)

WR	x	y	z
$r_{M2}[m]$	$\pm 1e-6$	$\pm 1e-6$	$\pm 1e-6$
$v_{M2}[m/s]$	$\pm 1e-6$	$\pm 1e-6$	$\pm 1e-7$
$\theta_{M2}[rad]$	$\pm 1e-5$	$\pm 1e-4$	$\pm 1e-5$
$\omega_{M2}[rad/s]$	$\pm 1e-5$	$\pm 1e-5$	$\pm 1e-5$
HR	x	y	z
$r_{M2}[m]$	$\pm 1e-6$	$\pm 1e-7$	$\pm 1e-6$
$v_{M2}[m/s]$	$\pm 1e-8$	$\pm 1e-8$	$\pm 1e-8$
$\theta_{M2}[rad]$	$\pm 1e-5$	$\pm 1e-4$	$\pm 1e-4$
$\omega_{M2}[rad/s]$	$\pm 1e-7$	$\pm 1e-7$	$\pm 1e-6$

In the following figures, the input actuation of one of the two thousand runs are presented for the TMs control both for position and attitude. The plots of the actuation forces and torques are scaled wrt the maximum value for each variable:

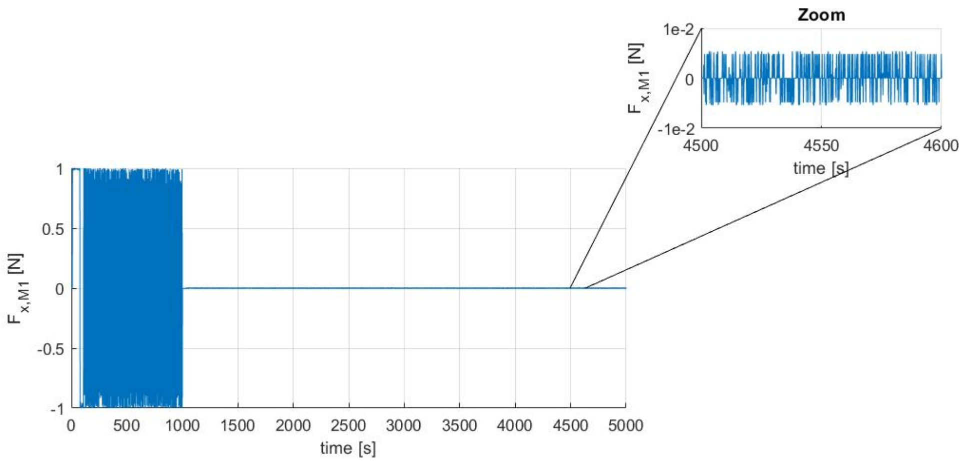

Figure 5.26. STW SMC - TM1 actuation force along X axis

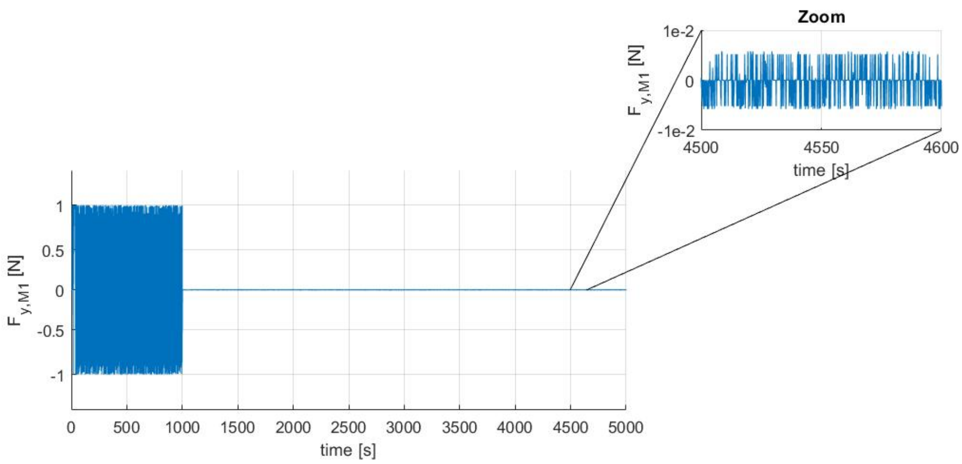

Figure 5.27. STW SMC - TM1 actuation force along Y axis

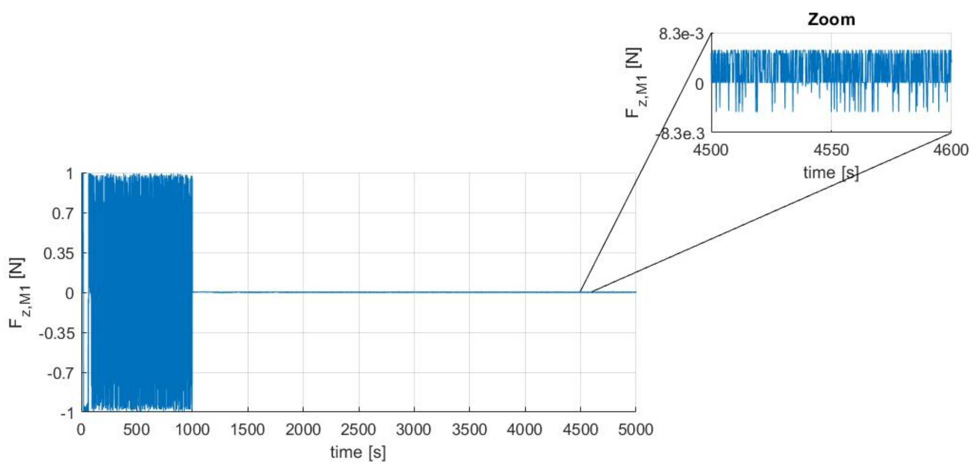

Figure 5.28. STW SMC - TM1 actuation force along Z axis

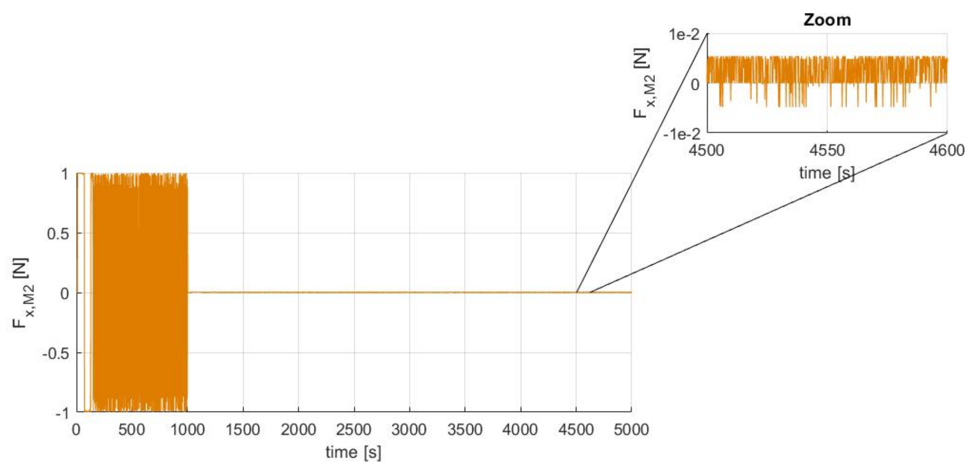

Figure 5.29. STW SMC - TM2 actuation force along X axis

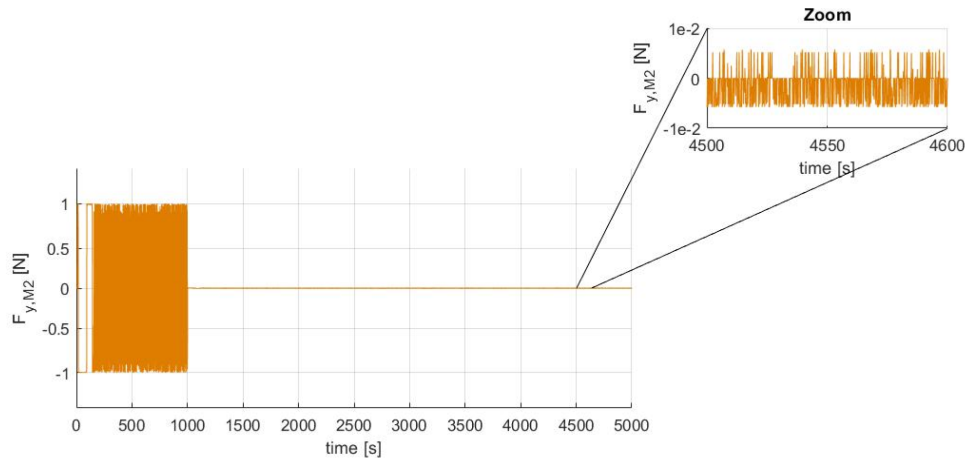

Figure 5.30. STW SMC - TM2 actuation force along Y axis

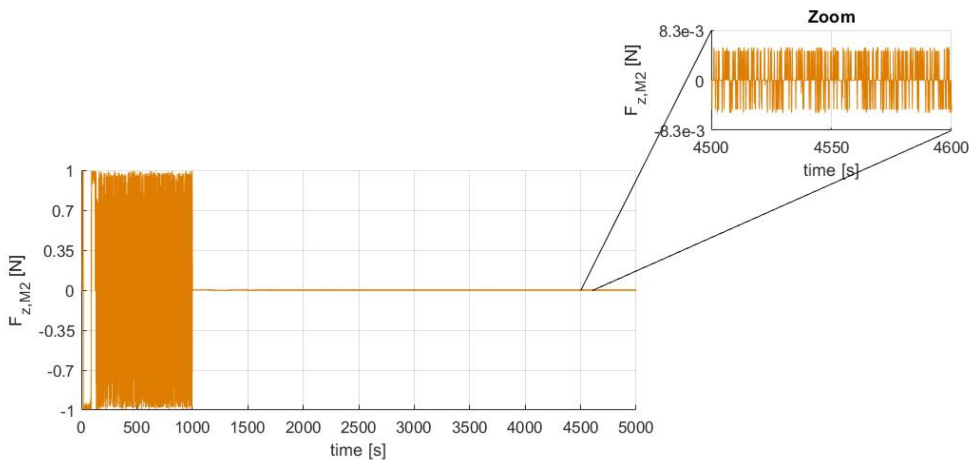

Figure 5.31. STW SMC - TM2 actuation force along Z axis

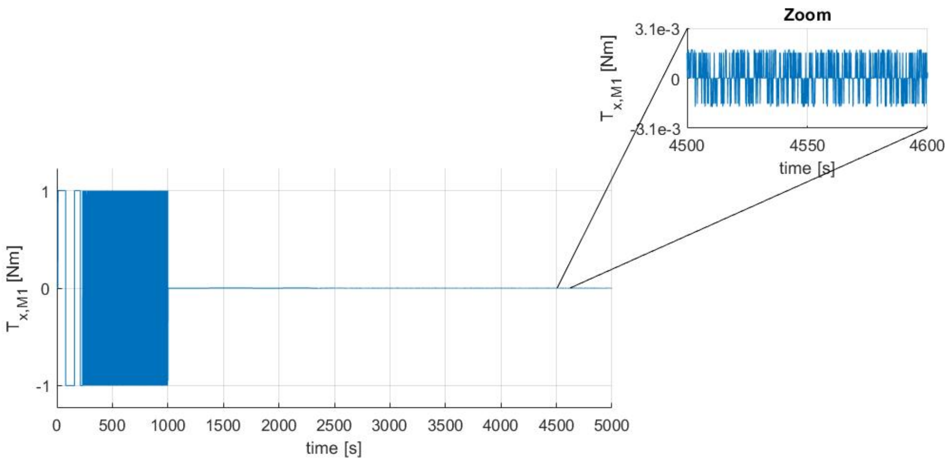

Figure 5.32. STW SMC - TM1 actuation torque around X axis

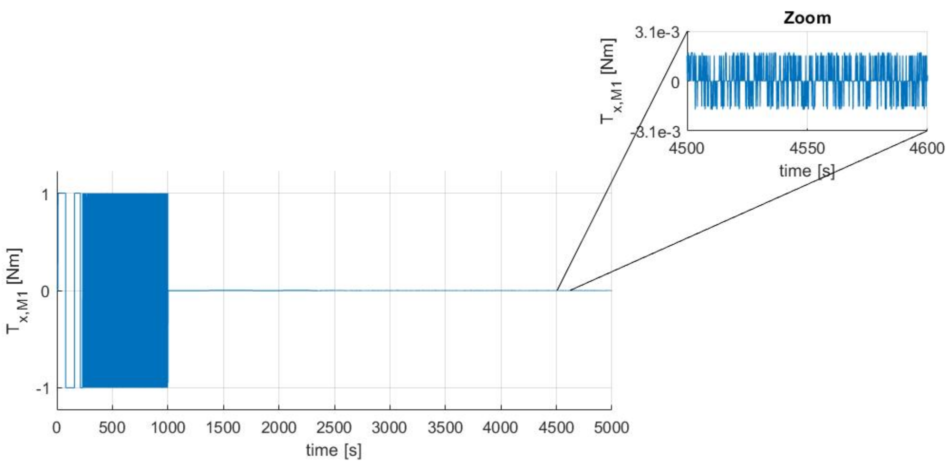

Figure 5.33. STW SMC - TM1 actuation torque around Y axis

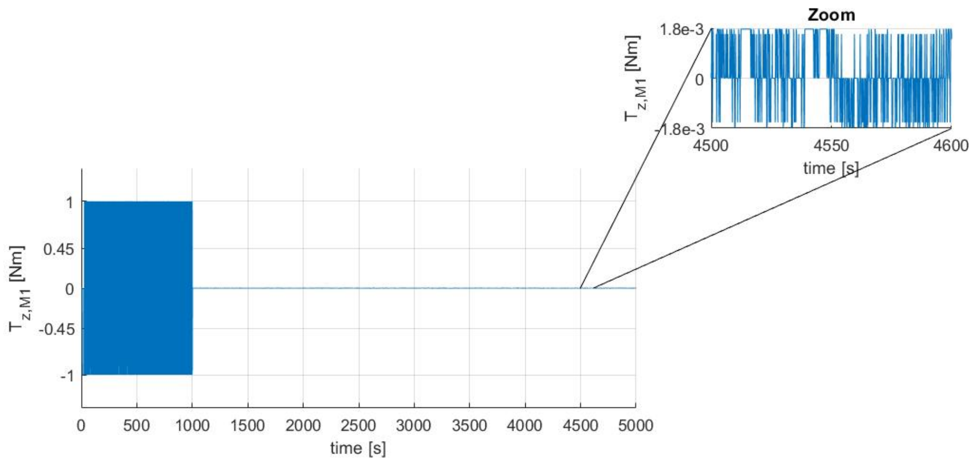

Figure 5.34. STW SMC - TM1 actuation torque around Z axis

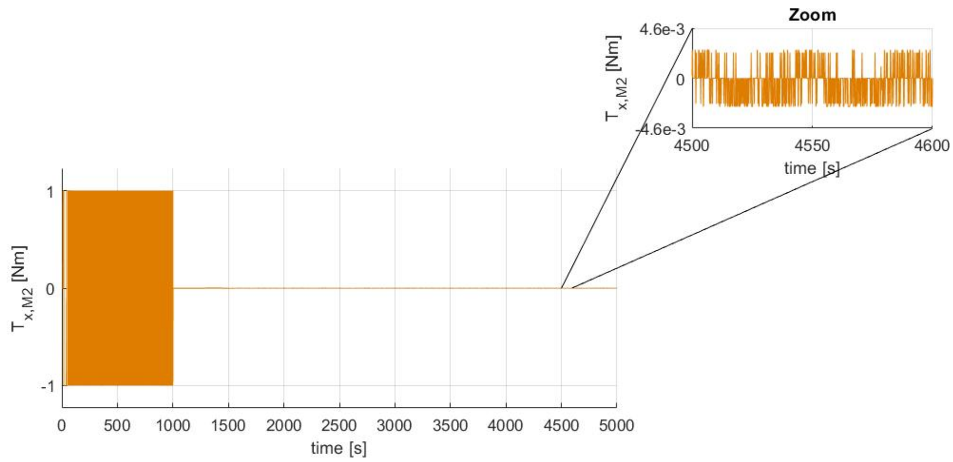

Figure 5.35. STW SMC - TM2 actuation torque around X axis

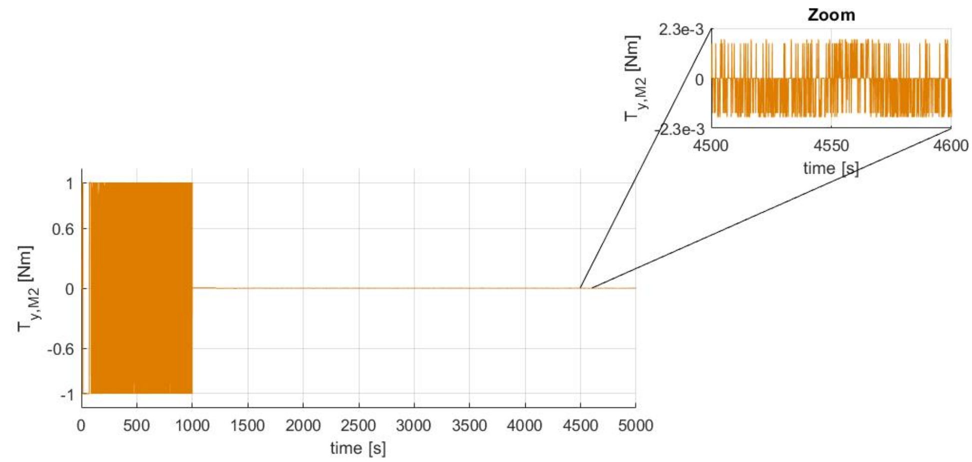

Figure 5.36. STW SMC - TM2 actuation torque around Y axis

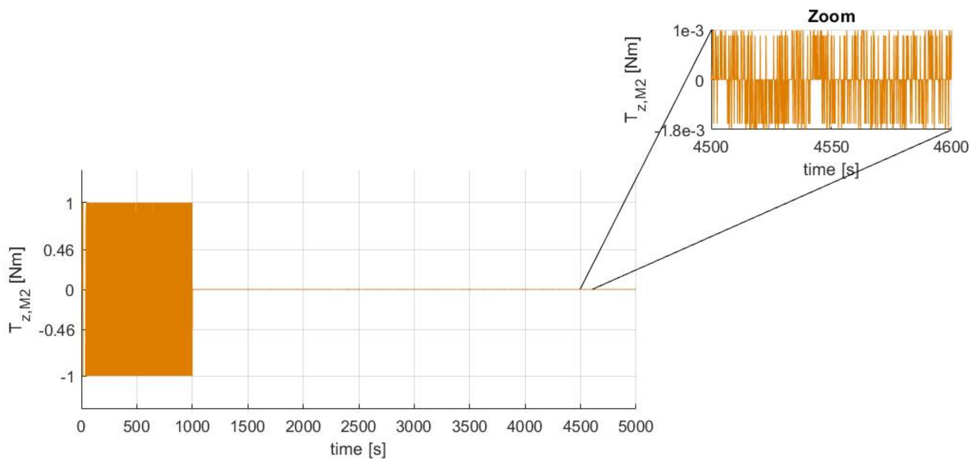

Figure 5.37. STW SMC - TM2 actuation torque around Z axis

From Fig.5.26 to Fig.5.37, the actuation forces and torques in the HR mode are about 2-3 orders of magnitude lower than the actuation authority in the WR mode as it was expected and described in the Chapter 2 about the operative configuration and in which are given as reference the real order of magnitude of actuation forces and torques. Moreover, the saturation in the WR and HR mode is about the 98% of the real available actuation authority in the way to not overload the TMs actuation system.

Finally, the performance of the sliding surface are described in Table 5.6 and Table 5.7 in terms of chattering amplitude but just about their orders of magnitude, both for position and attitude control. In this case, the continuous control law implemented in the STW SMC control is able to reduce the chattering of the sliding variable and to improve the accuracy performance in respect of the behaviour of the first order SMC with its discontinuous control law.

Table 5.6. STW SMC - TM1 Sliding surface chattering in WR and HR mode

WR	x	y	z
$\sigma_{pos,M1}[m]$	$\pm 1e-6$	$\pm 1e-6$	$\pm 1e-6$
$\sigma_{rot,M1}[rad]$	$\pm 1e-4$	$\pm 1e-3$	$\pm 1e-3$
HR	x	y	z
$\sigma_{pos,M1}[m]$	$\pm 1e-7$	$\pm 1e-7$	$\pm 1e-7$
$\sigma_{rot,M1}[rad]$	$\pm 1e-3$	$\pm 1e-3$	$\pm 1e-3$

Table 5.7. STW SMC - TM2 Sliding surface chattering in WR and HR mode

WR	x	y	z
$r_{M2}[m]$	$\pm 1e-6$	$\pm 1e-6$	$\pm 1e-6$
$\sigma_{rot,M2}[rad]$	$\pm 1e-4$	$\pm 1e-3$	$\pm 1e-3$
HR	x	y	z
$\sigma_{pos,M2}[m]$	$\pm 1e-7$	$\pm 1e-7$	$\pm 1e-7$
$\sigma_{rot,M2}[rad]$	$\pm 1e-4$	$\pm 1e-3$	$\pm 1e-3$

Moreover, the settling time of the sliding variables give a more detailed view about goodness of the STW SMC control performance. As showed in Table 5.8 and Table 5.9, the position sliding surface variables are not critical for both TMs and they have a settling time within $0-200s$ for the $80-100\%$ of runs in WR and HR mode except for the TM1 and TM2 position sliding variables along Z-axis which are equally distributed in the $0-800s$ time interval. As opposite, the rotation sliding surface variables are critical for both TMs as seen also for the angular displacements. In detail, in the WR the σ_{rot} have a settling time within $0-800s$ and in the HR mode they have a settling time within the $1201-5000s$.

Table 5.8. STW SMC performance - TM1 Sliding surface settling time in WR and HR mode

	[0; 199]s	[200; 800]s	[801; 1000]s
WR	[x;y;z]	[x;y;z]	[x;y;z]
$\sigma_{pos,M1}$	[80.5%; 88.5%; 56.5%]	[19.5%; 11.5%; 43.5%]	[0%; 0%; 0%]
$\sigma_{rot,M1}$	[58.5%; 3%; 8.5%]	[41.5%; 97.5%; 91.5%]	[0%; 0%; 0%]
	[1001; 1200]s	[1201; 4800]s	[4801; 5000]s
HR	[x;y;z]	[x;y;z]	[x;y;z]
$\sigma_{pos,M1}$	[99.5%; 100%; 100%]	[0.5%; 0%; 0%]	[0%; 0%; 0%]
$\sigma_{rot,M1}$	[100%; 8.5%; 3%]	[0%; 24%; 37%]	[0%; 67.5%; 60%]

Table 5.9. STW SMC performance - TM2 Sliding surface settling time in WR and HR mode

	[0; 199]s	[200; 800]s	[801; 1000]s
WR	[x;y;z]	[x;y;z]	[x;y;z]
$\sigma_{pos,M2}$	[80.5%; 88%; 53.5%]	[19.5%; 12%; 46.5%]	[0%; 0%; 0%]
$\sigma_{rot,M2}$	[46%; 3.5%; 5.5%]	[54%; 94%; 94.5%]	[0%; 2.5%; 0%]
	[1001; 1200]s	[1201; 4800]s	[4801; 5000]s
HR	[x;y;z]	[x;y;z]	[x;y;z]
$\sigma_{pos,M2}$	[100%; 97%; 100%]	[0%; 2%; 0%]	[0%; 0%; 0%]
$\sigma_{rot,M2}$	[6%; 0.5%; 19.5%]	[43.5%; 35%; 60.5%]	[50.5%; 64.5%; 20%]

5.5 Optimal performance results

In the following, a single run is showed between the 200 performed for STW SMC validation in the MonteCarlo campaign. This section could be useful to have a clear overview of the optimal performance achieved by the best simulations of the campaign.

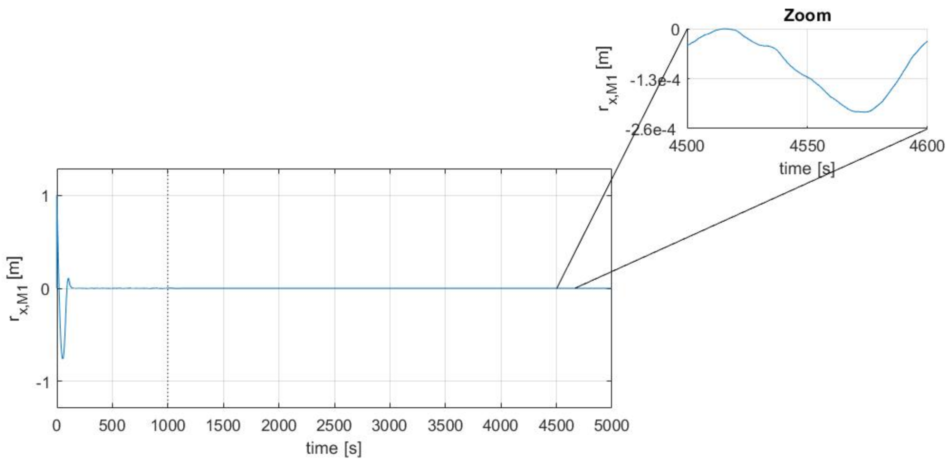

Figure 5.38. STW SMC optimal run - TM1 Linear position along X axis

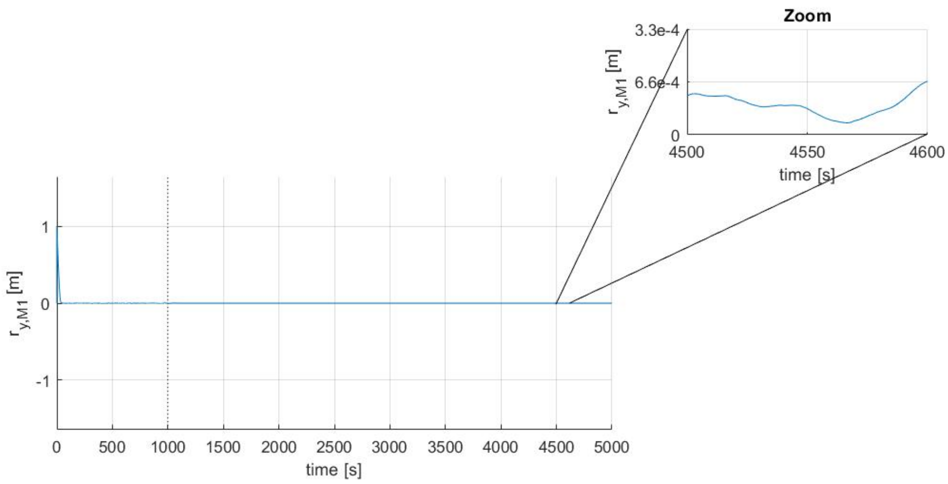

Figure 5.39. STW SMC optimal run - TM1 Linear position along Y axis

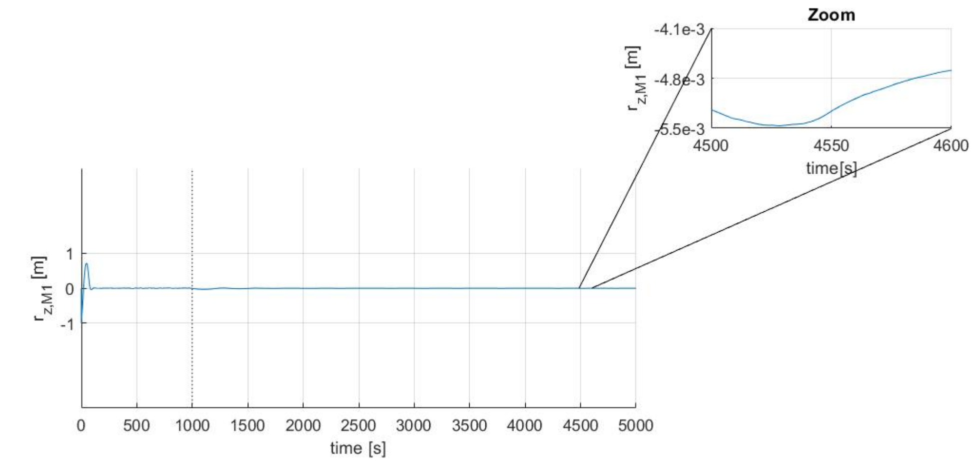

Figure 5.40. STW SMC optimal run - TM1 Linear position along Z axis

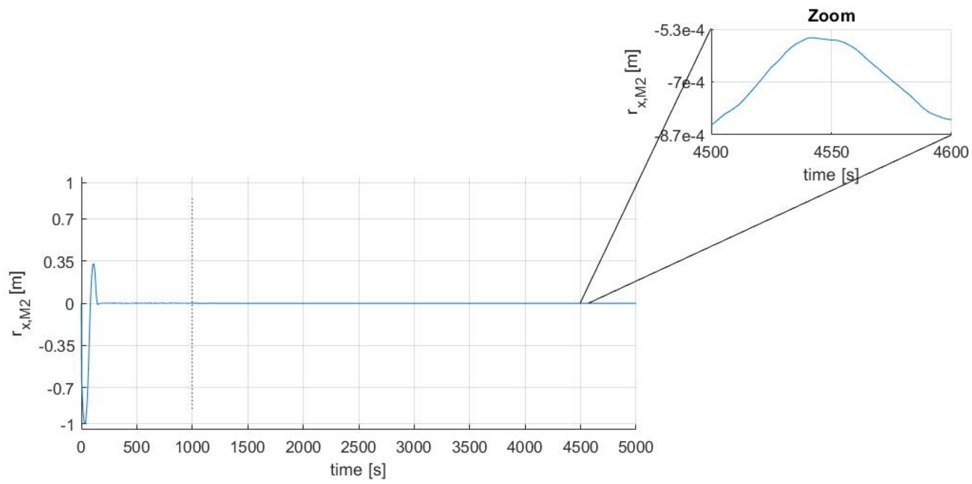

Figure 5.41. STW SMC optimal run - TM2 Linear position along X axis

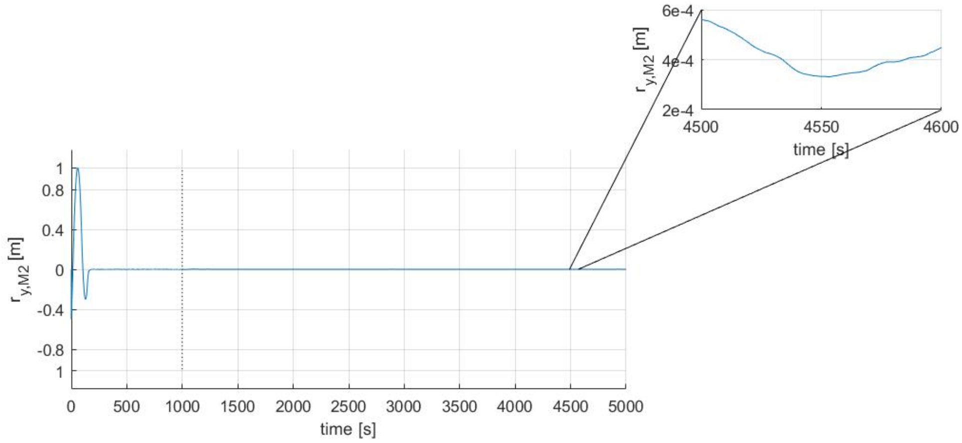

Figure 5.42. STW SMC optimal run - TM2 Linear position along Y axis

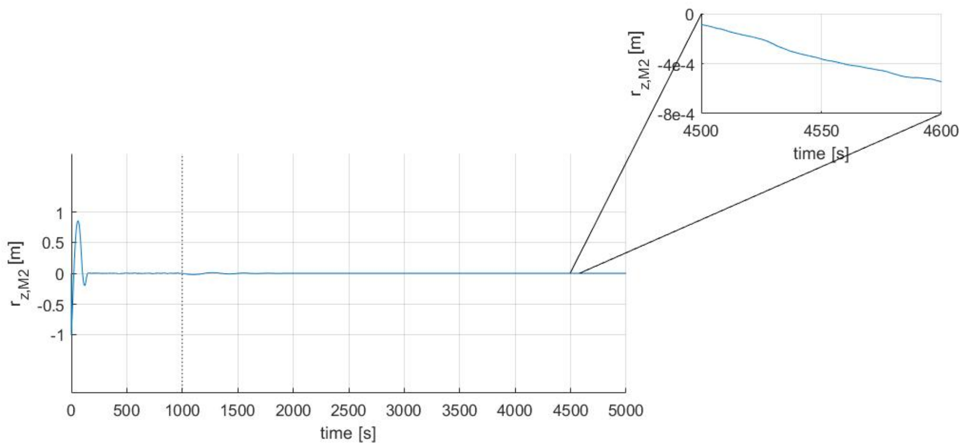

Figure 5.43. STW SMC optimal run - TM2 Linear position along Z axis

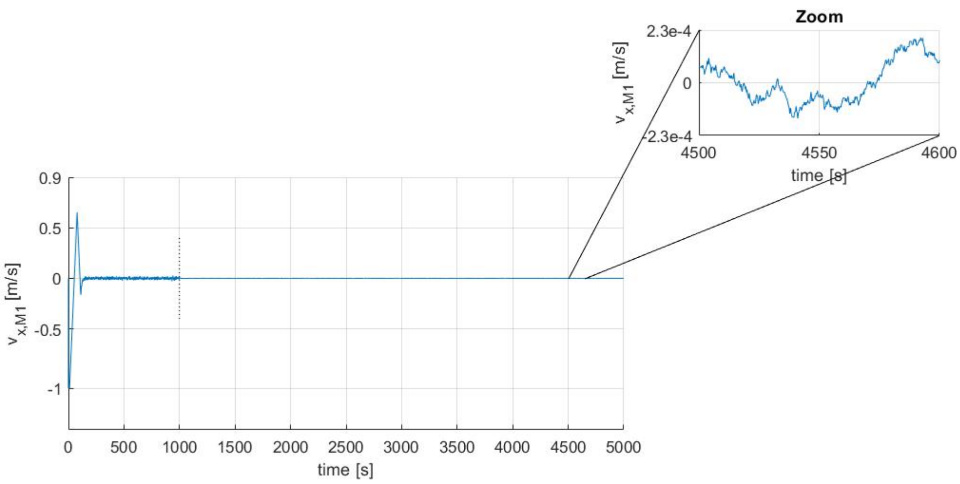

Figure 5.44. STW SMC optimal run - TM1 Linear velocity along X axis

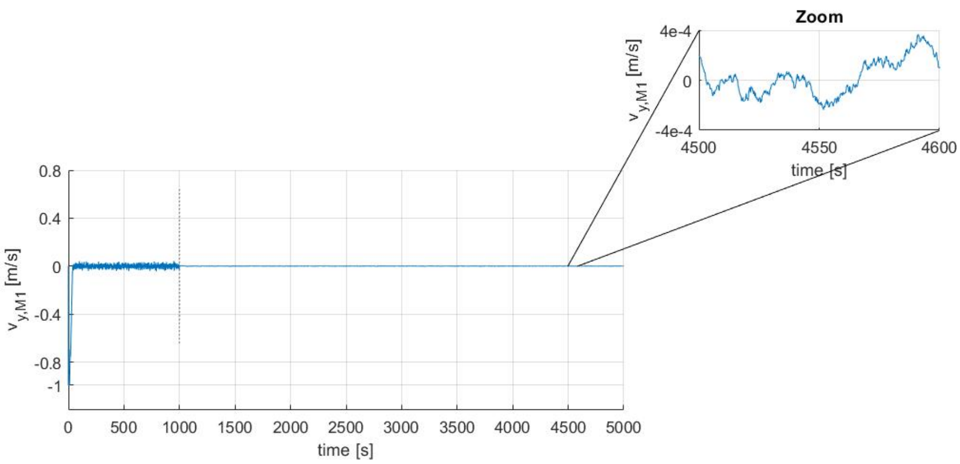

Figure 5.45. STW SMC optimal run - TM1 Linear velocity along Y axis

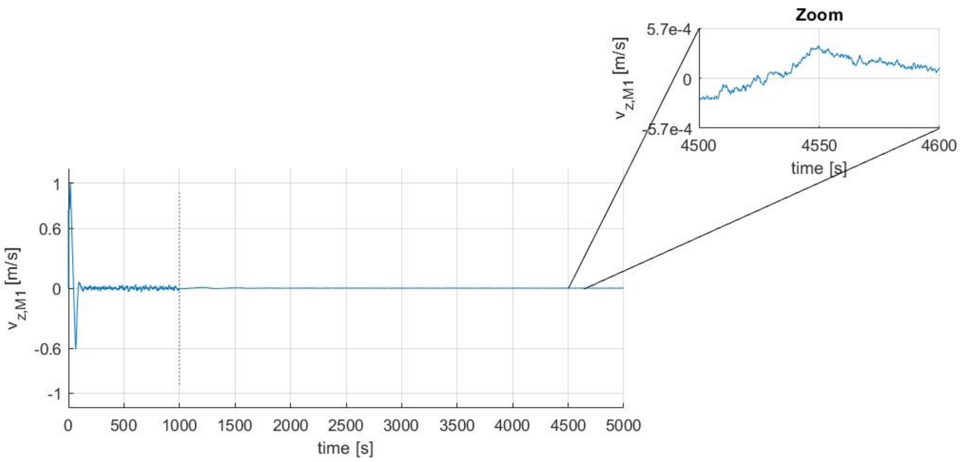

Figure 5.46. STW SMC optimal run - TM1 Linear velocity along Z axis

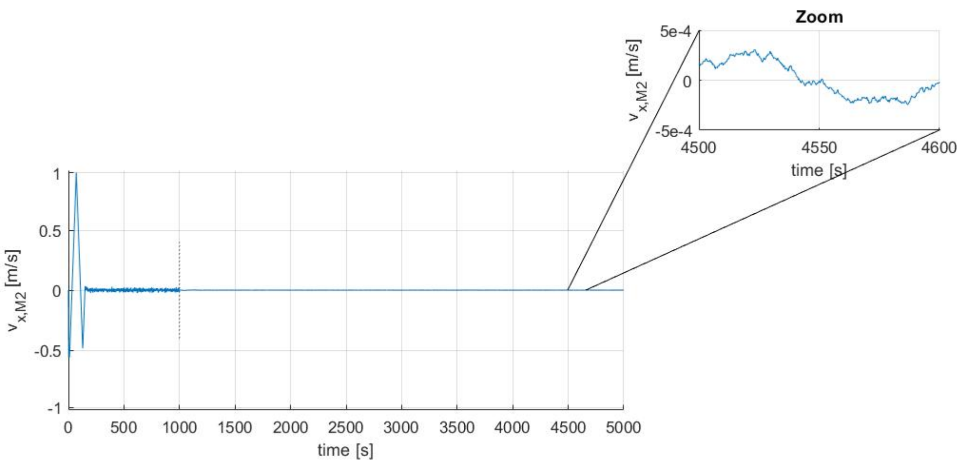

Figure 5.47. STW SMC optimal run - TM2 Linear velocity along X axis

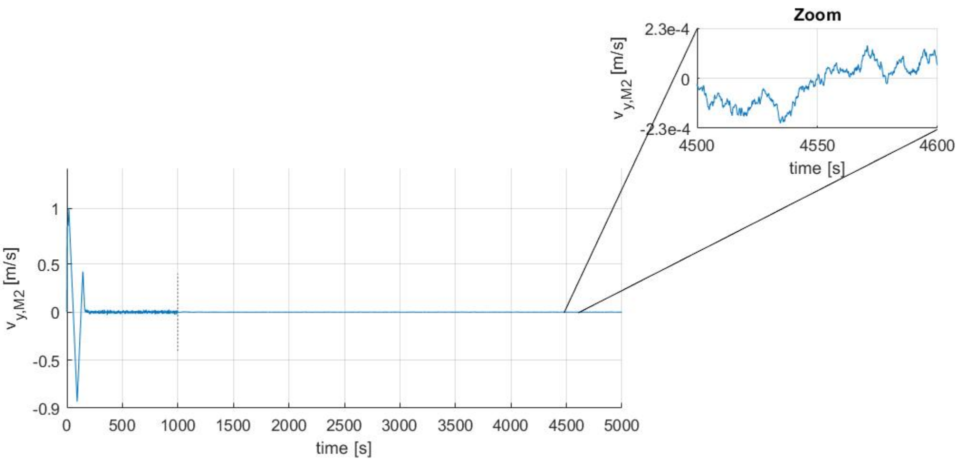

Figure 5.48. STW SMC optimal run - TM2 Linear velocity along Y axis

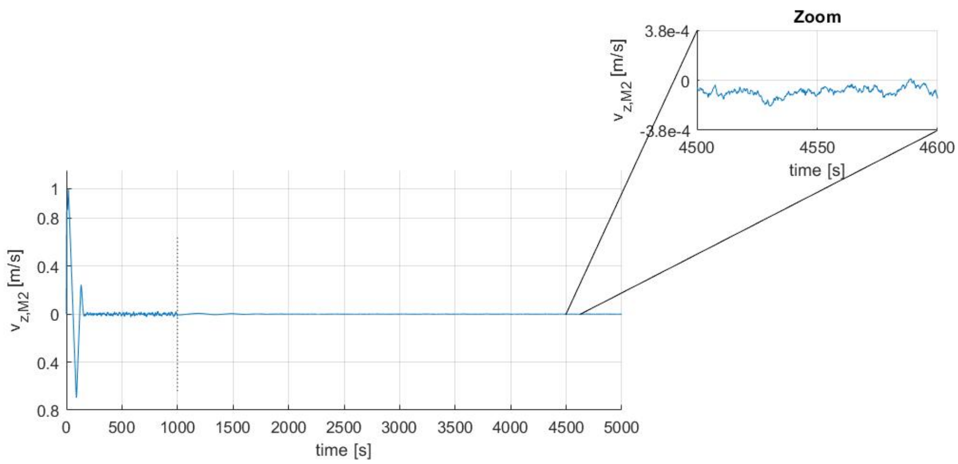

Figure 5.49. STW SMC optimal run - TM2 Linear velocity along Z axis

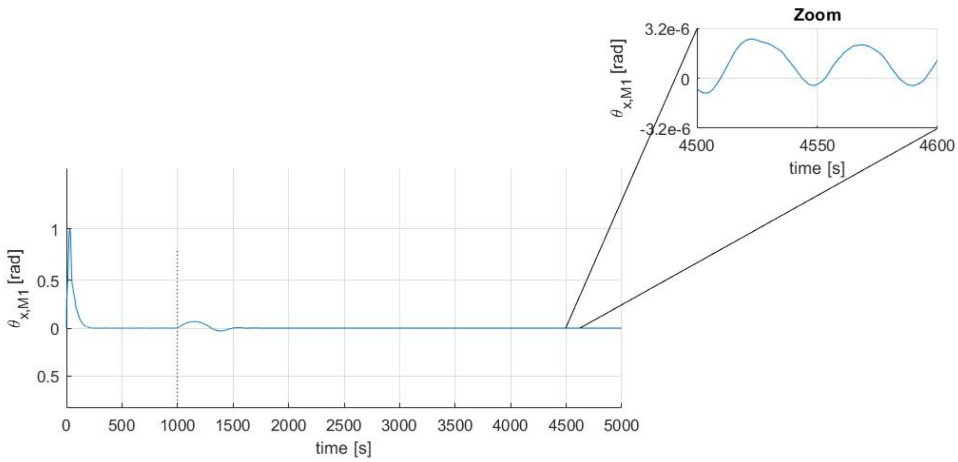

Figure 5.50. STW SMC optimal run - TM1 Angular position around X axis

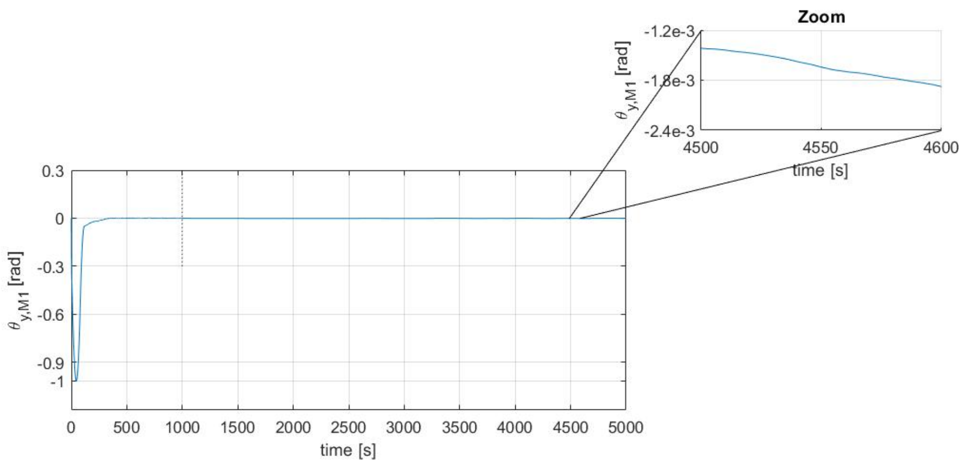

Figure 5.51. STW SMC optimal run - TM1 Angular position around Y axis

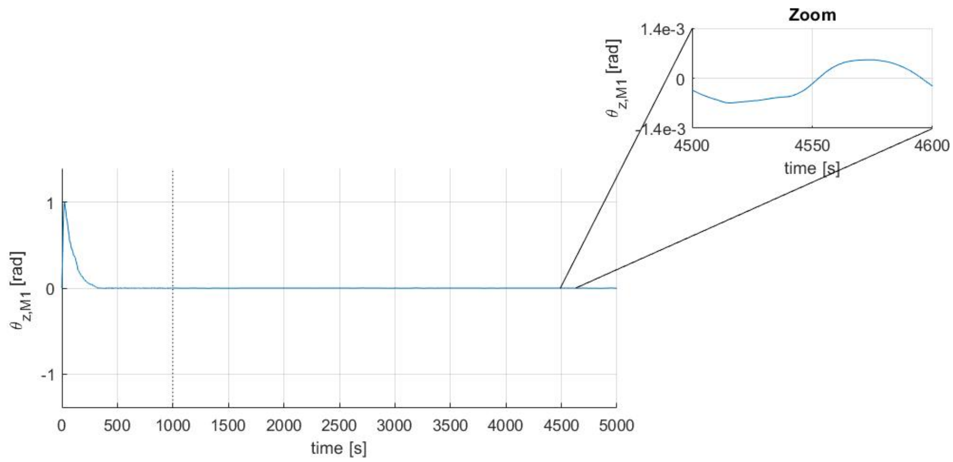

Figure 5.52. STW SMC optimal run - TM1 Angular position around Z axis

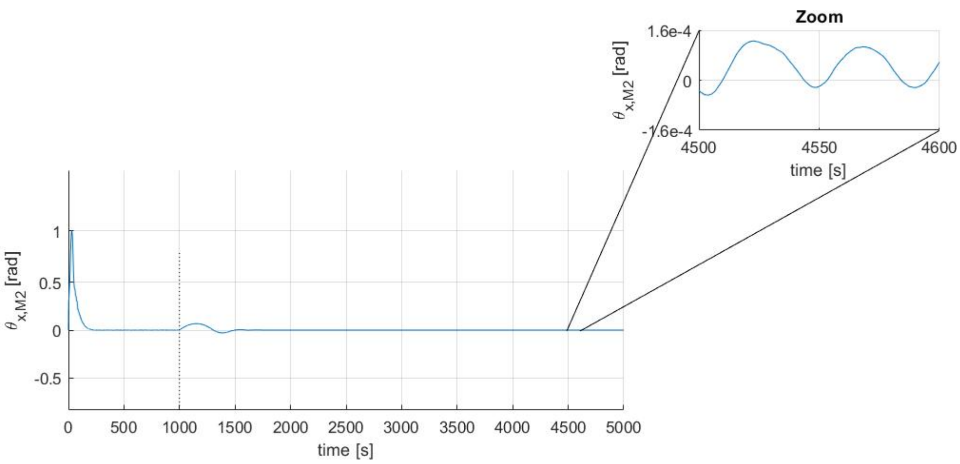

Figure 5.53. STW SMC optimal run - TM2 Angular position around X axis

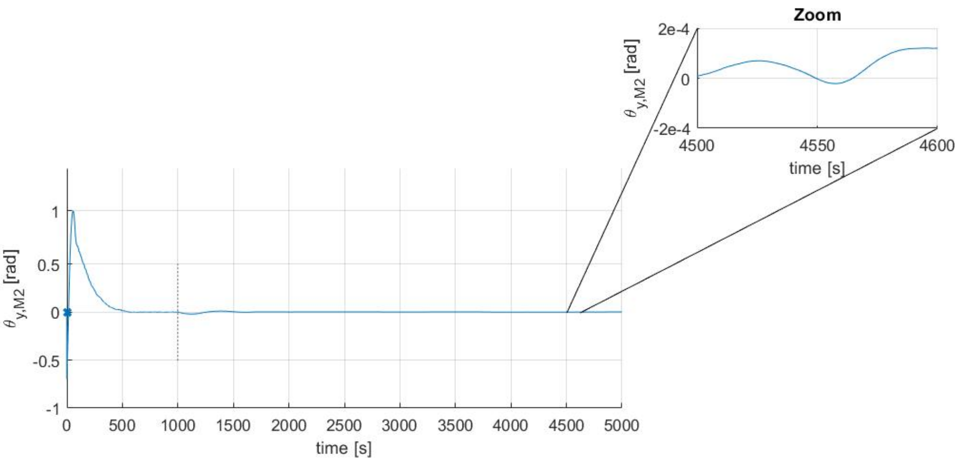

Figure 5.54. STW SMC optimal run - TM2 Angular position around Y axis

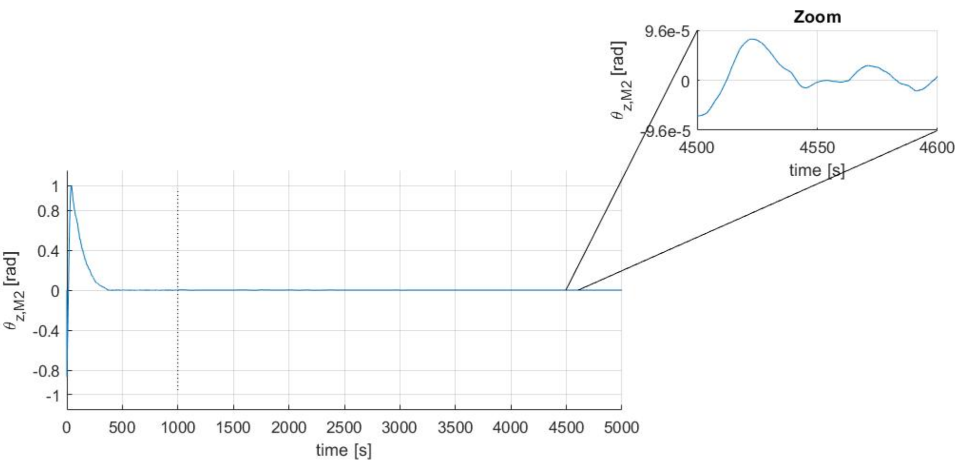

Figure 5.55. STW SMC optimal run - TM2 Angular position around Z axis

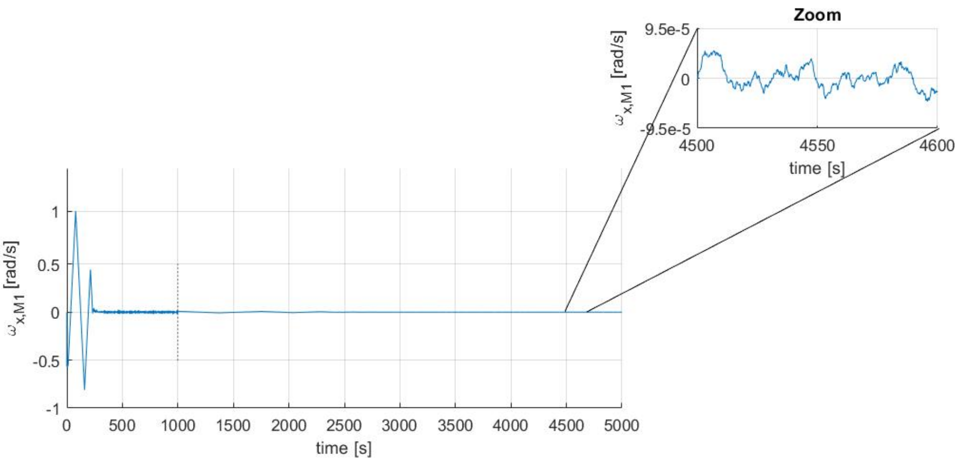

Figure 5.56. STW SMC optimal run - TM1 Angular velocity around X axis

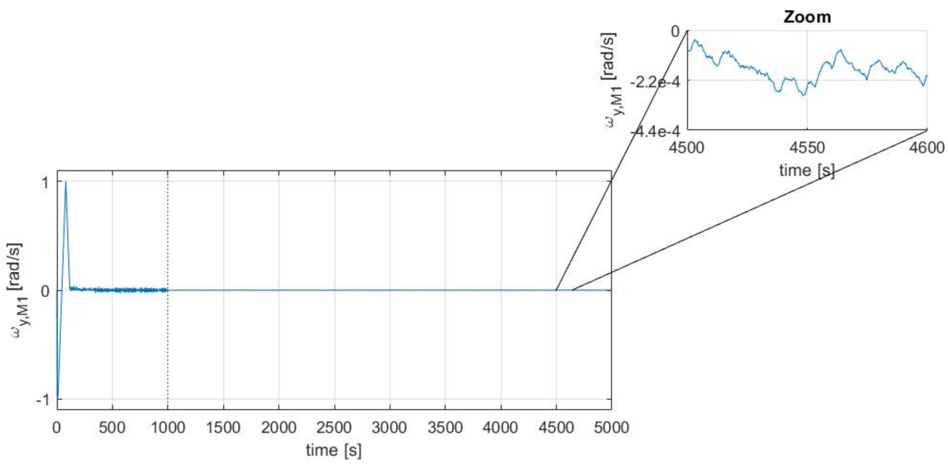

Figure 5.57. STW SMC optimal run - TM1 Angular velocity around Y axis

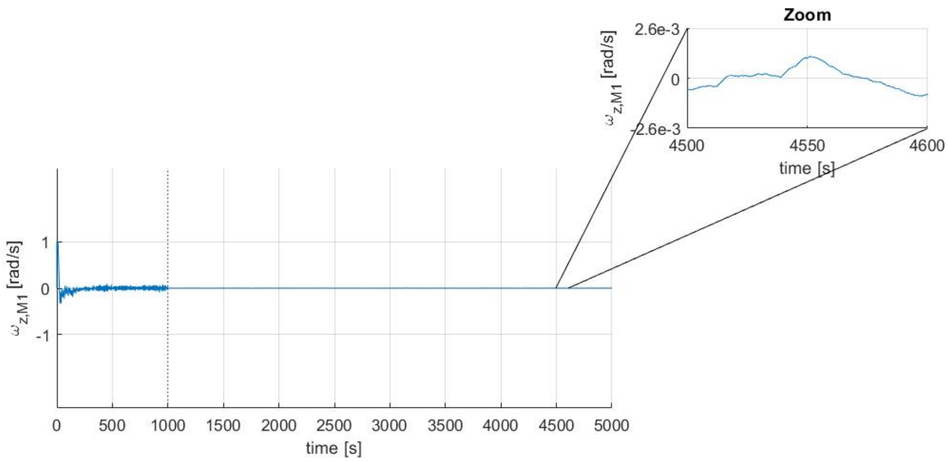

Figure 5.58. STW SMC optimal run - TM1 Angular velocity around Z axis

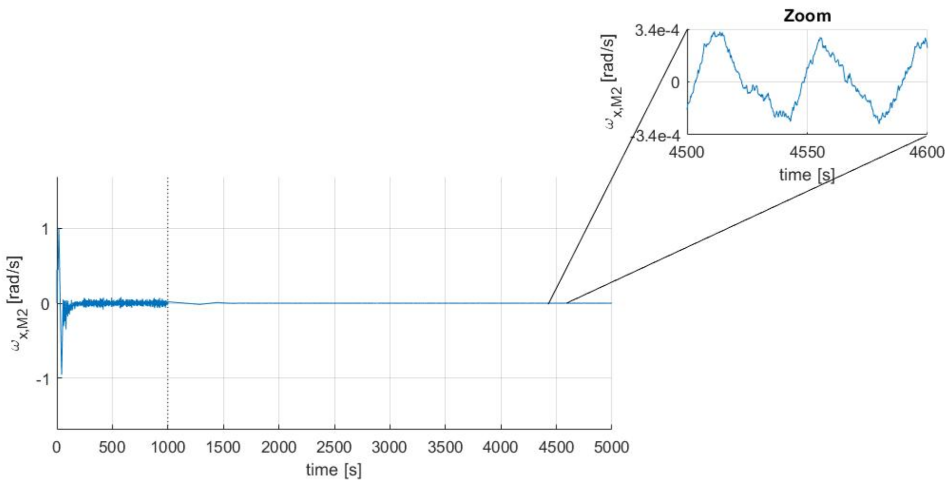

Figure 5.59. STW SMC optimal run - TM2 Angular velocity around X axis

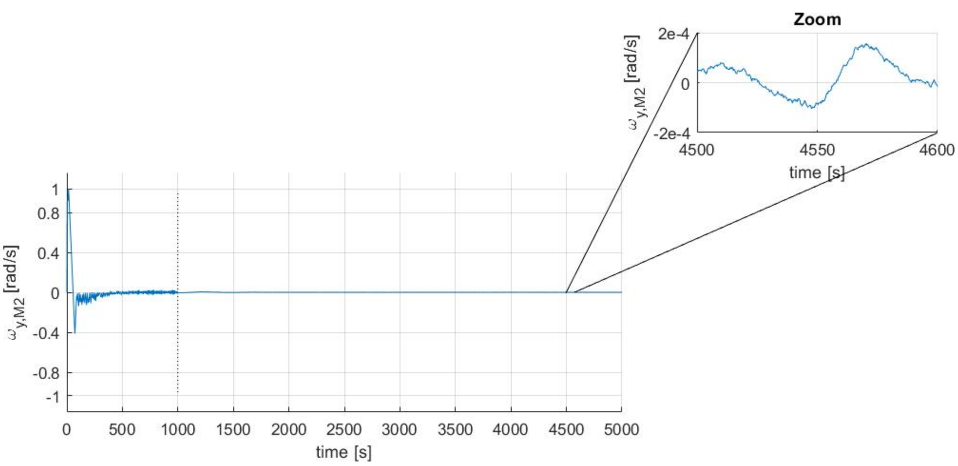

Figure 5.60. STW SMC optimal run - TM2 Angular velocity around Y axis

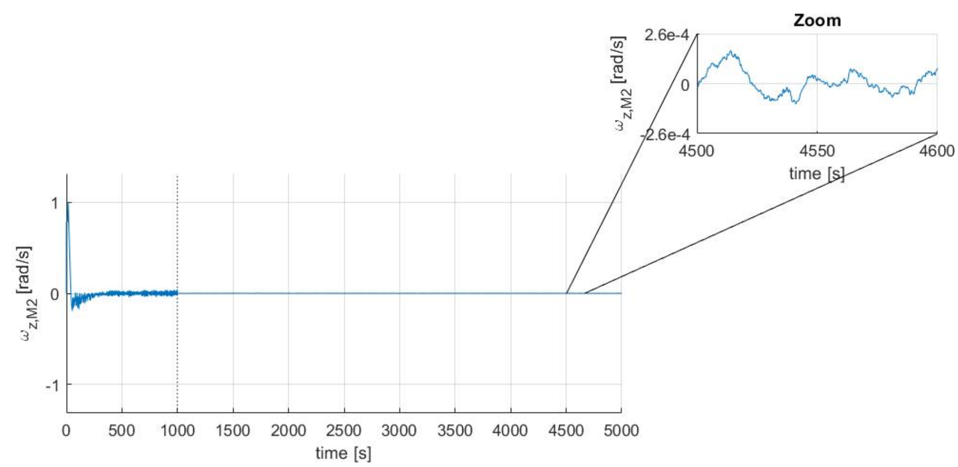

Figure 5.61. STW SMC optimal run - TM2 Angular velocity around Z axis

The performance of this run are similar, in terms of the steady-state accuracy, to the ones described for the 200 runs campaign, except for the attitude angles which are at least lower of 1-2 orders of magnitude.

5.6 First Order SMC vs STW SMC

In this section the performance of the first order SMC controller designed are presented and described in Chapter 4. The results are presented through overlapped plots and taking into account ten simulations featured with critical initial conditions. These latter will be considered too for the STW SMC runs which are used for the comparison of the two implemented control strategies. Morevoer, the decoupled dynamics between the two TMs, of which in Chapter 3, allows us to show just the TM1.

- First Order SMC results

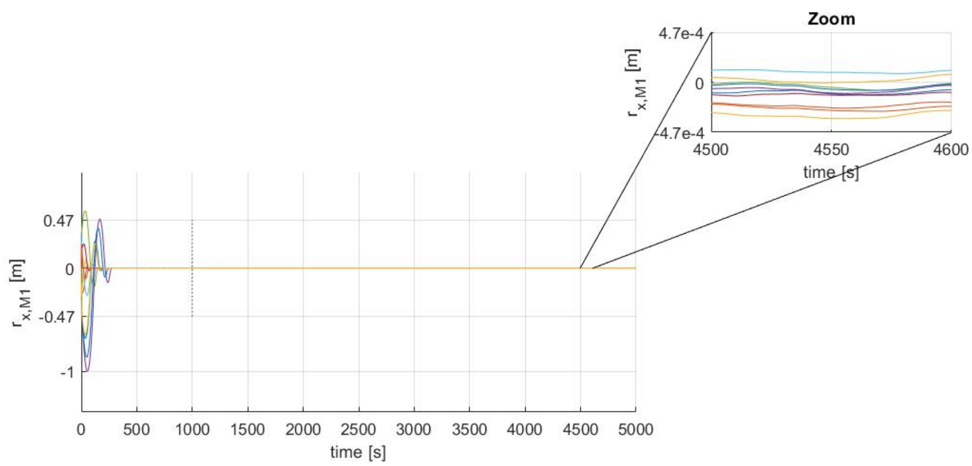

Figure 5.62. 1st Order SMC - Critical conditions - TM1 Linear position along X axis

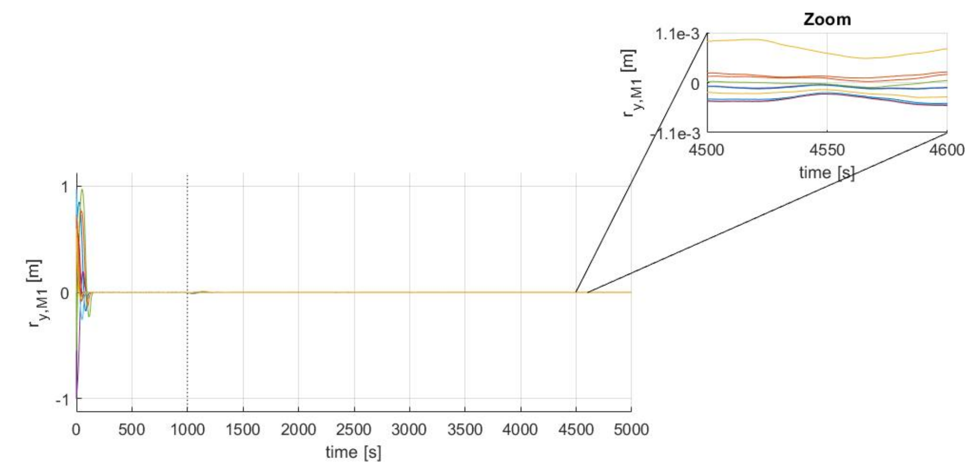

Figure 5.63. 1st Order SMC - Critical conditions - TM1 Linear position along Y axis

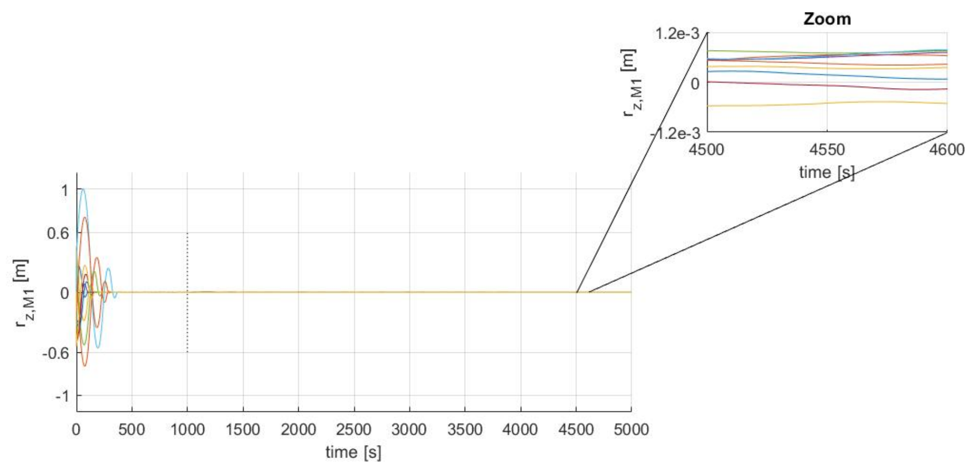

Figure 5.64. 1st Order SMC - Critical conditions - TM1 Linear position along Z axis

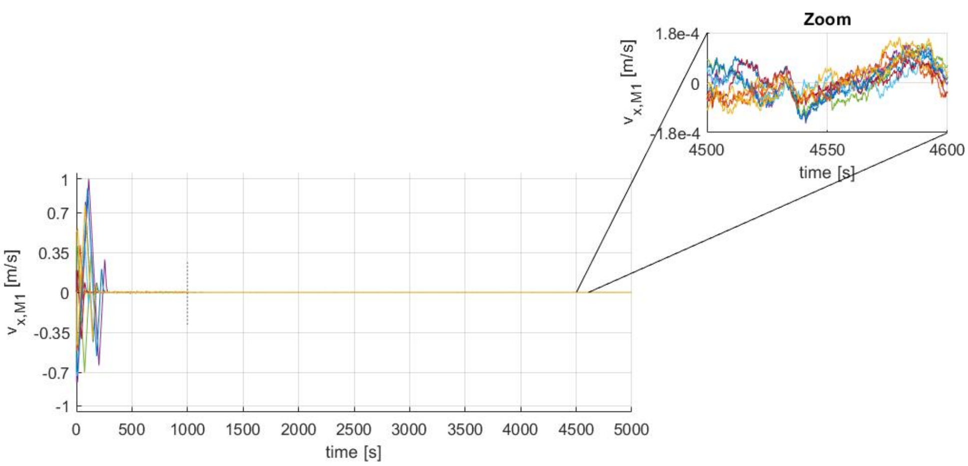

Figure 5.65. 1st Order SMC - Critical conditions - TM1 Linear velocity along X axis

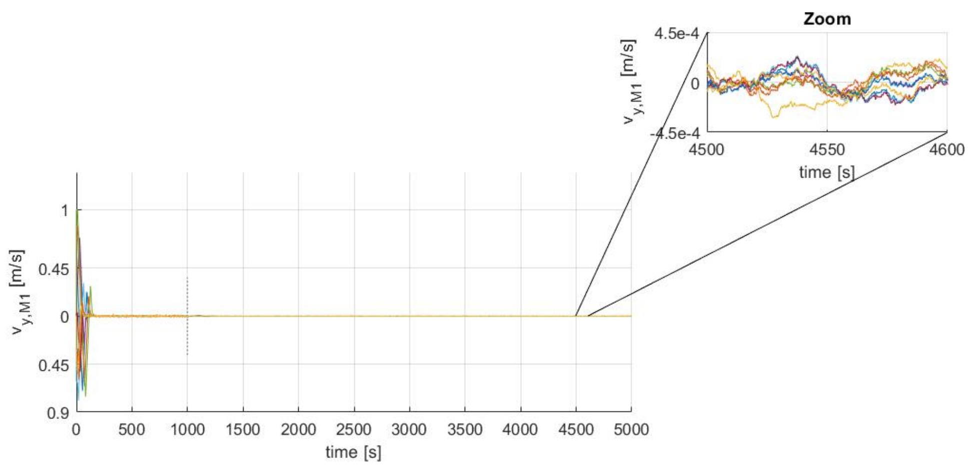

Figure 5.66. 1st Order SMC - Critical conditions - TM1 Linear velocity along Y axis

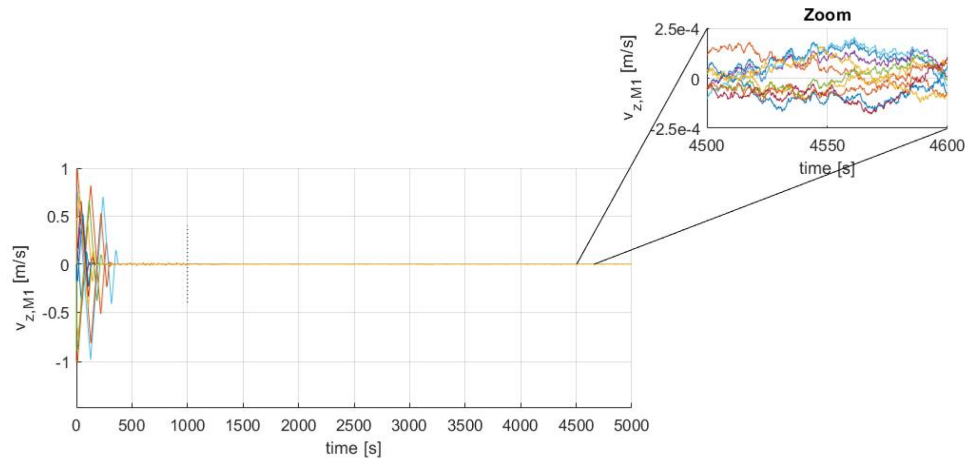

Figure 5.67. 1st Order SMC - Critical conditions - TM1 Linear velocity along Z axis

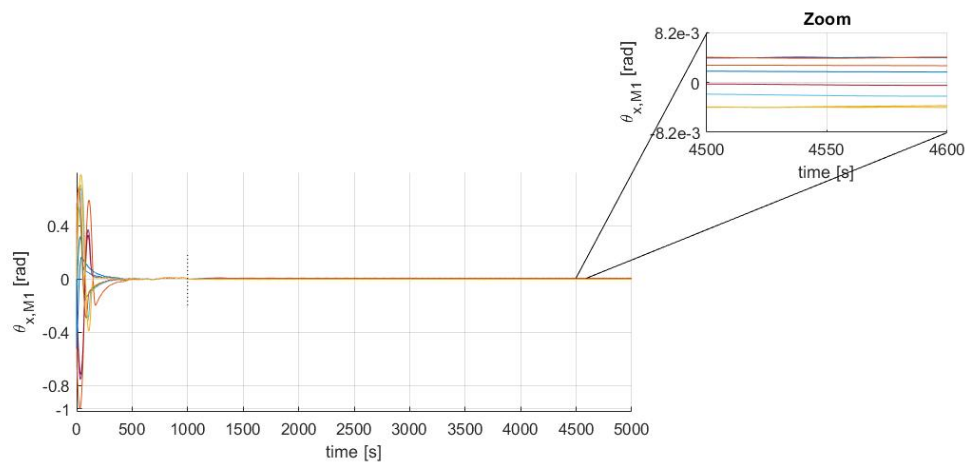

Figure 5.68. 1st Order SMC - Critical conditions - TM1 Angular position around X axis

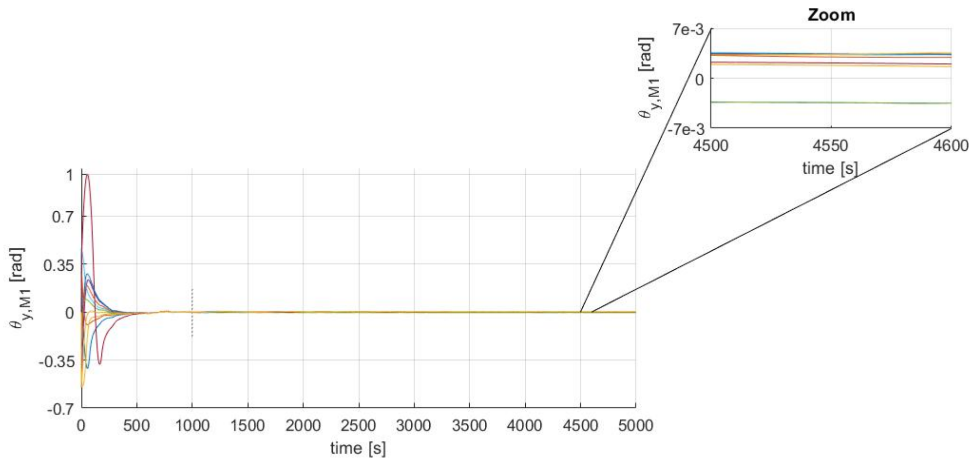

Figure 5.69. 1st Order SMC - Critical conditions - TM1 Angular position around Y axis

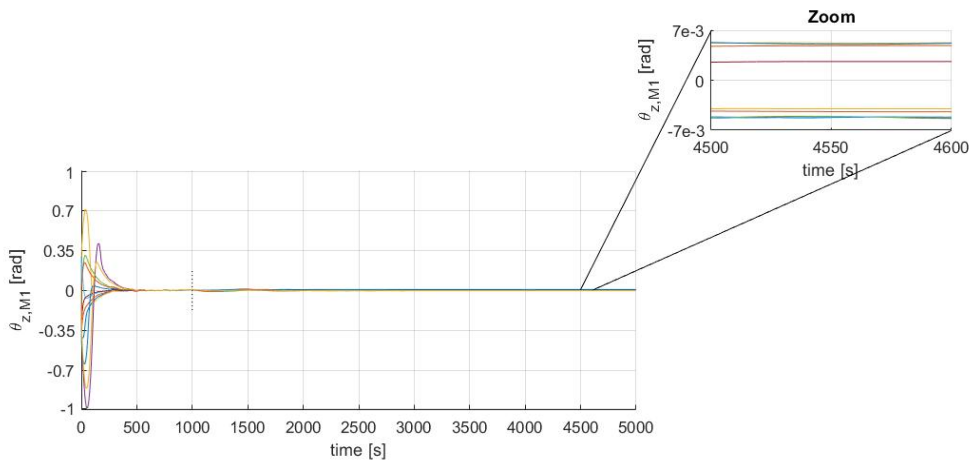

Figure 5.70. 1st Order SMC - Critical conditions - TM1 Angular position around Z axis

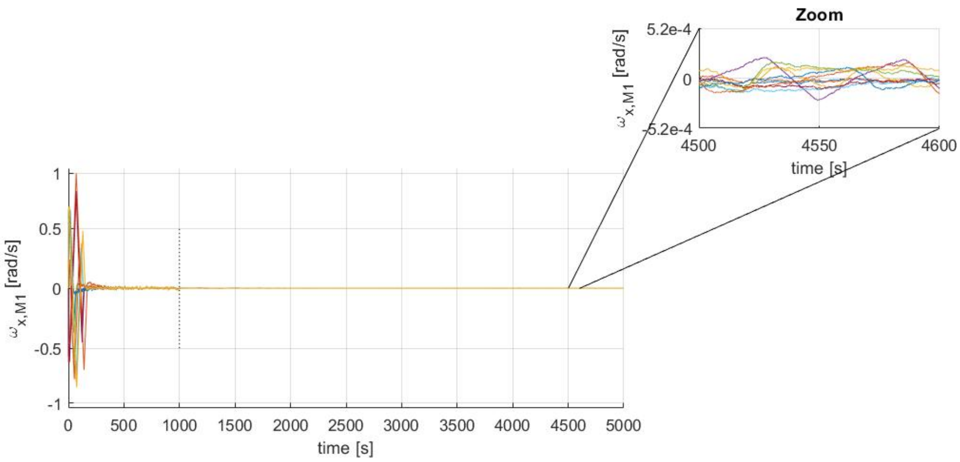

Figure 5.71. 1st Order SMC - Critical conditions - TM1 Angular velocity around X axis

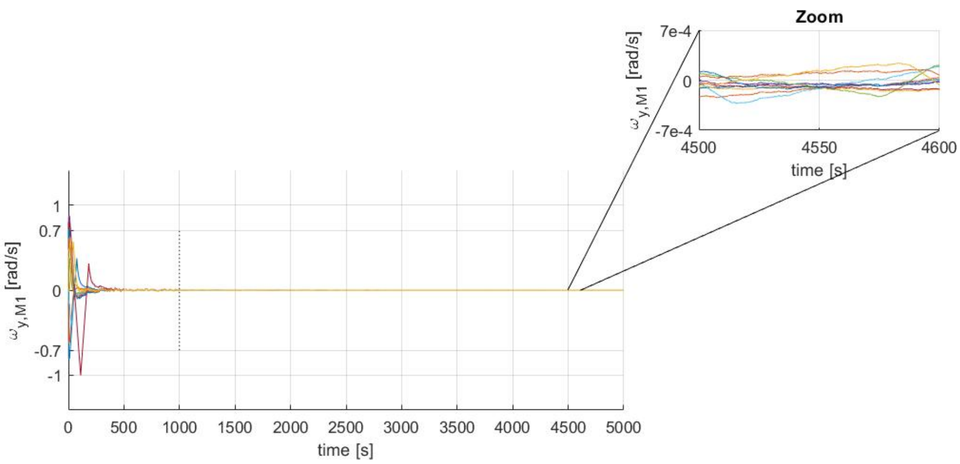

Figure 5.72. 1st Order SMC - Critical conditions - TM1 Angular velocity around Y axis

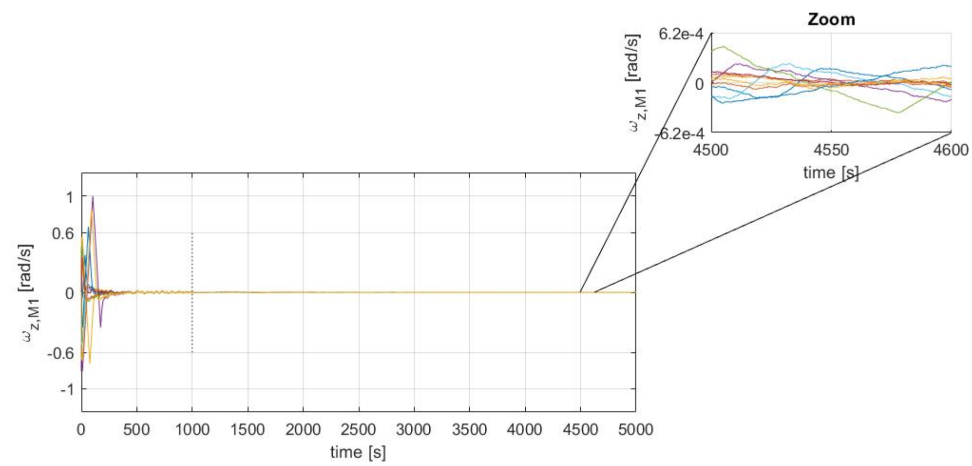

Figure 5.73. 1st Order SMC - Critical conditions - TM1 Angular velocity around Z axis

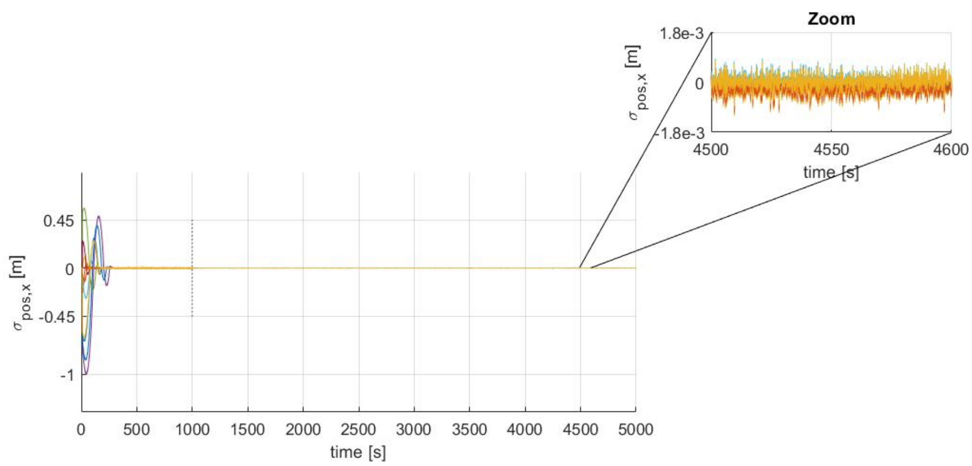

Figure 5.74. 1st Order SMC - Critical conditions - TM1 Position sliding surface along X axis

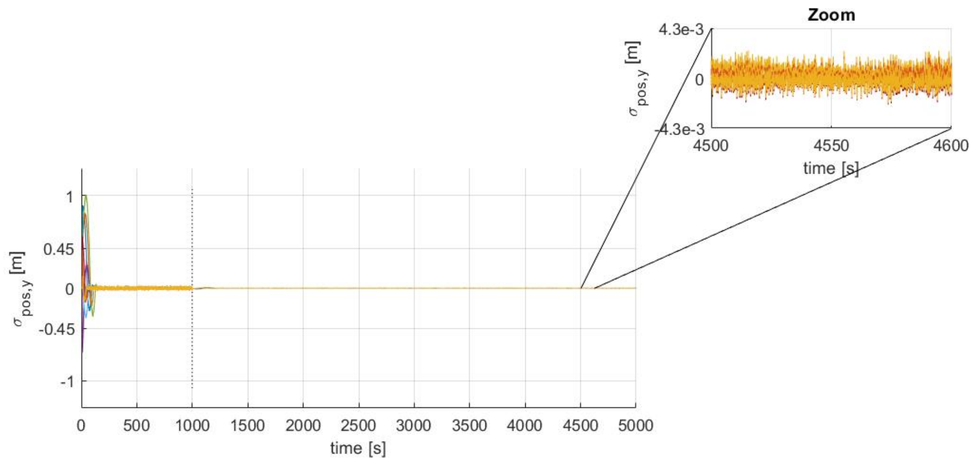

Figure 5.75. 1st Order SMC - Critical conditions - TM1 Position sliding surface along Y axis

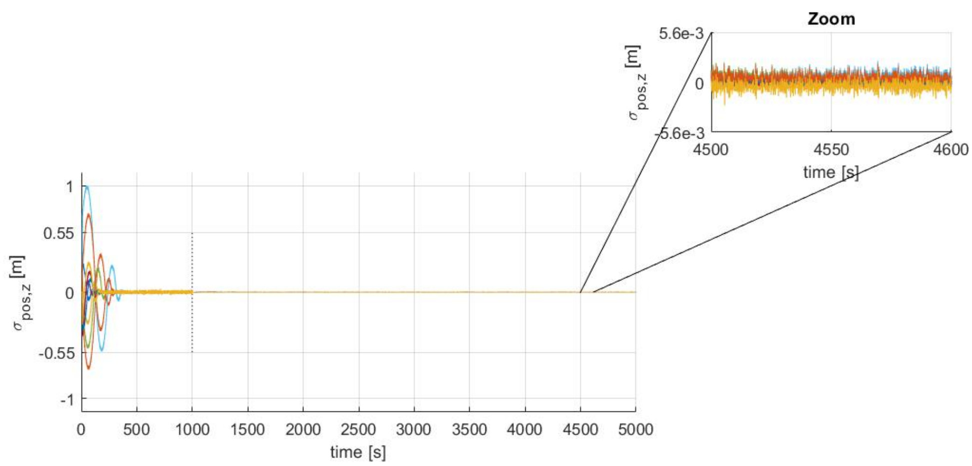

Figure 5.76. 1st Order SMC - Critical conditions - TM1 Position sliding surface along Z axis

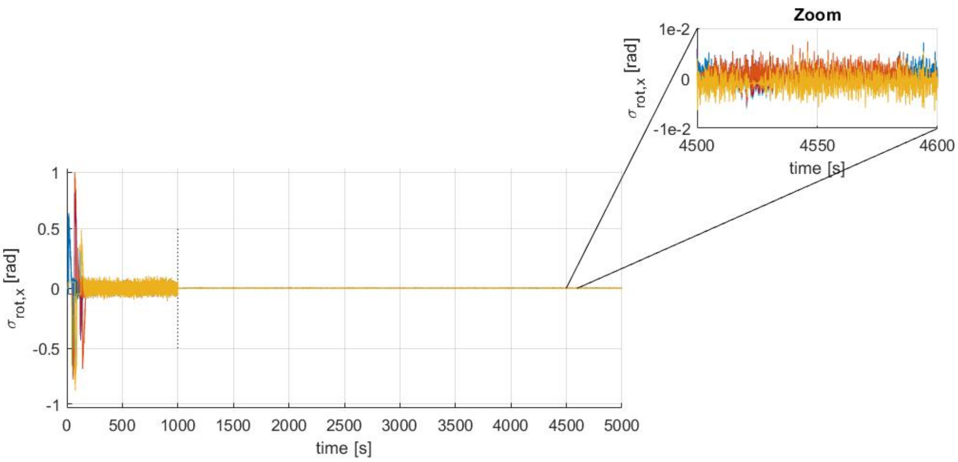

Figure 5.77. 1st Order SMC - Critical conditions - TM1 Rotation sliding surface around X axis

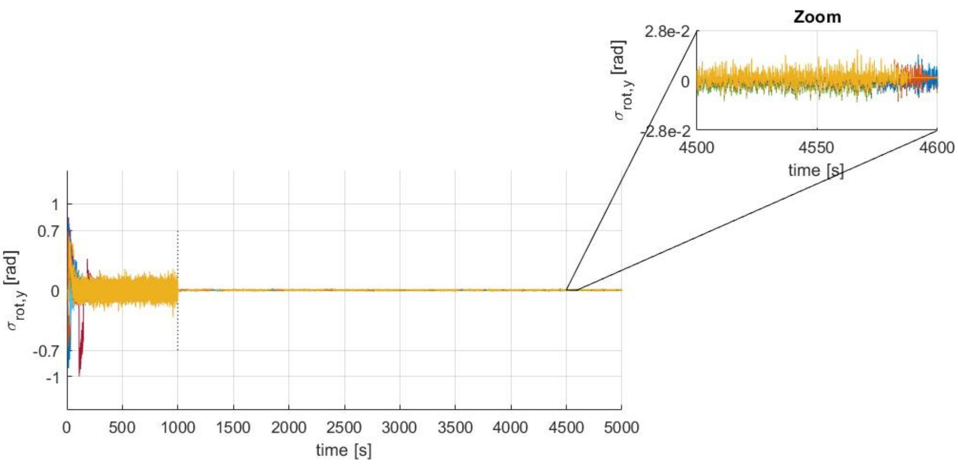

Figure 5.78. 1st Order SMC - Critical conditions - TM1 Rotation sliding surface around Y axis

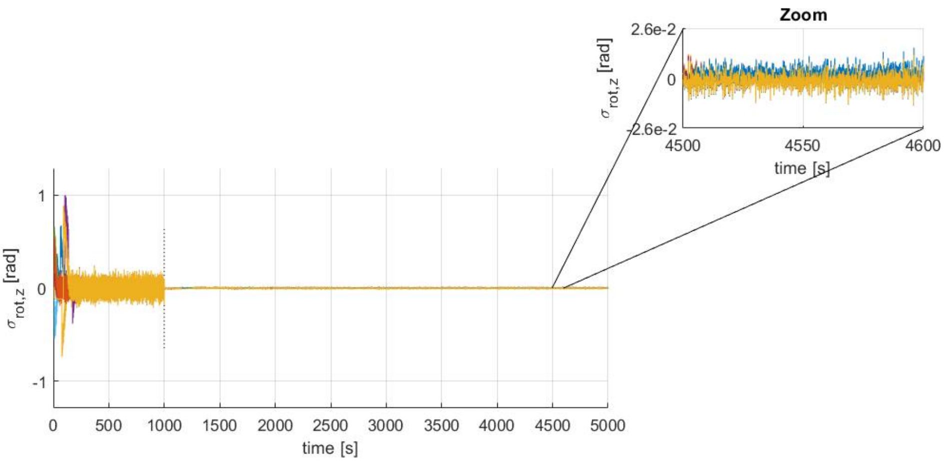

Figure 5.79. 1st Order SMC - Critical conditions - TM1 Rotation sliding surface around Z axis

In the following tables are also described the first order SMC performance needed for comparison purposes:

Table 5.10. First Order SMC - Accuracy in WR and HR mode (3σ)

WR	x	y	z
$r_{M1}[m]$	$\pm 3.68e-6$	$\pm 3.05e-6$	$\pm 4.71e-6$
$v_{M1}[m/s]$	$\pm 9.54e-7$	$\pm 9.17e-7$	$\pm 8.06e-7$
$\theta_{M1}[rad]$	$\pm 7.25e-4$	$\pm 2.87e-4$	$\pm 4.44e-4$
$\omega_{M1}[rad/s]$	$\pm 7.80e-5$	$\pm 3.43e-5$	$\pm 4.86e-5$
HR	x	y	z
$r_{M1}[m]$	$\pm 7.19e-7$	$\pm 6.23e-7$	$\pm 1.59e-6$
$v_{M1}[m/s]$	$\pm 1.58e-8$	$\pm 1.59e-8$	$\pm 1.55e-8$
$\theta_{M1}[rad]$	$\pm 2.56e-4$	$\pm 2.86e-4$	$\pm 4.16e-4$
$\omega_{M1}[rad/s]$	$\pm 5.29e-7$	$\pm 4.96e-7$	$\pm 5.71e-7$

Table 5.11. First Order SMC - Settling time in WR and HR mode

	[0; 199]s	[200; 800]s	[801; 1000]s
WR	[x;y;z]	[x;y;z]	[x;y;z]
r_{M1}	[80%; 100%; 60%]	[20%; 0%; 40%]	[0%; 0%; 0%]
v_{M1}	[80%; 100%; 60%]	[20%; 0%; 40%]	[0%; 0%; 0%]
θ_{M1}	[0%; 0%; 0%]	[0%; 0%; 0%]	[100%; 100%; 100%]
ω_{M1}	[100%; 90%; 80%]	[0%; 10%; 20%]	[0%; 0%; 0%]
	[1001; 1200]s	[1201; 4800]s	[4801; 5000]s
HR	[x;y;z]	[x;y;z]	[x;y;z]
r_{M1}	[100%; 80%; 100%]	[0%; 20%; 0%]	[0%; 0%; 0%]
v_{M1}	[100%; 50%; 0%]	[0%; 50%; 100%]	[0%; 0%; 0%]
θ_{M1}	[0%; 10%; 0%]	[10%; 10%; 10%]	[90%; 80%; 90%]
ω_{M1}	[70%; 20%; 50%]	[20%; 80%; 50%]	[0%; 0%; 0%]

Table 5.12. First Order SMC - Maximum overshoot

WR	x	y	z
$r_{M1}[m]$	1.10e-3	4.4e-4	8.60e-4
$v_{M1}[m/s]$	2.80e-5	2.20e-5	2e-5
$\theta_{M1}[rad]$	2.4e-2	2.9e-2	3e-2
$\omega_{M1}[rad/s]$	9.60e-4	7.10e-4	8e-4

- STW SMC results

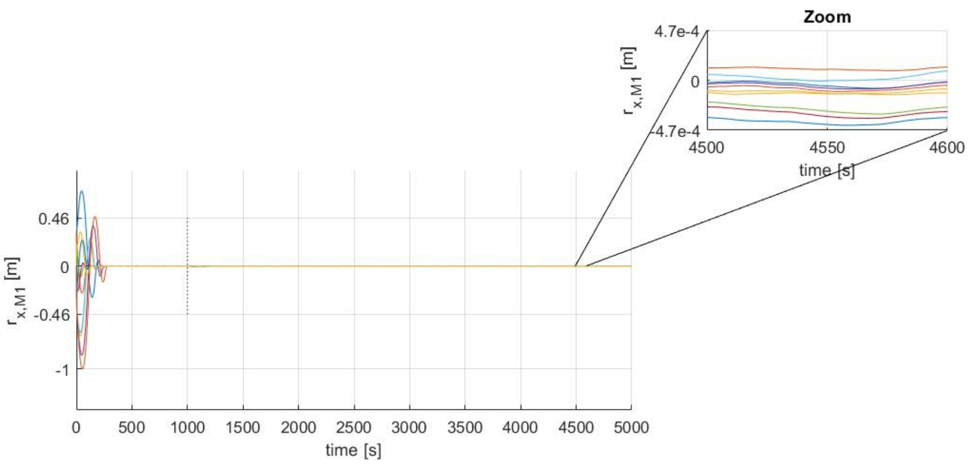

Figure 5.80. STW SMC - Critical conditions - TM1 Linear position along X axis

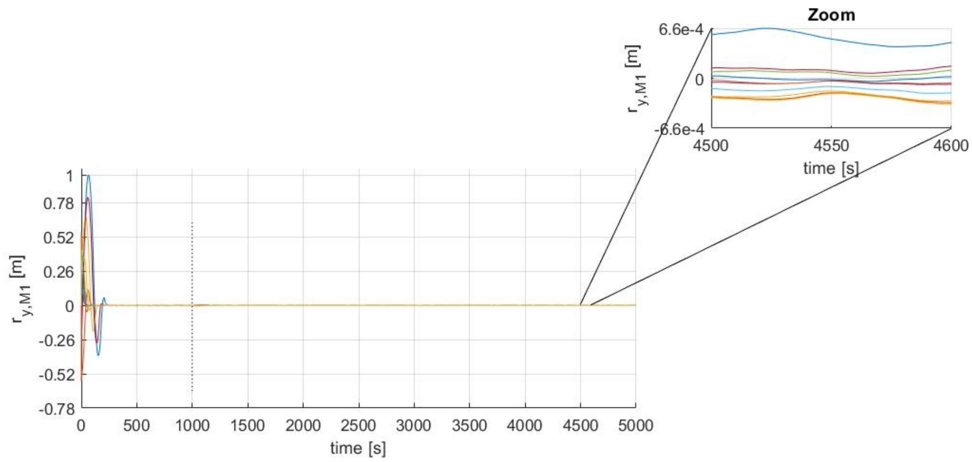

Figure 5.81. STW SMC - Critical conditions - TM1 Linear position along Y axis

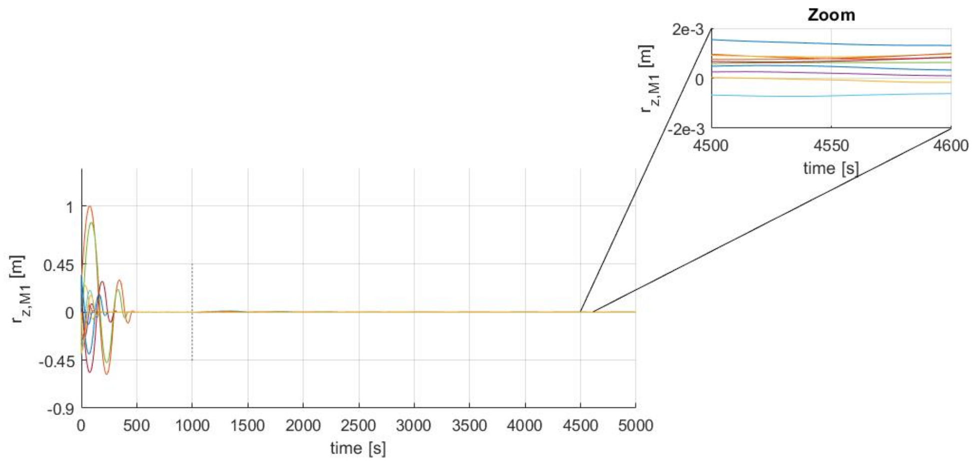

Figure 5.82. STW SMC - Critical conditions - TM1 Linear position along Z axis

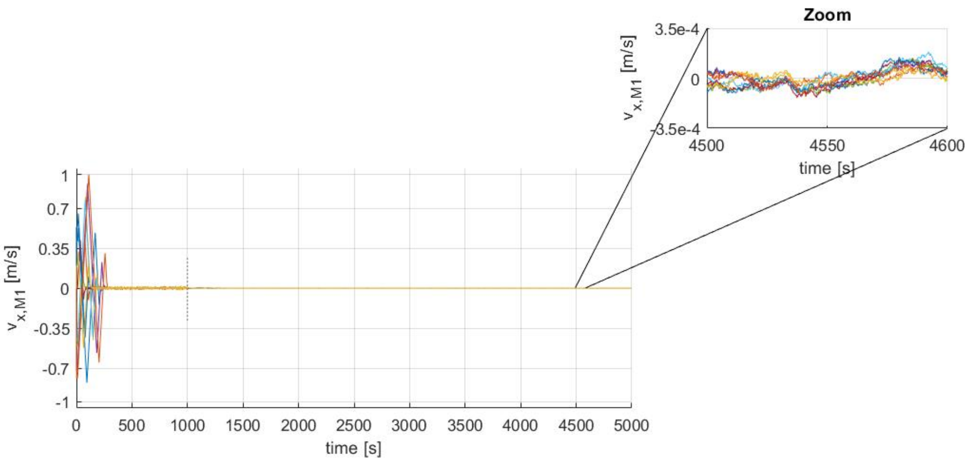

Figure 5.83. STW SMC - Critical conditions - TM1 Linear velocity along X axis

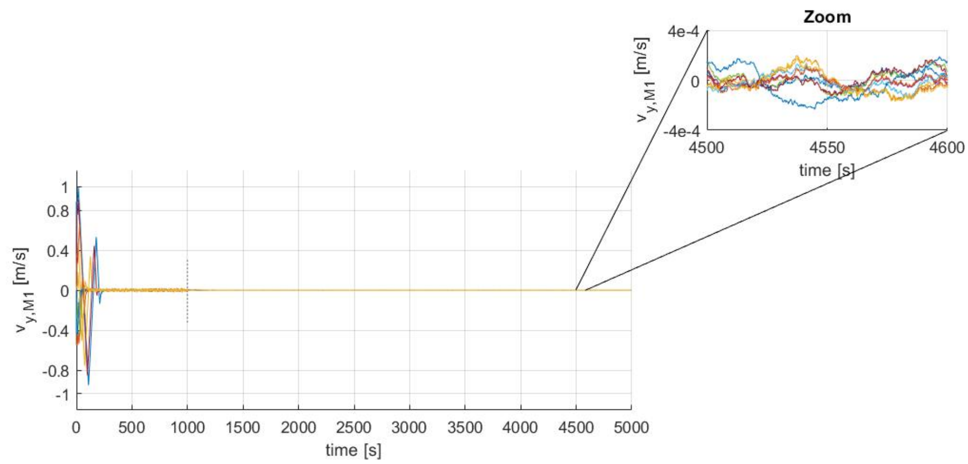

Figure 5.84. STW SMC - Critical conditions - TM1 Linear velocity along Y axis

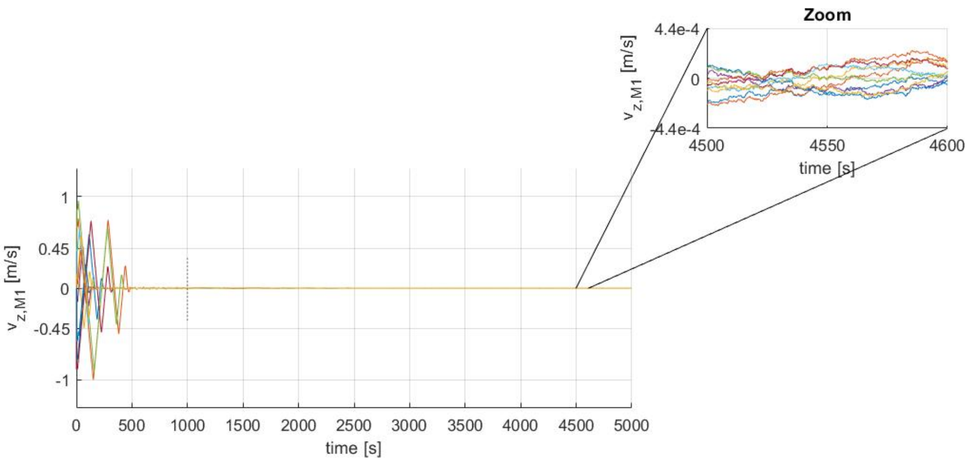

Figure 5.85. STW SMC - Critical conditions - TM1 Linear velocity along Z axis

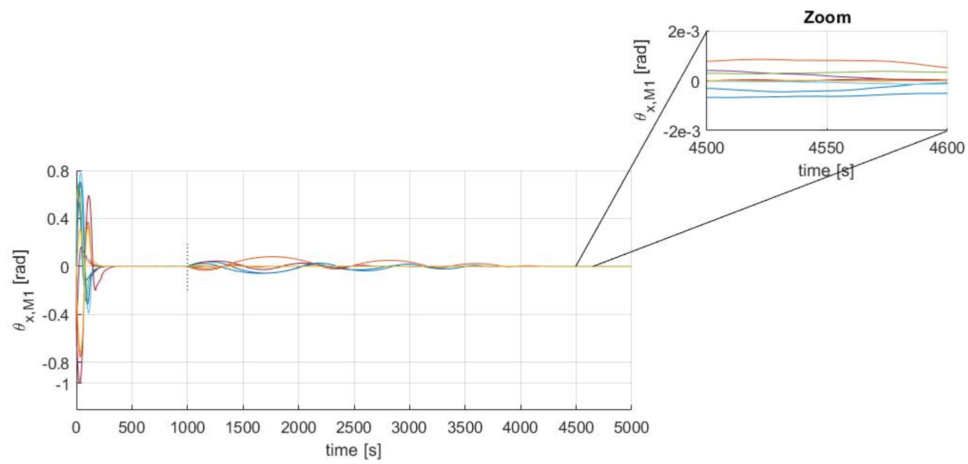

Figure 5.86. STW SMC - Critical conditions - TM1 Angular position around X axis

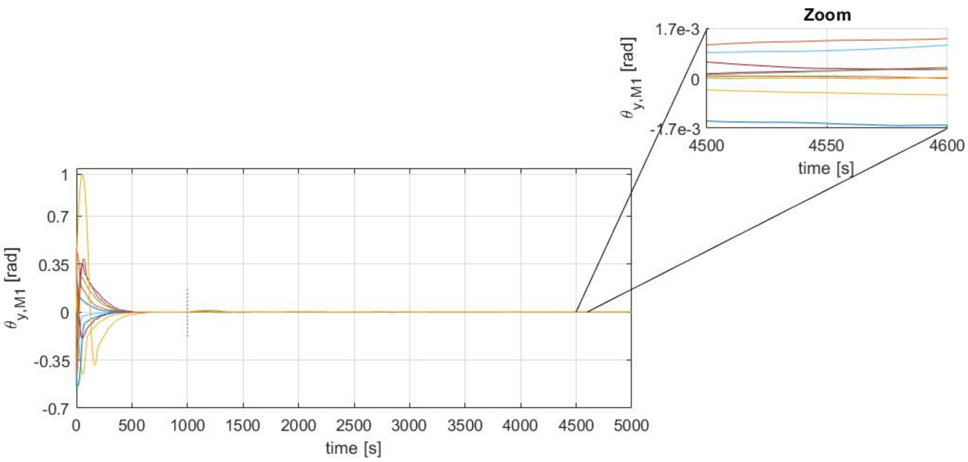

Figure 5.87. STW SMC - Critical conditions - TM1 Angular position around Y axis

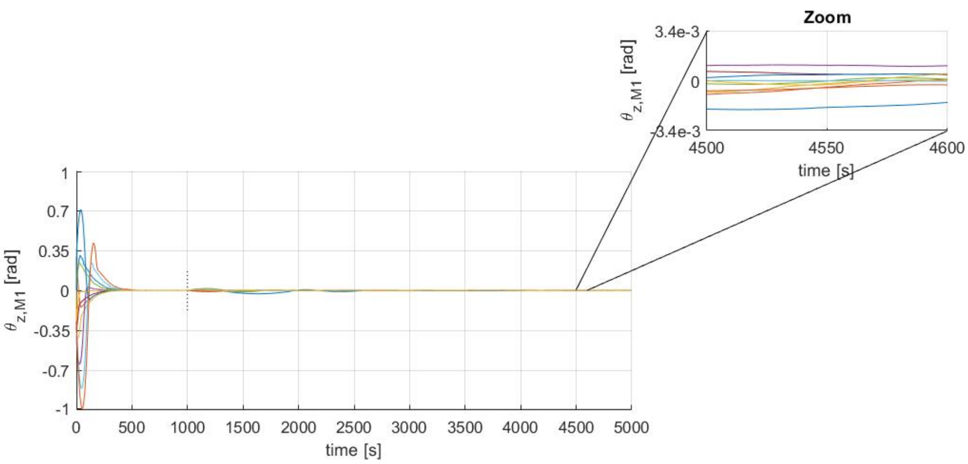

Figure 5.88. STW SMC - Critical conditions - TM1 Angular position around Z axis

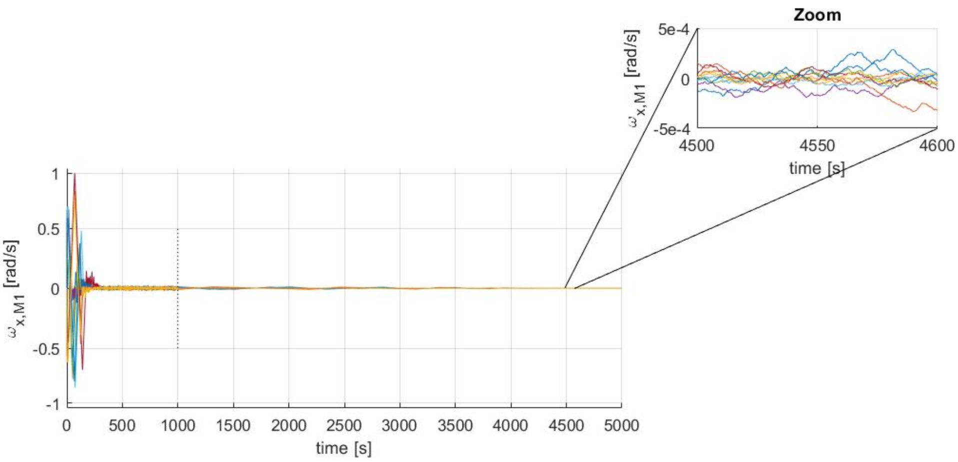

Figure 5.89. STW SMC - Critical conditions - TM1 Angular velocity around X axis

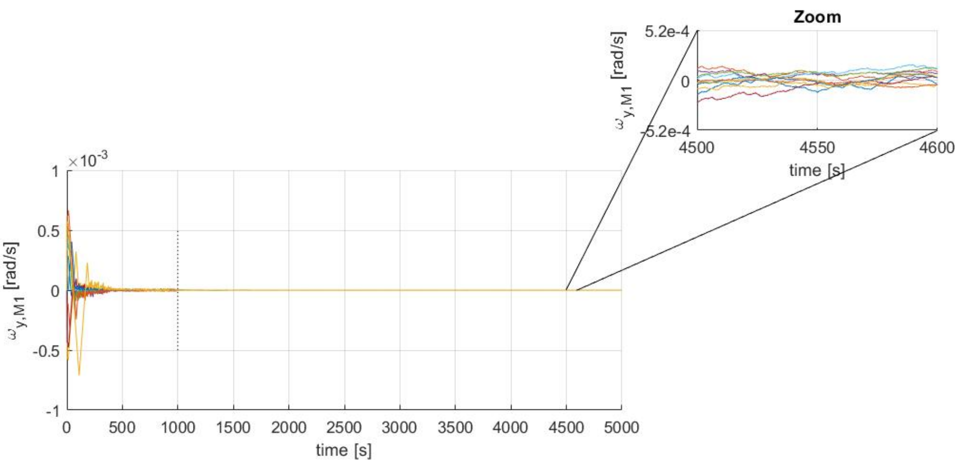

Figure 5.90. STW SMC - Critical conditions - TM1 Angular velocity around Y axis

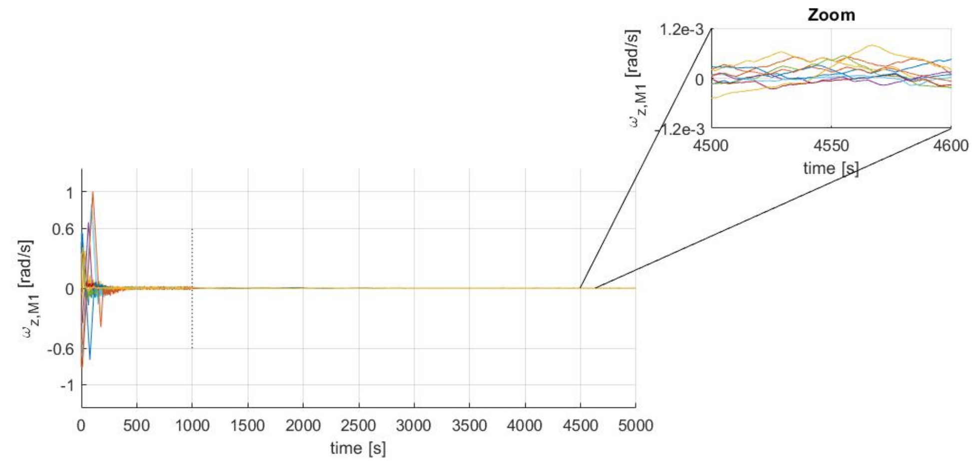

Figure 5.91. STW SMC - Critical conditions - TM1 Angular velocity around Z axis

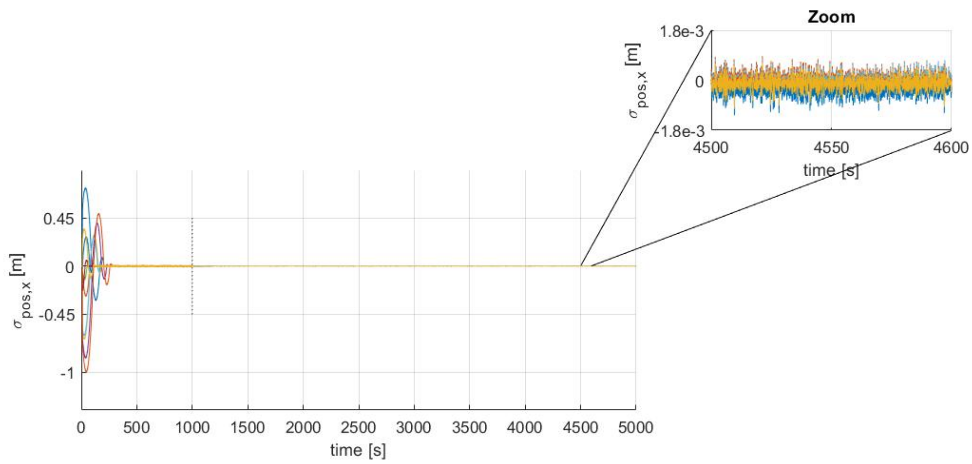

Figure 5.92. STW SMC - Critical conditions - TM1 Position sliding surface along X axis

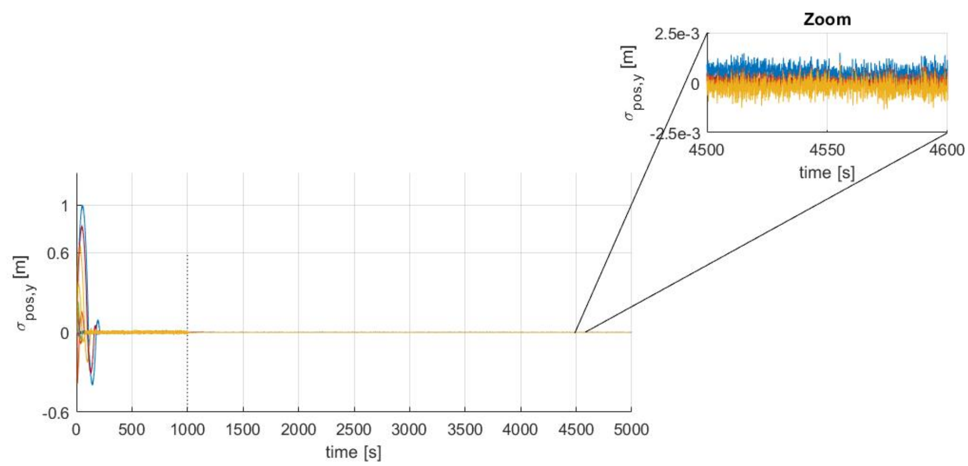

Figure 5.93. STW SMC - Critical conditions - TM1 Position sliding surface along Y axis

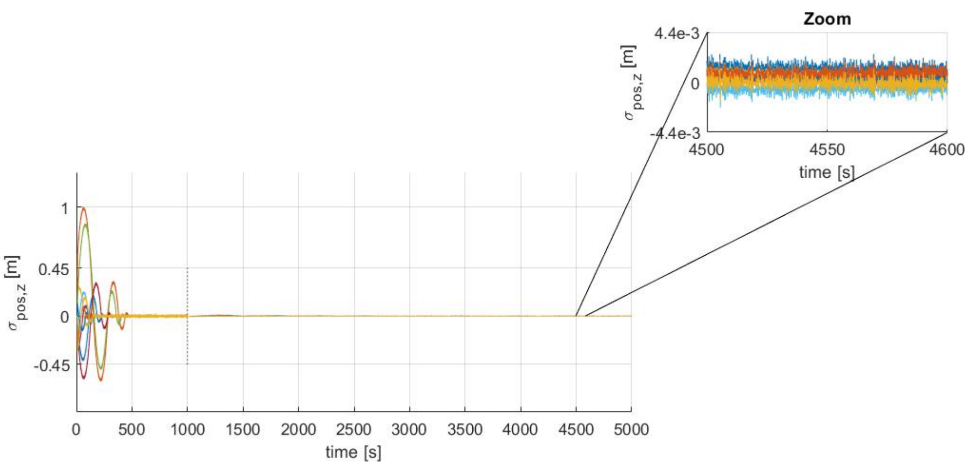

Figure 5.94. STW SMC - Critical conditions - TM1 Position sliding surface along Z axis

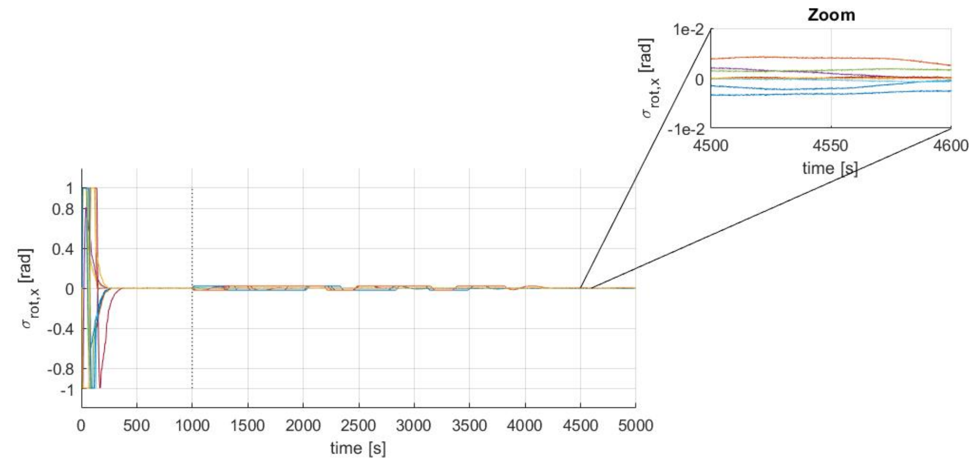

Figure 5.95. STW SMC - Critical conditions - TM1 Rotation sliding surface around X axis

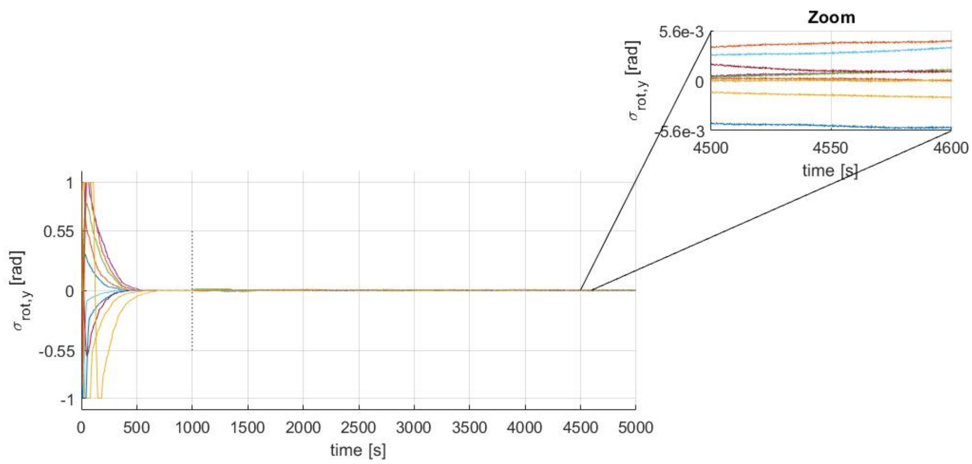

Figure 5.96. STW SMC - Critical conditions - TM1 Rotation sliding surface around Y axis

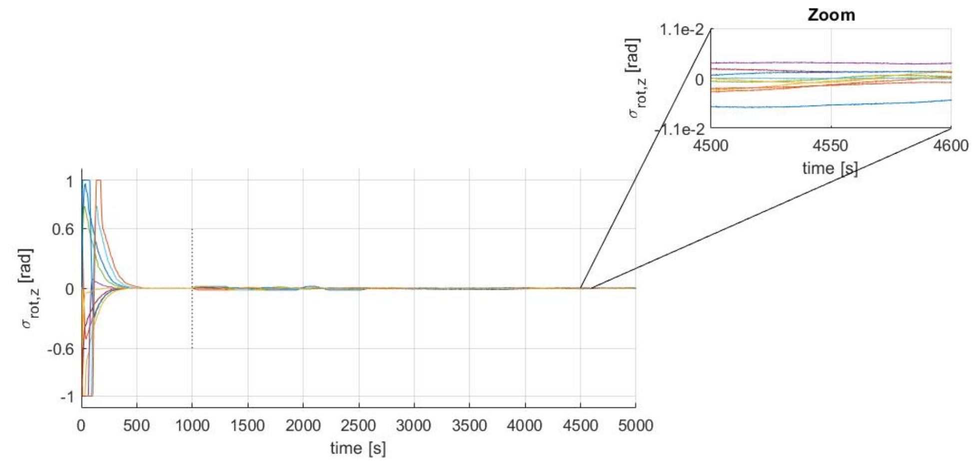

Figure 5.97. STW SMC - Critical conditions - TM1 Rotation sliding surface around Z axis

In the following are exposed the STW SMC results for comparison purposes in terms of accuracy, settling time and maximum overshoot:

Table 5.13. STW SMC comparison performance - Accuracy in WR and HR mode (3σ)

WR	x	y	z
$r_{M1}[m]$	$\pm 4.91e-6$	$\pm 4.15e-6$	$\pm 4.33e-6$
$v_{M1}[m/s]$	$\pm 1.73e-6$	$\pm 1.60e-6$	$\pm 8.27e-7$
$\theta_{M1}[rad]$	$\pm 6.12e-5$	$\pm 6.15e-5$	$\pm 6.73e-5$
$\omega_{M1}[rad/s]$	$\pm 6.24e-5$	$\pm 4e-5$	$\pm 4.45e-5$
HR	x	y	z
$r_{M1}[m]$	$\pm 8.83e-7$	$\pm 7.18e-7$	$\pm 4.09e-6$
$v_{M1}[m/s]$	$\pm 1.66e-8$	$\pm 1.55e-8$	$\pm 1.49e-8$
$\theta_{M1}[rad]$	$\pm 3.62e-5$	$\pm 8.26e-5$	$\pm 8.80e-5$
$\omega_{M1}[rad/s]$	$\pm 7.33e-7$	$\pm 5.44e-7$	$\pm 1.71e-6$

Table 5.14. STW SMC comparison performance - Settling time in WR and HR mode

	[0; 199]s	[200; 800]s	[801; 1000]s
WR	[x;y;z]	[x;y;z]	[x;y;z]
r_{M1}	$[60\%; 90\%; 60\%]$	$[40\%; 10\%; 40\%]$	$[0\%; 0\%; 0\%]$
v_{M1}	$[70\%; 90\%; 60\%]$	$[30\%; 10\%; 40\%]$	$[0\%; 0\%; 0\%]$
θ_{M1}	$[20\%; 0\%; 10\%]$	$[80\%; 100\%; 90\%]$	$[0\%; 0\%; 0\%]$
ω_{M1}	$[90\%; 50\%; 70\%]$	$[10\%; 50\%; 30\%]$	$[0\%; 0\%; 0\%]$
	[1001; 1200]s	[1201; 4800]s	[4801; 5000]s
HR	[x;y;z]	[x;y;z]	[x;y;z]
r_{M1}	$[90\%; 100\%; 40\%]$	$[10\%; 0\%; 60\%]$	$[0\%; 0\%; 0\%]$
v_{M1}	$[60\%; 80\%; 0\%]$	$[40\%; 20\%; 100\%]$	$[0\%; 0\%; 0\%]$
θ_{M1}	$[30\%; 90\%; 40\%]$	$[70\%; 10\%; 60\%]$	$[0\%; 0\%; 0\%]$
ω_{M1}	$[30\%; 60\%; 40\%]$	$[70\%; 40\%; 60\%]$	$[0\%; 0\%; 0\%]$

Table 5.15. STW SMC comparison performance - Maximum overshoot

WR	x	y	z
$r_{M1}[m]$	1.10e-3	7.61e-4	1.10e-3
$v_{M1}[m/s]$	2.84e-5	2.60e-5	2.30e-5
$\theta_{M1}[rad]$	2.4e-2	2.88e-2	2.96e-2
$\omega_{M1}[rad/s]$	9.58e-4	7.10e-4	8.05e-4

This analysis shows how both control strategies are able counteract the external disturbances, high sensor noises and uncertainties, with similar performance. As said before, the performance metrics are the settling time and the accuracy. The displacements (as from Fig.5.62 to Fig.5.64 and from the Fig.5.80) to the Fig.5.82) are not critical variables and both controllers are able to reach the desired requirements. In general, velocities are not critical and both controller achieve the required performance, as can be seen for the linear velocities from Fig.5.65 to 5.67 and from 5.83 to 5.85. As the same for the angular velocities, as seen from the 5.71 to the 5.73 and from 5.89 to the 5.91. Instead, as from Fig.5.68 to the Fig.5.70 and from Fig.5.86 to the Fig.5.88, the angular displacements have a critical behavior. In detail, the first order SMC has a settling time higher with respect to

STW-SMC time, even if it is able to handle disturbances and noises. Moreover, the accuracy is one order of magnitude greater than the second order SMC. The STW-SMC is able to counteract disturbances, uncertainties, noises, even for critical initial conditions. A nominal self gravity of 50 % of the control authority is considered for these simulations. Whereas, control performances are summarized about the first order SMC in Table 5.10, Table 5.11 and Table 5.12 and about the STW SMC in Table 5.13, Table 5.14 and 5.15.

We first analyzed the WR mode results. As in Tables 5.11 and 5.14, a settling time of about 200 s is obtained for the linear displacements, for both control strategies, only $20 - 40$ % of the simulations have a maximum settling time of 800 s. Instead, as previously said, for the first order SMC, all the simulations related to the angular displacements have a settling time between 800-1000 s for the first order SMC. For the STW-SMC, the rotational displacements have a maximum settling time of 800 s. The linear and angular velocities are the same for both controller with more than 50% runs have a settling time within the 200s and the others have are within the 800s. In terms of maximum overshoot, se seen in the Table 5.15 and 5.12 both controllers have similar performance for all the states and are able to not allow to the TMs to hit the inner walls of the holding cages.

We now analyze the HR mode results. As for the previous mode, a settling time of about 200 s is observed in Tables 5.11 and 5.14, for linear displacements and for both controllers. As in the previous case, for the angular displacements, the maximum settling time of 1000 s is observed for the first order SMC, with an accuracy of about 10^{-5} rad for all the DoFs. Instead, for the second order SMC in terms of angular displacements, most of the simulations have a settling time of maximum 800 s, with an accuracy of about 10^{-5} rad for all the DoFs. In terms of linear and angular velocities, they have a more critical behaviour wrt the WR performance, with their own three components having a settling time equally distributed between $0 - 800s$ Even if an oscillatory behavior can be observed in zoom of Figures 5.86, 5.87, 5.88, high accuracy is obtained, one order of magnitude less than the first order SMC.

Finally, the sliding surface results of both control strategies are showed from Fig.5.74 to Fig.5.79 and from Fig.5.92 to Fig.5.97. For both controllers, the positions sliding surface are not critical and they show similar behaviours in terms of settling time, as the same showed with the linear positions performance. The rotations sliding surface are critical both for WR and HR mode. In detail, in the figures zoom box can be seen that the chattering is achieved with a reduced amplitude for the STW SMC in respect of the first order SMC. This difference is due to the continuous control law implemented to the STW SMC which allow to reduce the chattering amplitude. As opposite, the higher chattering amplitude of the first order SMC is due to the implemented discontinuous control law. Moreover, the advantages of a continuous control law is also the reduction of the actuation effort to achieve and keep the desired trajectories for the simulation variables.

5.7 Self gravity disturbance analysis

This section highlight the STW SMC controller behaviour in respect of the strong environmental disturbance which strongly leads the control design, mostly about the HR mode. In detail, the SG is analyzed because it is one of the main disturbance to cause a strong deviation in the desired performance, mostly in terms of attitude control, because it is comparable to the maximum actuation authority. Considering self gravity disturbances fixed at the 50% and 25% of the maximum actuation authority, ten simulations for each level of disturbances are performed, with critical initial conditions.

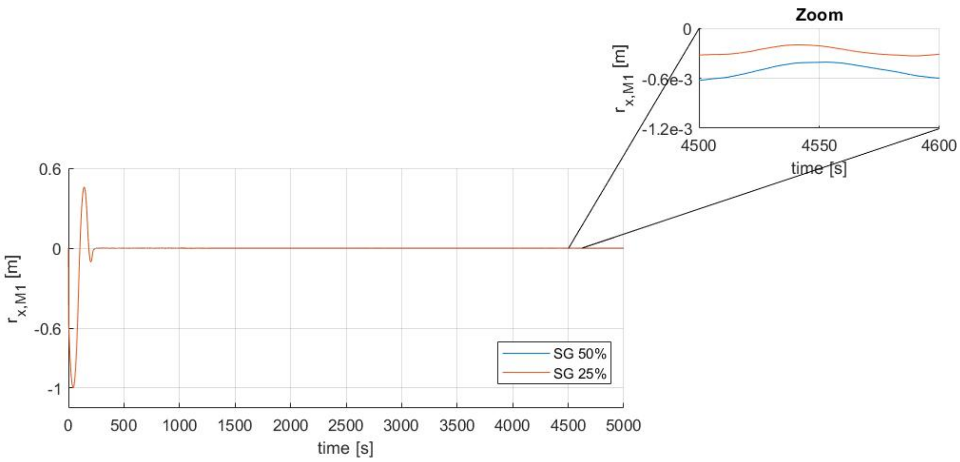

Figure 5.98. SG disturbance analysis - TM1 Linear position along X axis

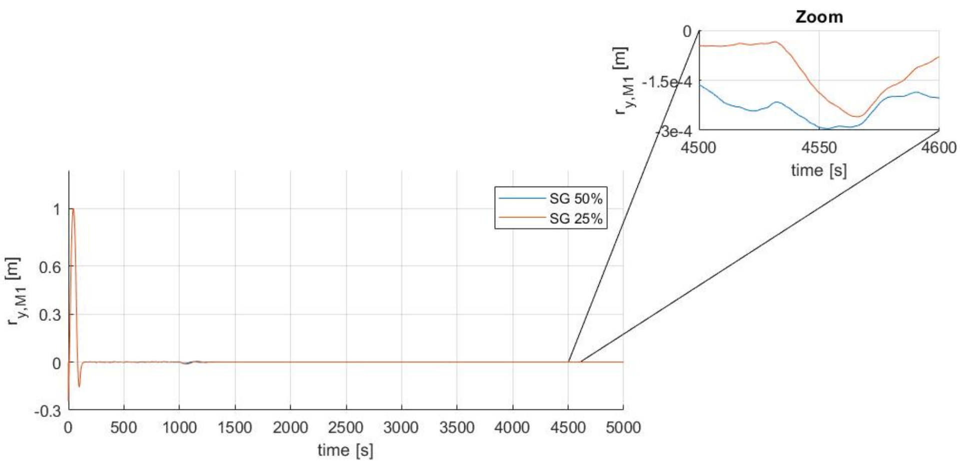

Figure 5.99. SG disturbance analysis - TM1 Linear position along Y axis

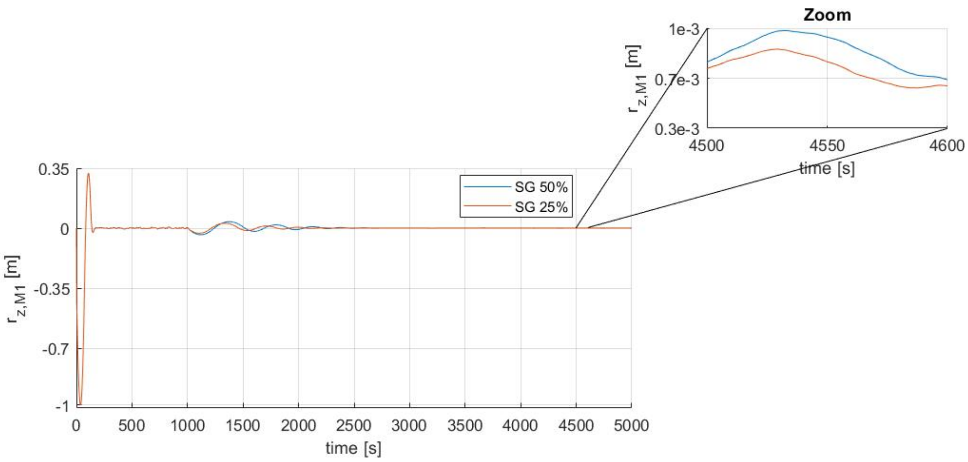

Figure 5.100. SG disturbance analysis - TM1 Linear position along Z axis

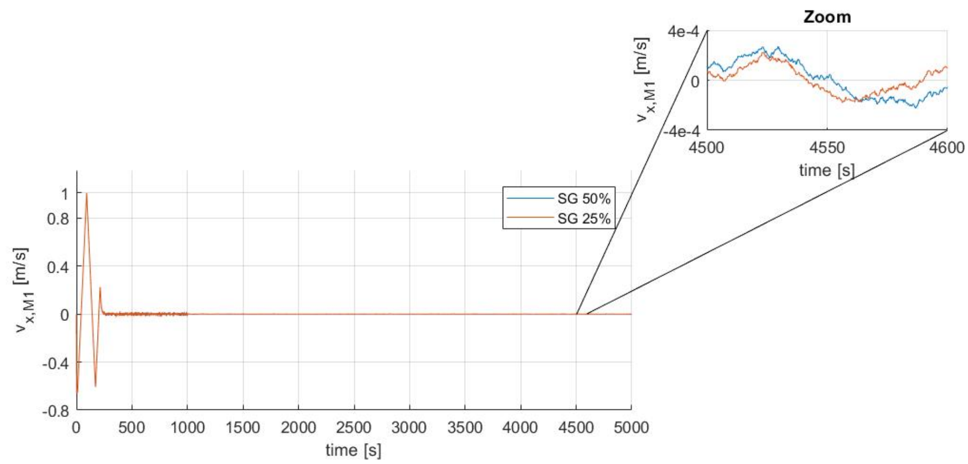

Figure 5.101. SG disturbance analysis - TM1 Linear velocity along X axis

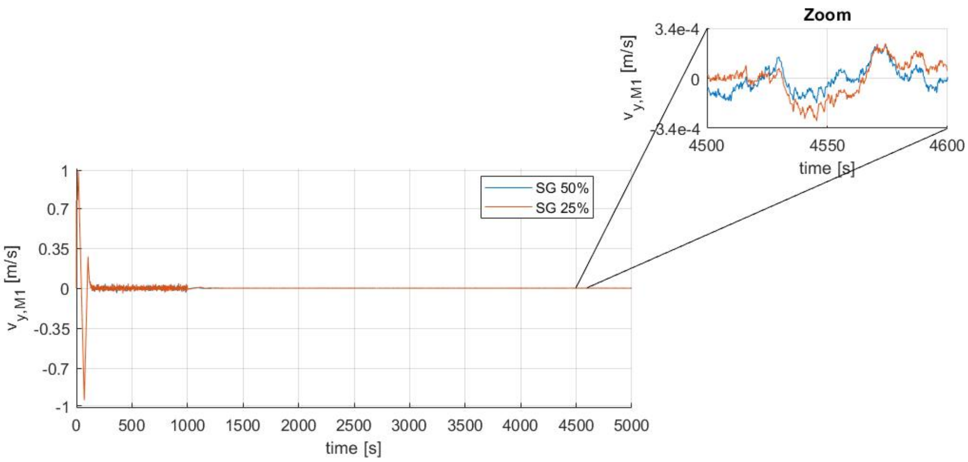

Figure 5.102. SG disturbance analysis - TM1 Linear velocity along Y axis

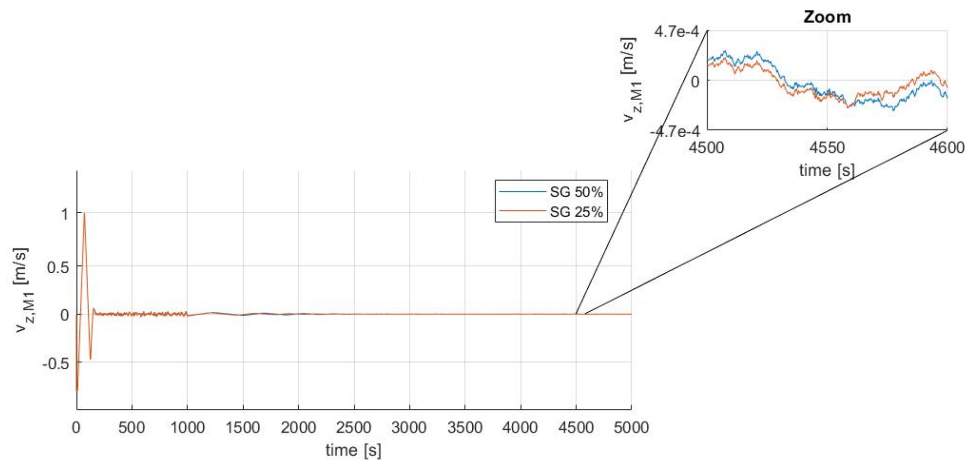

Figure 5.103. SG disturbance analysis - TM1 Linear velocity along Z axis

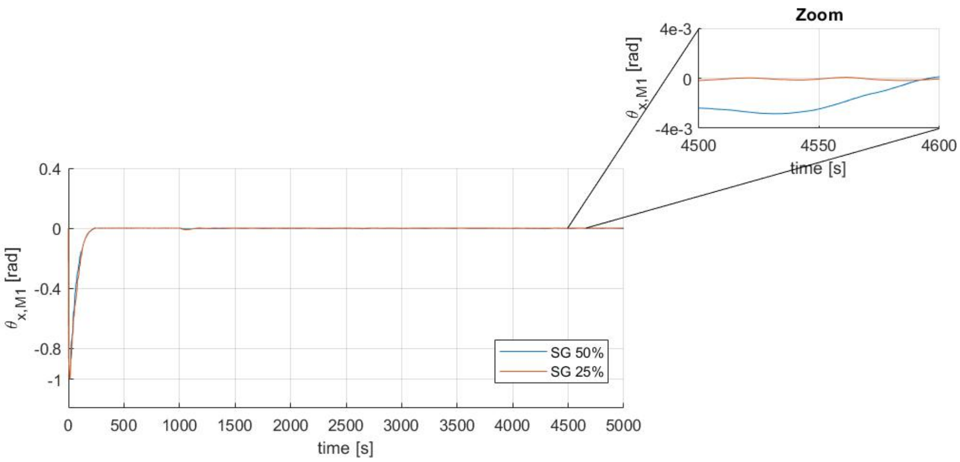

Figure 5.104. SG disturbance analysis - TM1 Angular position around X axis

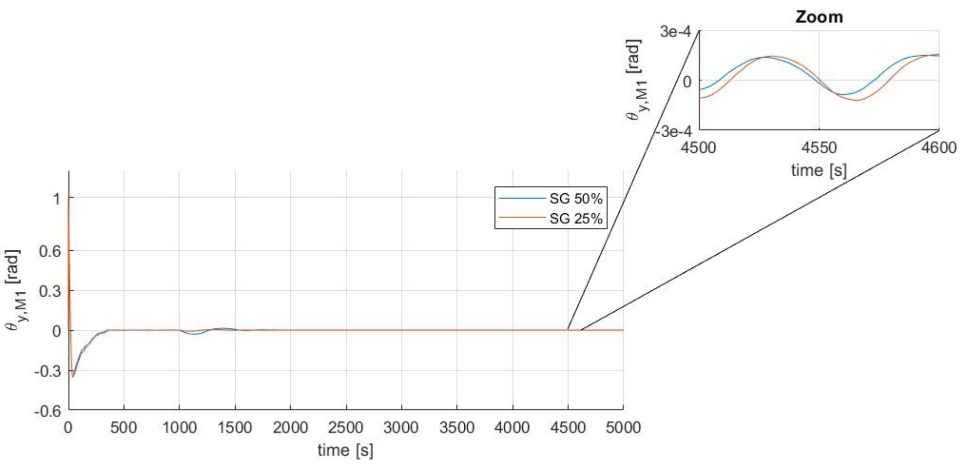

Figure 5.105. SG disturbance analysis - TM1 Angular position around Y axis

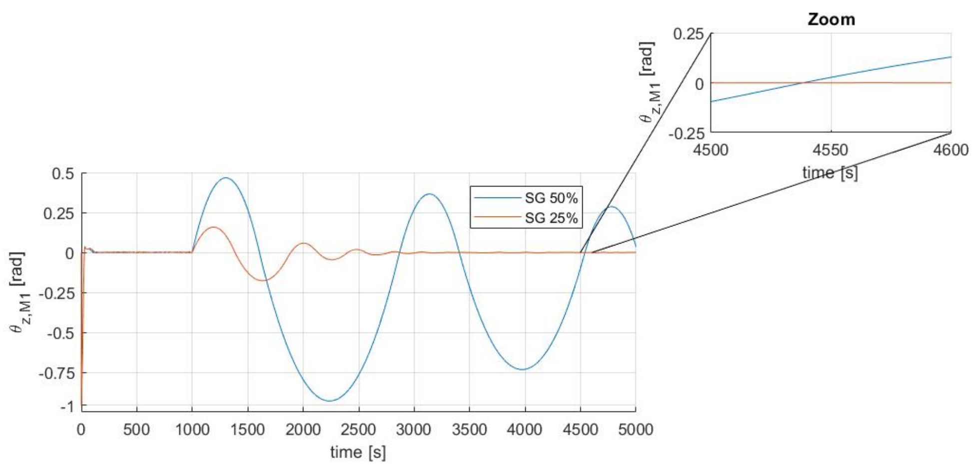

Figure 5.106. SG disturbance analysis - TM1 Angular position around Z axis

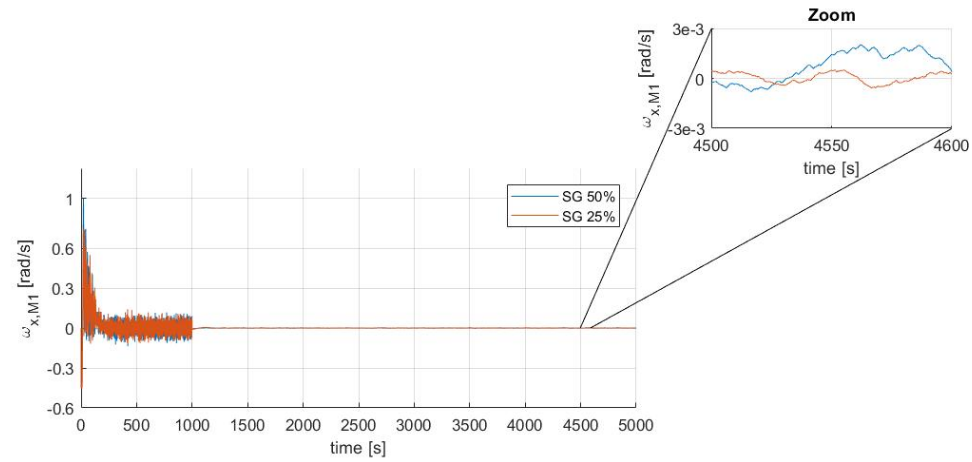

Figure 5.107. SG disturbance analysis - TM1 Angular velocity around X axis

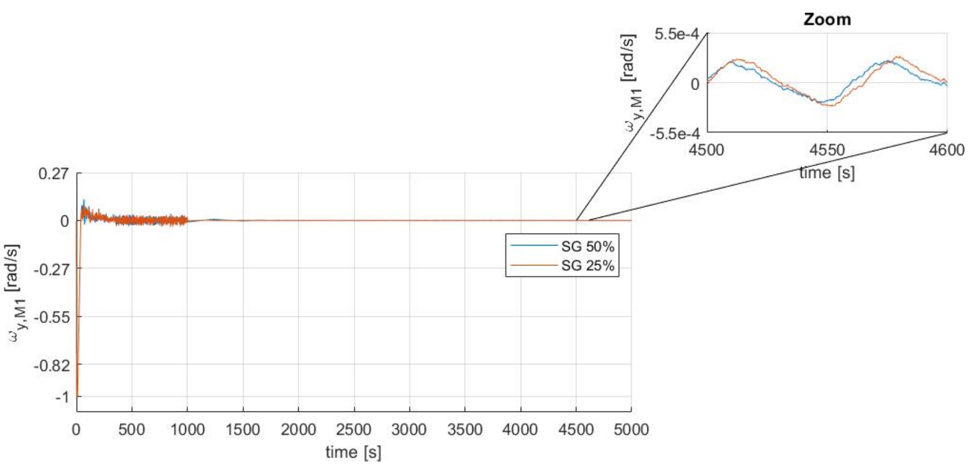

Figure 5.108. SG disturbance analysis - TM1 Angular velocity around Y axis

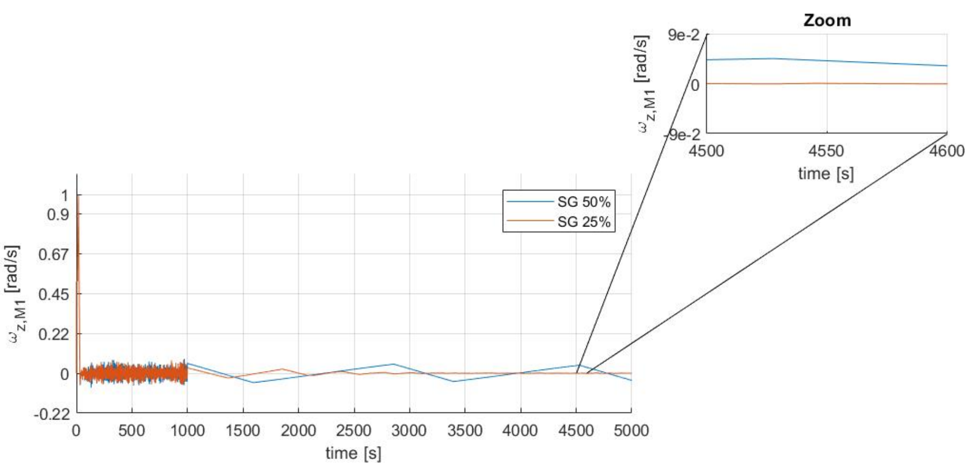

Figure 5.109. SG disturbance analysis - TM1 Angular velocity around Z axis

As explained above, the self gravity disturbance is considered in the mathematical model as the main TM external disturbances. Its effects are deeply analyzed since the maximum magnitude of the disturbances is close to the control authority, with a self gravity force of about 10^{-9} N and a SG torque of about 10^{-12} Nm. This section highlights the behaviour of only the STW-SMC controller when different environmental disturbances are considered, since these disturbances mainly influenced the control design, especially for the HR mode. An oscillatory behavior can be observed for both the linear, angular displacements and velocities. Moreover, the settling time is about 12000 s for the angular displacement around Z axis (see Figure 5.106). As seen for the position and attitude cases, the linear and angular velocities follow a similar behaviour. In detail, the linear velocities have no variation in varying SG disturbance. As opposite, the angular velocities, in the SG 25% case, show a reduced and more stable oscillation in respect of the case with SG setted to 50%. All the figures have a maximum simulation time of 5000 s, since most of the simulations have this maximum convergence time.

Chapter 6

Conclusions and future works

6.1 Conclusions

This work is focused on the design of a STW SMC control for the TMs release phase of LISA mission, which is a space observatory with the goal to detect gravitational waves to validate Einstein's theory of gravity as it is explained in detail in the first chapter together with the main goal to catch and stabilize the masses in the TMs release phase. The useful information are carried out by LISA Pathfinder reports about the LISA configuration and its related operative environment. Then, in the second chapter, the simulation environment, given by Thales Alenia Space for the MonteCarlo campaign, and the adopted models are presented in detail in terms of sensors, actuators, noises and disturbance. Instead, the mathematical model implemented in the plant and the adopted reference systems are deeply described together with the S/C and TM nonlinear dynamics. In the fourth chapter, a deep study of the SMC control is done and the two proposed control strategies, the first order SMC and STW SMC algorithm are presented and designed for control purposes in the TMs release phase. The controllers are tested in the fifth chapter, through a MonteCarlo campaign in a wide range of cases with a critical configuration due to varying initial conditions and environmental disturbance and noises. Moreover, a comparison between the STW SMC and a first order SMC is performed in the same simulation environment and with critical initial conditions, in reference of the experience done in LISA Pathfinder mission. A performance analysis is presented and described about its fundamental criteria and it is carried out to compare the campaign results. The STW SMC is validated in terms of performance to be in ESA requirements and to achieve the initial conditions requested to switch to the SCI operations, the main phase of LISA mission. These results are achieved thanks to STW SMC properties such as the robustness and insensibility to the external disturbance and model uncertainties and due to the continuous control law adopted. The comparison between the two control strategies showed that the first order have a similar result compared to the STW SMC for position control but not for the attitude angles which are critical in the HR mode. The first order SMC is implemented with a discontinuous control law which is able to counteract the high environmental disturbance and noises for position control but it doesn't satisfy, for the attitude control, the steady-state accuracy requirements needed to switch to the SCI operations. In detail, the accuracy bounds 3σ of the Euler angles are one order of magnitude higher than the STW SMC performance, with a slow settling time which is equal or higher than the simulation time. So this work demonstrates the effectiveness and the suitability of the STW SMC control and its own properties for LISA, in respect of the designed first order control similar to the one applied in LISA Pathfinder. This latter could not counteract the strong influence of the external disturbance, noises and model uncertainties. Finally, a brief analysis is done about the control performance to the SG disturbance variation because of its magnitude which is similar or greater than the actuation authority of the TMs actuators. This last analysis is done as a tip to validate in a more accurate analysis an improved model for the disturbance and noises.

6.2 Future works

In this thesis there are many aspects which could be considered for future works, to improve the control design and its integration between different operative phases. The division of the TMs release phase in two modes put in evidence that the transitions between different phases could be critical and this problem should be deeply analyzed to better understand the convergence time needed by the implemented controllers to achieve the desired steady-state accuracy and to evaluate the influence of the different configurations assumed for each operative phases and sub-phases provided for LISA mission. A detailed study of the environmental disturbance and noises could be useful to better understand the GRS and SG contribution to the slow converging runs. These latter are not defined by any ESA specifications and they are assumed independently in a conservative way which involved, as negative aspect, a negative design due to environmental disturbance and noises with a magnitude similar, or higher, than the maximum actuation authority. This is due to the maximum boundary value of the SG set to 50% of the GRS saturation and it can exceed the maximum actuation authority, as experimented mostly in HR mode. So, an improved modeling of the disturbance and noises, in terms of magnitude and shape, and their validation through a new MonteCarlo campaign could be considered as next step to obtain more reliable results closer to the real environment experimented in LISA Pathfinder. In the end, an experimental control design about the STW SMC could be done in future taking into account the SMC equivalent control terms, which are not studied in this work, in the way to improve the STW SMC performance reducing actuation effort and the saturation time.

Appendix A

Notation

- Elementary rotation:
$$X(\phi)=\begin{bmatrix}1 & 0 & 0\\ 0 & c(\phi) & -s(\phi)\\ 0 & s(\phi) & c(\phi)\end{bmatrix};\ Y(\theta)=\begin{bmatrix}c(\theta) & 0 & s(\theta)\\ 0 & 1 & 0\\ -s(\theta) & 0 & c(\theta)\end{bmatrix};\ Z(\psi)=\begin{bmatrix}c(\psi) & -s(\psi) & 0\\ s(\psi) & c(\psi) & 0\\ 0 & 0 & 1\end{bmatrix}$$
with $\Theta = [\phi, \theta, \psi]$ Euler angles and $c = cos$ and $s = sin$.

- Rotation matrix (3-2-1):
$T(\Theta) = Z(\psi)Y(\theta)X(\phi);$
$T^{-1}(\Theta) = T^T(\Theta) = X(-\phi)Y(-\theta)Z(-\psi);$

  as function of the Euler angles.

$$T(q) = \begin{bmatrix} q_0^2+q_1^2-q_2^2-q_3^2 & 2(q_1q_2+q_0q_3) & 2(q_1q_3+q_0q_2)\\ 2(q_1q_2+q_0q_3) & q_0^2-q_1^2+q_2^2-q_3^2 & 2(q_2q_3-q_0q_1)\\ 2(q_1q_3-q_0q_2) & 2(q_2q_3+q_0q_1) & q_0^2-q_1^2-q_2^2+q_3^2\end{bmatrix}$$
$T_a^b = T(q_a^b)$ for quaternion rotation from b to a.

  as function of quaternions.

  $q = [q_0\ q_1\ q_2\ q_3]^T = [q_0\ \mathbf{q}]$

  with q_0 the scalar component and $\mathbf{q} = [q_1\ q_2\ q_3]^T \in \mathrm{R}^3$

- Kinematic matrices (3-2-1):

$$Q(\mathbf{\Theta}) = \frac{1}{cos(\theta)} \begin{bmatrix} cos(\theta) & sin(\phi)sin(\theta) & cos(\phi)sin(\theta) \\ 0 & cos(\phi)cos(\theta) & -sin(\phi)cos(\theta) \\ 0 & sin(\phi) & cos(\phi) \end{bmatrix}$$

- Quaternion multiplication:
  $$p = q \otimes r = \begin{bmatrix} p_0 \\ p_1 \\ p_2 \\ p_3 \end{bmatrix} = \begin{bmatrix} q_0 & -q_1 & -q_2 & -q_3 \\ q_1 & q_0 & -q_3 & q_2 \\ q_2 & q_3 & q_0 & -q_1 \\ q_3 & -q_2 & q_1 & q_0 \end{bmatrix} \cdot \begin{bmatrix} r_0 \\ r_1 \\ r_2 \\ r_3 \end{bmatrix}$$

- Rotation matrix derivative:
  $\dot{T} = T\boldsymbol{\omega} \wedge$
  $\ddot{T} = T\mathbf{\Omega}$
  with $\Omega = \boldsymbol{\omega} \wedge \boldsymbol{\omega} \wedge + \dot{\boldsymbol{\omega}}\wedge$.

- Gyroscopic acceleration:
  $\mathbf{\Lambda}(\boldsymbol{\omega}) = \mathbf{\Lambda}(\boldsymbol{\omega}, J) = -J^{-1}\boldsymbol{\omega} \wedge J\boldsymbol{\omega}$.

Appendix B

Variables

The variables used in the TM and S/C dynamics are presented below:

- $\mathbf{r}_I$: S/C CoM position w.r.t. the IF origin - components in IF
- $\mathbf{r}_M$: S/C CoM position w.r.t. the IF origin - components in IF
- $\mathbf{r}_M^I$: TM CoM position w.r.t. the cage center - components in IF
- $\mathbf{r}_{MI}$: TM CoM position w.r.t. the IF origin - components in IF
- $\mathbf{q}_M$: quaternion of the rotation OF $\rightarrow$ MF
- $\mathbf{q}_S$: quaternion of the rotation CF local $\rightarrow$ SF
- $\mathbf{q}_{SI}$: quaternion of the rotation IF $\rightarrow$ SF
- $\mathbf{q}_{MI}$: quaternion of the rotation IF $\rightarrow$ MF
- $\boldsymbol{\omega}_M$: TM angular velocity w.r.t. OF - components in MF
- $\boldsymbol{\omega}_{MI}$: TM angular velocity w.r.t. IF - components in MF
- $\boldsymbol{\omega}_S$: S/C angular velocity w.r.t. the local CF - components in SF
- $\boldsymbol{\omega}_{SI}$: S/C angular velocity w.r.t. IF - components in SF
- $\boldsymbol{\omega}_O$: OA angular velocity w.r.t. IF - components in OF
- $\boldsymbol{\omega}_C$: local CF origin angular velocity w.r.t. IF - components in local CF
- ζ: OF angle with respect to its rest position (the rest positions of the two OFs x-axes are given by the SF $x - axis \pm \pi/6$)

- $\mathbf{b}_M$: vector from the OA pivot to the cage center - components in OF
- $\mathbf{b}_S$: vector from the S/C CoM to the OA pivot - components in SF
- m_M: Test mass
- m_s: Total S/C mass
- J_M: inertia matrix of a TM w.r.t TM CoM
- J_S: inertia matrix of a S/C w.r.t S/C CoM (including the two OAs)
- $\mathbf{F}_E$: commanded electrostatic suspension force
- $\mathbf{F}_T$: commanded MPS force
- $\mathbf{M}_E$: commanded electrostatic suspension torque
- $\mathbf{M}_T$: commanded MPS torque
- $\mathbf{d}_M$: force of the disturbance acting on the TM - components in OF
- $\mathbf{d}_S$: force of the disturbance acting on the S/C - components in SF
- $\mathbf{D}_M$: moment of the disturbance acting on the TM - components in MF
- $\mathbf{D}_S$: moment of the disturbance acting on the S/C - components in SF
- K_R: TM angular stiffness matrix

Bibliography

Amaro-Seoane, Pau et al. (2017). "Laser interferometer space antenna". In: *arXiv preprint arXiv:1702.00786*.

Antonucci, F et al. (2012). "The LISA pathfinder mission". In: *Classical and Quantum Gravity* 29.12, p. 124014.

Capello, Elisa, Elisabetta Punta, and Giorgio Bartolini (2017). "Simplex sliding mode control strategies for spacecraft rendezvous maneuvers". In: *IFAC-PapersOnLine* 50.1, pp. 8496–8501.

Capello, Elisa et al. (2017). "Sliding-mode control strategies for rendezvous and docking maneuvers". In: *Journal of Guidance, Control, and Dynamics* 40.6, pp. 1481–1487.

ESSB HB-E-003 Working Group, ESA (2011). *ESA Pointing Error Engineering Handbook*.

Levant, Arie (1993). "Sliding order and sliding accuracy in sliding mode control". In: *International journal of control* 58.6, pp. 1247–1263.

– (2003). "Introduction to high-order sliding modes". In: *School of Mathematical Sciences, Israel* 58.6, p. 1.

Merkowitz, Stephen M et al. (2005). "Self-gravity modelling for LISA". In: *Classical and Quantum Gravity* 22.10, S395.

Montemurro, Fabio et al. (2006). "Control design of the test mass release mode for the lisa pathfinder mission". In: *AIP Conference Proceedings*. Vol. 873. 1. American Institute of Physics, pp. 583–587.

Moore, Christopher J, Davide Gerosa, and Antoine Klein (2019). "Are stellar-mass black-hole binaries too quiet for LISA?" In: *Monthly Notices of the Royal Astronomical Society: Letters* 488.1, pp. L94–L98.

Pukdeboon, Chutiphon (July 2011). "Optimal Sliding Mode Controllers for Attitude Stabilization of Flexible Spacecraft". In: *Mathematical Problems in Engineering* 863092. DOI: 10.1155/2011/863092.

Schleicher, A et al. (2018). “In-orbit performance of the LISA Pathfinder drag-free and attitude control system”. In: *CEAS Space Journal* 10.4, pp. 471–485.

Shtessel, Yuri et al. *Sliding mode control and observation*. Springer.

Tiwari, Pyare Mohan, S. Janardhanan, and Mashuq un Nabi (2014). “Rigid spacecraft attitude tracking using finite time sliding mode control”. In: *IFAC Proceedings Volumes* 47.1. 3rd International Conference on Advances in Control and Optimization of Dynamical Systems (2014), pp. 263 –270. ISSN: 1474-6670. DOI: https://doi.org/10.3182/20140313-3-IN-3024.00168. URL: http://www.sciencedirect.com/science/article/pii/S1474667016326660.

Utkin, Vadim I (1992). *Sliding modes in optimization and control problems*.

Yeh, F-K (2010). “Sliding-mode adaptive attitude controller design for spacecrafts with thrusters”. In: *IET control theory & applications* 4.7, pp. 1254–1264.